

INFORMATION TO USERS

This manuscript has been reproduced from the microfilm master. UMI films the text directly from the original or copy submitted. Thus, some thesis and dissertation copies are in typewriter face, while others may be from any type of computer printer.

The quality of this reproduction is dependent upon the quality of the copy submitted. Broken or indistinct print, colored or poor quality illustrations and photographs, print bleedthrough, substandard margins, and improper alignment can adversely affect reproduction.

In the unlikely event that the author did not send UMI a complete manuscript and there are missing pages, these will be noted. Also, if unauthorized copyright material had to be removed, a note will indicate the deletion.

Oversize materials (e.g., maps, drawings, charts) are reproduced by sectioning the original, beginning at the upper left-hand corner and continuing from left to right in equal sections with small overlaps. Each original is also photographed in one exposure and is included in reduced form at the back of the book.

Photographs included in the original manuscript have been reproduced xerographically in this copy. Higher quality 6" x 9" black and white photographic prints are available for any photographs or illustrations appearing in this copy for an additional charge. Contact UMI directly to order.

UMI

A Bell & Howell Information Company
300 North Zeeb Road, Ann Arbor MI 48106-1346 USA
313/761-4700 800/521-0600

University of Alberta

**Finite Amplitude Waves and Eddy Development
on a Baroclinically Unstable Front
over a Sloping Bottom**

by

Mateusz K. Reszka



A thesis submitted to the Faculty of Graduate Studies and Research
in partial fulfillment of the requirements for the degree of
Master of Science

in

Applied Mathematics

Department of Mathematical Sciences

Edmonton, Alberta

Fall, 1997



National Library
of Canada

Acquisitions and
Bibliographic Services

395 Wellington Street
Ottawa ON K1A 0N4
Canada

Bibliothèque nationale
du Canada

Acquisitions et
services bibliographiques

395, rue Wellington
Ottawa ON K1A 0N4
Canada

Your file *Votre référence*

Our file *Notre référence*

The author has granted a non-exclusive licence allowing the National Library of Canada to reproduce, loan, distribute or sell copies of this thesis in microform, paper or electronic formats.

The author retains ownership of the copyright in this thesis. Neither the thesis nor substantial extracts from it may be printed or otherwise reproduced without the author's permission.

L'auteur a accordé une licence non exclusive permettant à la Bibliothèque nationale du Canada de reproduire, prêter, distribuer ou vendre des copies de cette thèse sous la forme de microfiche/film, de reproduction sur papier ou sur format électronique.

L'auteur conserve la propriété du droit d'auteur qui protège cette thèse. Ni la thèse ni des extraits substantiels de celle-ci ne doivent être imprimés ou autrement reproduits sans son autorisation.

0-612-22662-X

University of Alberta
Library Release Form

Name of Author: Mateusz K. Reszka

Title of Thesis: Finite Amplitude Waves and Eddy Development on a
Baroclinically Unstable Front over a Sloping Bottom

Degree: Master of Science

Year this Degree Granted: 1997

Permission is hereby granted to the University of Alberta Library to reproduce single copies of this thesis and to lend or sell such copies for private, scholarly, or scientific research purposes only.

The author reserves all other publication and other rights in association with the copyright in the thesis, and except as hereinbefore provided, neither the thesis nor any substantial portion thereof may be printed or otherwise reproduced in any material form whatever without the author's prior written permission.

A handwritten signature in dark ink, reading "Mateusz Reszka", is written over a horizontal line.

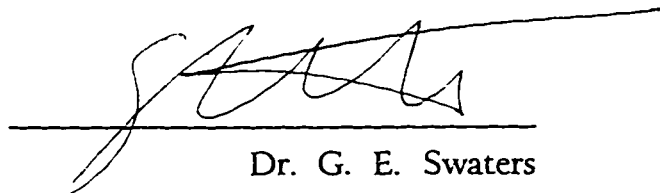
Permanent Address:
Department of Mathematical Sciences
University of Alberta
Edmonton, Alberta
Canada T6G 2G1

September 15, 1997

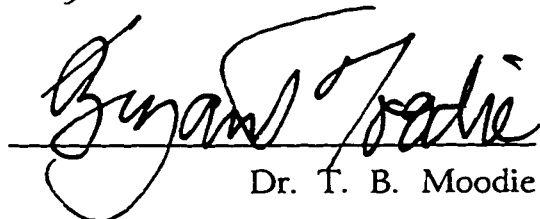
University of Alberta

Faculty of Graduate Studies and Research

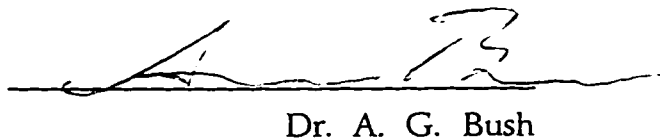
The undersigned certify that they have read and recommend to the Faculty of Graduate Studies and Research for acceptance, a thesis entitled **Finite Amplitude Waves and Eddy Development on a Baroclinically Unstable Front over a Sloping Bottom** submitted by **Mateusz K. Reszka** in partial fulfillment of the requirements for the degree of **Master of Science in Applied Mathematics**.



Dr. G. E. Swaters



Dr. T. B. Moodie



Dr. A. G. Bush

Date: 10 SEPTEMBER 1997

Abstract

We study the baroclinic dynamics of buoyancy-driven flows over a sloping bottom, as described by a two layer Shallow Water model derived in Swaters (1993). The model filters out barotropic instabilities and, in contrast with traditional two-layer Quasigeostrophic models, allows for $O(1)$ variations in the upper layer thickness. It also couples the two layers, unlike models based on the reduced-gravity ansatz. The resulting system of partial differential equations allows us to study the dominant physical processes and, though highly nonlinear, is still amenable to analytical investigation.

First, we derive the Shallow Water equations and the model itself. Then, conditions for linear stability/instability are demonstrated and, in particular, the role of bottom topography is elucidated. Next, we derive an amplitude equation to examine the growth of perturbations in a marginally unstable, highly idealized flow. It is found that such perturbations oscillate in time due to the interaction of linear and nonlinear terms, but under certain conditions, may also exhibit explosive growth. The latter situation corresponds to rapid evolution of the mean flow. A modified, space-dependent

amplitude equation is also derived, which allows soliton solutions.

Various numerical experiments were performed by integrating the model equations forward in time using a finite difference scheme. The results of linear theory were easily verified, however the search for weakly-nonlinear oscillations proved problematic due to a peculiar numerical instability. Some evidence of weakly-nonlinear interaction was found. Encouragingly, experiments involving very realistic isolated and coupled front profiles yielded meandering, warm-core and cold-core vortex shedding, as well as vortex merging/splitting.

Acknowledgements

Most importantly, I would like to extend my sincere thanks to my supervisor, Dr. Gordon E. Swaters. Both his guidance and his enthusiasm were invaluable to the completion of this work, as well as to my academic growth. I should also thank my colleagues, Richard Karsten and Francis Poulin, with whom I have had many discussions concerning various aspects of Geophysical Fluid Dynamics. Finally, I wish to thank my parents, for their constant support.

Funding for this research was provided by the Natural Sciences and Engineering Research Council under a PGS A grant, by the Department of Mathematical Sciences at the University of Alberta, as well as by my supervisor.

Contents

1	Introduction	1
2	Derivation of the Governing Equations	5
2.1	Introduction	5
2.2	The Two Layer Shallow Water Equations	6
2.3	Scalings for the Variables	13
2.4	Governing Equations	16
2.5	Derivation from Potential Vorticity	22
3	The Linear Stability Problem	26
3.1	Linear Stability Equations	26
3.2	Perturbation Energetics	28
3.3	Normal Mode Analysis	32
4	Weakly Nonlinear Analysis	42
4.1	Introduction	41
4.2	The Nonlinear Problem	43
4.2.1	Non-linear Perturbation Equations	43
4.2.2	Scaling for Slow Time	45
4.2.3	$O(1)$ Problem	48
4.2.4	$O(s)$ Problem	49
4.2.5	$O(s^2)$ Problem	58
4.3	Solutions to the Amplitude Equation	70
4.3.1	Region I	71
4.3.2	Region II	79

4.3.3 Region III	85
4.3.4 Region IV	89
5 Dependence on Spatial Scales	95
5.1 $O(1)$ Problem	97
5.2 $O(s)$ Problem	97
5.3 $O(s^2)$ Problem	100
5.4 Steadily Travelling Solitons	103
6 Numerical Analysis	109
6.1 Introduction	109
6.2 The Algorithm	110
6.3 Linear Theory Results	115
6.4 Weakly Non-linear Results	123
6.5 Jet Simulations	129
6.5.1 Warm-Core Eddy Simulation	131
6.5.2 Cold-Core Eddy Simulation	136
6.5.3 Effect of Bottom Slope	139
6.6 Coupled Front Simulations	141
6.7 A word about comparisons	148
7 Conclusions	149
Bibliography	151
Appendix A: Some Limits	156
A.1 Point a	156
A.2 Point b	157
A.3 Region I	157
A.4 Region II	160

A.5 Region III	164
Appendix B: Expressions for σ	166
B.1 Upper Branch, $l^2-2>0$	166
B.2 Upper Branch, $l^2-2<0$	167
B.3 Lower Branch	168
Appendix C: Numerical Solver	170

List of Figures

2.1 - Model Geometry	10
3.1 - Marginal Stability Curves (MSC)	38
3.2 - Marginal Stability Curves, alternate plot	39
3.3 - Phase speed, Upper Branch of MSC	40
3.4 - Phase speed, Lower Branch of MSC	41
4.1 - MSC and supercriticality curves	47
4.2 - σ and N for Lower Branch	65
4.3 - σ and N for Upper Branch	66
4.4 - σ and N for Lower Branch, α not negligible	67
4.5 - σ and N for Upper Branch, α not negligible	68
4.6 - Zoom-in of Figure 4.5	69
4.7 - Snoidal Wave solution in Region I	77
4.8 - Time for Blow-up of solution, Region I	78
4.9 - Cnoidal Wave solution in Region II	84
4.10 - Dnoidal Wave solution in Region III	88
4.11 - Time for Blow-up of solution in Region IV	93
4.12 - Solution in wavenumber space	94
5.1 - Soliton solution time series	107
6.1 - Typical perturbation contour plot	118
6.2 - Wedge front + perturbation contour plot	118
6.3 - Time series for wedge profile at Point 1	119
6.4 - Time series for wedge profile at Point 2	121

6.5 - Lower layer KE versus time for wedge simulation	125
6.6 - Time series of weakly unstable isolated front	126
6.7 - Lower layer KE versus time for weakly unstable front	128
6.8 - Isolated front profile (a jet)	130
6.9 - Time series of isolated front	133
6.10 a, b - h and p at t=206 for isolated front	135
6.11 - Time series of isolated front (cold pool forming)	137
6.12 - Time of first eddy pinch-off versus bottom slope	140
6.13 - Coupled front profile (a shear flow)	144
6.14 - Time series of coupled front simulation	145
6.15 a, b - Eddy merging and splitting	147

Chapter 1

Introduction

Buoyancy-driven surface currents play a major role in ocean circulation. These “rivers” in the ocean can exist wherever a thin layer of fluid overlies a thicker layer with greater density. The density difference may be a manifestation of differences in temperature or salinity, or both, and while the density gradient is never discontinuous, it is often quite sharp. When isopycnals (surfaces of constant density) intersect the surface, the interfacial region is called a front. If the spatial extent is large enough, and the time scale on which motion takes place is long enough, effects due to the rotation of the earth become important. In fact, when these effects are roughly equal to buoyancy stresses, the flow is in geostrophic balance and it is this relationship which, to a first approximation, determines the motion and drives the current.

Many of the world’s currents are close to geostrophic balance (Robinson, 1983). Examples include the Brazil (South Atlantic) Current, the Kuroshio (North Pacific) Current, the Agulhas (Indian Ocean) Current, as well as the archetypal Gulf Stream off the eastern coast of North America. All of these are western boundary currents whose courses run, at least in part, through the shallow water atop a continental shelf. A buoyancy current may also form at the freshwater overflow

from a river (e.g. Mertz *et al.*, 1989 and 1990) or where cold, fresh water from the Arctic meets the ambient ocean to the south (Griffiths & Linden, 1981).

A great deal of attention has, in recent years, been focused on departures from geostrophy and the apparent instability of such flows to perturbations (e.g. Griffiths & Linden, 1982, Olson & Evans, 1986, Ghil & Paldor, 1994). It is these effects which give rise to interesting and significant features, most noticeably in but not limited to, the Gulf Stream. For example, as it leaves the continental shelf off Cape Hatteras, N.C., this intense jet begins to meander and shed large, stable vortices (Bush *et al.*, 1995). The Gulf Stream lies at the boundary between the warm waters of the Sargasso Sea and the colder, denser water of the ambient ocean. A warm vortex, composed of Sargasso water, will propagate north into the slope water region, while a cold vortex will move into the Sargasso (Verzicco *et al.*, 1997). In this way, eddies are able to transport the physical, biological and chemical components of the water across the Stream (Chassignet & Cushman-Roisin, 1991). Indeed, eddies are ubiquitous along the whole length of the Gulf Stream, as well as other surface currents.

Many models, mathematical and numerical, have been proposed in order to understand the basic instability mechanism and the subsequent evolution of the flow. A considerable amount of progress has been made using layer models, which assume that an interface between two layers is in fact marked by a density discontinuity. Some results have been obtained using Quasigeostrophic theory which, in a two-layer context, requires that interfacial variations be small in relation to the overall depth of the upper layer (see, for example, Flierl, 1984). The stipulation that isopycnal deflections are small, however, explicitly prevents the possibility of a true front (which outcrops on the surface, as described previously).

The frontal model introduced by Griffiths *et al.* (1982), (hereafter referred to as "GKS") and the one introduced by Cushman-Roisin (1986) both relied on

the approximation of an infinitely deep lower layer whose motion does not feed back into the upper layer. These so-called “reduced gravity” models, however, effectively decoupled the dynamics of the two layers, an approximation which may not be valid, especially if the length scale is somewhat larger than the Rossby deformation radius (Chassignet & Cushman-Roisin, 1991). GKS also reported the existence of an instability unaccounted for by their theory, and possibly resulting from the influence of the lower layer.

Swaters (1993) has proposed a two-layer model based on an intermediate length scaling which does allow isopycnal outcroppings and couples the two layers. It focuses on *baroclinic* instability, known to play a major role in the evolution of buoyancy fronts (Robinson, 1983; Griffiths & Linden, 1981). *Baroclinic* instability is the release of potential energy stored in density gradients within the fluid, which inevitably leads to horizontal motion, through a process called vortex tube stretching (Cushman-Roisin, 1994). This is fundamentally different from *barotropic* instability, which relies on the release of kinetic energy only, as is usually observed in flows with horizontal shear. While the lower layer in this model is quasigeostrophic, the upper layer is not. The velocities in the lower layer are small compared to the upper layer. Interaction takes place via vortex tube stretching, and the model also includes the effect of bottom topography.

The governing equations are derived in an asymptotic expansion of the appropriately scaled shallow water equations. High frequency waves and barotropic instability are filtered out through an appropriate choice of velocity scalings and the rigid-lid approximation, both to be discussed later. It should be pointed out that a similar model, with no bottom topography, was derived by Cushman-Roisin (1992) in the context of a midlatitude β -plane. The Swaters (1993) paper discusses the relevant linear stability problem and presents a comprehensive analysis of stability characteristics within the framework of a Hamiltonian formulation. Karsten

& Swaters (1996) have extended the Hamiltonian analysis.

The goal of this thesis is two-fold. We develop a finite amplitude theory for a wedge-shaped front, building on the earlier linear work, and we motivate further analysis using a series of numerical experiments. The results of computational integration of the governing equations have been very encouraging. Meandering, formation of warm and cold core eddies, mean flow - eddy interaction, eddy merging and splitting have all been observed. In fact, it is suggested that the reader can start with Section 6.5 for inspiration, before tackling the main body of the thesis. The finite amplitude analysis examines the development of a perturbation on a marginally unstable flow, taking into account weakly-nonlinear interactions. It is found that the equation which governs the behavior of the perturbation admits oscillatory solutions, as well as solutions which become unbounded in finite time. A more general equation is also derived (by including spatial dependence) which is known to allow soliton solutions.

The advantage of the Swaters model seems to be a concise formulation which nevertheless captures the essential physical processes involved in the evolution of buoyancy fronts over sloping topography. Results of linear and weakly nonlinear theories as well as numerical simulations up to this point are very much in keeping with real-world observations, laboratory experiments and primitive equation numerical models. Research contained in this thesis marks the end of the first stage of model analysis. The ideas presented here can be extended and investigated in more detail.

Chapter 2

Derivation of the Governing Equations

2.1 Introduction

The essential equations governing fluid flow are the Navier-Stokes (conservation of momentum) equations and the Continuity (conservation of mass) equation. However this system contains more unknowns than equations, and in order to close it, additional relations or assumptions must be introduced. In this form, the primitive set of equations has no known general solution and is all but impossible to analyze theoretically in any direct manner. Luckily, by carefully considering the relative magnitudes of all the terms, and focusing on one or two aspects of the particular physical problem at hand, we can arrive at a reduced system which does lend itself to analytical treatment. In this chapter we will derive our model with the aid of scaling arguments and asymptotic expansions. Large-scale motion in the oceans is, for the most part, horizontal and the fluid is stably stratified. This will lead us to the Shallow Water equations, often the first step in model derivation.

Scalings, appropriate for buoyancy-driven fronts, will ensure that geostrophic balance is maintained to leading order, and that high frequency (superinertial) waves are filtered out. Next, we will expand all variables in powers of a small parameter and systematically match terms of similar magnitude, generating a series of problems. Finally, we must consider a sufficient number of these problems to obtain equations which involve only the leading order terms in the asymptotic expansions. This will determine the leading order behavior of the unknown quantities. For a more detailed discussion of asymptotic methods we refer the reader to the book by Zauderer (1989). In the last section of the chapter we present an alternate derivation of the model using the concept of Potential Vorticity (PV).

2.2 The Two-Layer Shallow Water Equations

Our starting point will be the inviscid form of the Navier-Stokes (i.e. momentum) equations for a rotating, incompressible fluid of constant density. Unlike gases, water is not compressible to any significant degree, and viscosity may be neglected on large scales, except perhaps at boundaries. If we consider fronts which are located far enough away from any boundary, then this last assumption is also justified. The equations for conservation of momentum and mass, respectively, can be written

$$\mathbf{u}_t + (\mathbf{u} \cdot \nabla) \mathbf{u} + f(\mathbf{k} \times \mathbf{u}) = -\frac{1}{\rho} \nabla p - \mathbf{k}g. \quad (2.1)$$

$$\nabla \cdot \mathbf{u} = 0. \quad (2.2)$$

where $\mathbf{u}(x, y, z, t) = (u, v, w)$ is the fluid velocity with u , v , and w the along-channel, cross-channel and vertical velocities respectively, ρ is the fluid density, $p(x, y, z, t)$ is the total pressure, $\nabla = (\partial_x, \partial_y, \partial_z)$ is the usual gradient operator, and \mathbf{k} is the unit vector normal to the earth's surface. The rotation of the earth is

taken into account by the Coriolis parameter f . We will assume that the spatial extent of the phenomena to be studied is small enough that f will not vary greatly from its value at some reference latitude, θ_o . For the oceans, it is usually adequate that the horizontal scale is less than about 100 km (Pond & Pickard, 1983). This is certainly true for the mesoscale phenomena we wish to study, we thus take f to be the constant $f_o = 2\Omega \sin(\theta_o)$, where $\Omega = 2\pi$ rad / day. This is known as the f -plane approximation.

Now, the typical depth of the ocean is 5 km. Moreover, on continental shelves, where we are likely to find surface currents, the oceanic depth is even less. The Shallow Water equations are obtained by arguing that the vertical scale of motion is much smaller than the horizontal. We express this statement as

$$D = \frac{H}{L} \ll 1. \quad (2.3)$$

where L is the typical horizontal scale, H is the vertical scale, and D is the *aspect ratio*.

We can rewrite the continuity equation (2.2) with appropriate scales underneath the terms, where U and W represent the typical horizontal and vertical velocity scales, respectively:

$$u_x + v_y + w_z = 0. \quad (2.4)$$

$$\frac{U}{L} \quad \frac{U}{L} \quad \frac{W}{H}$$

It is certainly possible that $W/H \ll U/L$ or $W/H \sim U/L$ to achieve a balance between these terms. However, it is not possible that $W/H \gg U/L$ since the sum of the first two terms is still $O(U/L)$ and there is nothing to balance with the third term. Effectively, U/L is an upper bound for the scale of w_z . Rearranging,

we may write

$$W \leq O(UH/L). \quad (2.5)$$

Let us now examine the momentum equations (2.1) in component form, where again, the appropriate scales are written underneath:

$$u_t + uu_x + vu_y + wu_z - f_o v = -\frac{1}{\rho} p_x. \quad (2.6)$$

$$\begin{array}{ccccccc} \frac{U}{T} & \frac{UU}{L} & \frac{UU}{L} & \frac{UW}{H} & fU & & \\ v_t + uv_x + vv_y + wv_z + f_o u = -\frac{1}{\rho} p_y. & & & & & & \end{array} \quad (2.7)$$

$$\begin{array}{ccccccc} \frac{U}{T} & \frac{UU}{L} & \frac{UU}{L} & \frac{UW}{H} & fU & & \\ w_t + uw_x + vw_y + ww_z = -\frac{1}{\rho} p_z - g. & & & & & & \end{array} \quad (2.8)$$

$$\frac{W}{T} \quad \frac{UW}{L} \quad \frac{UW}{L} \quad \frac{WW}{H}$$

If we take T to be simply the ratio of the typical length scale L over the horizontal velocity U (i.e. an *advective time scale*), then all the terms on the left hand side of (2.8) are of the same magnitude, which then implies

$$-\frac{1}{\rho} p_z - g = O\left(\frac{HU^2}{L^2}\right). \quad (2.9)$$

The right-hand side of (2.9) is a very small quantity for the mid ocean. Even considering the rather large values $H \simeq 5$ km, $U \simeq 0.5$ m/s and the modest length scale $L \simeq 50$ km, we conclude that the right hand side is $O(10^{-6})$. Therefore, the fluid is hydrostatic to a very good approximation, i.e.

$$p_z = -\rho g. \quad (2.10)$$

One may now argue that, since p is simply a linear function of z , its gradients in (2.6) and (2.7) will be independent of z . It is reasonable to expect that, if u and v are initially independent of z , they will remain this way indefinitely. We will assume this is the case in our investigation. Furthermore, the vertical velocity w is small. For example, typical scales for the Gulf Stream are $U = 1 \text{ m/s}$, $L = 10^5 \text{ m}$, $H = 10^3 \text{ m}$ (Pond & Pickard, 1983), which sets the upper bound for w at about 10^{-7} m/s . These arguments all suggest that the fluid motion is essentially two-dimensional, which is the main tenet of Shallow Water theory.

Because surface undulations of the fluid will be small compared to the vertical extent of the atmosphere, we can take the pressure at the surface to be essentially constant. In fact we can scale the pressure so that this constant is zero. In our model the upper layer thickness and the deformation of the fluid surface will be denoted by h and η , respectively. The assumption of constant density within each layer allows for a simple relationship between pressure and depth. Exploiting the hydrostatic condition (2.10), the pressure on a fluid parcel at vertical position z will be equal to the weight of water directly above it. Using Figure 2.1 we obtain the following expressions for the pressure in the upper and lower layer respectively

$$\begin{aligned} p_1 &= \rho_1 g(H + \eta - z) \\ &= \rho_1 g(H - z) + \rho_1 g\eta, \end{aligned} \tag{2.11}$$

$$\begin{aligned} p_2 &= \rho_1 g(h + \eta) + \rho_2 g(H - h - z) \\ &= \rho_2 g(H - z) + \bar{p}_2, \end{aligned} \tag{2.12}$$

where $\rho_1 g\eta$ and $\bar{p}_2 = \rho_1 g\eta - g(\rho_2 - \rho_1)h$ represent the dynamic pressures.

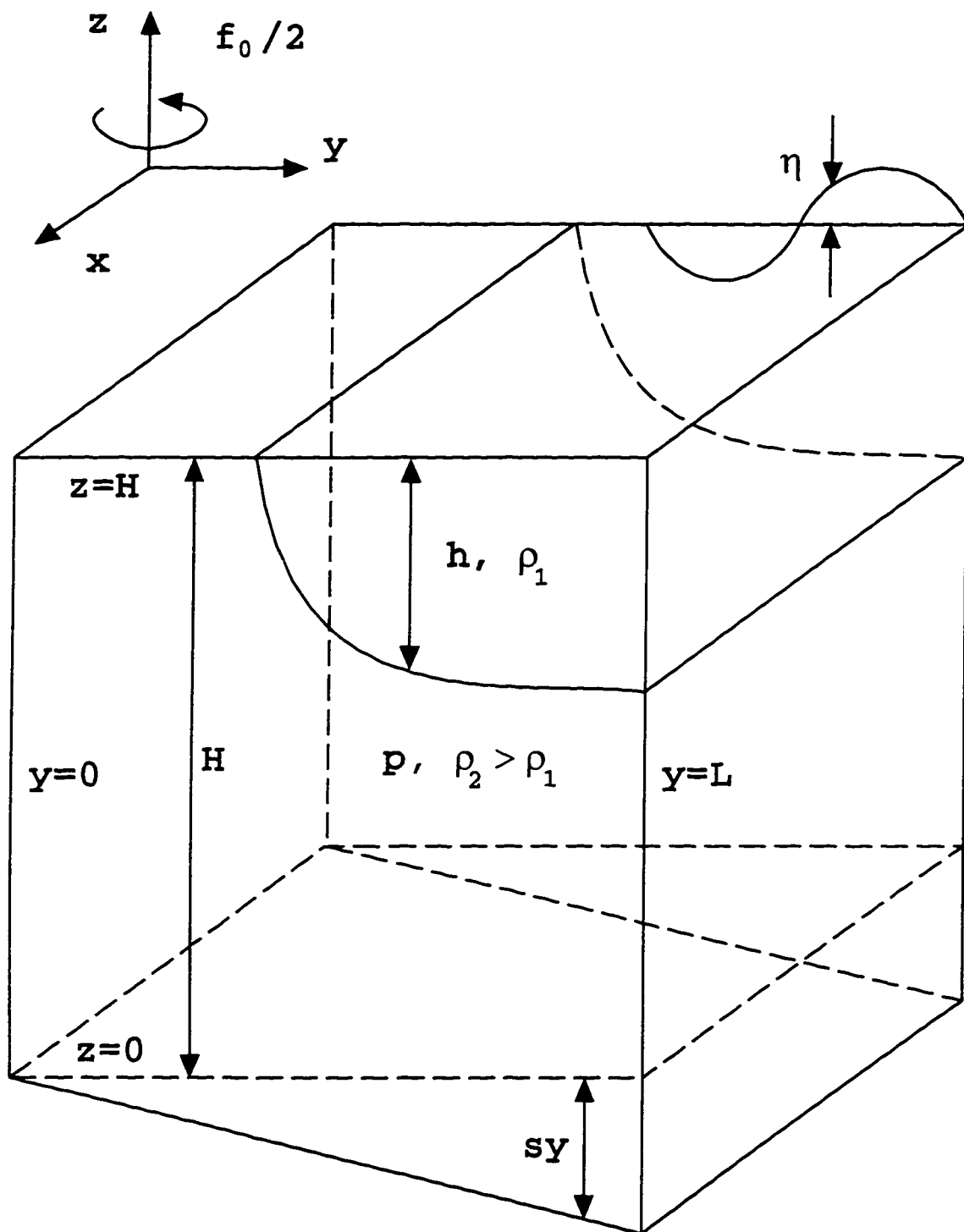


Figure 2.1: Model Geometry

We now transform the mass conservation condition (2.4) into a statement of mass conservation appropriate for shallow water. This is accomplished by requiring that a fluid parcel on the surface remains there for all time, and similarly for a parcel at the interface between the two layers. Here we will use the operator $D/Dt = \partial_t + \mathbf{u} \cdot \nabla$, known as the *total* derivative (or *material* derivative), where \mathbf{u} refers to the velocity in the layer under consideration. This derivative is a rate of change, following the fluid motion. Throughout the thesis the coordinates x and y will refer to the along-channel and cross-channel coordinates respectively, while z will measure vertical distance. We consider y to increase in the off-shore direction, and z to increase upward. Also, from this point on, ∇ will represent the two-dimensional gradient operator (∂_x, ∂_y) . The above kinematic conditions for layer one are stated as follows

$$w_1 = \frac{D}{Dt}(H + \eta) \quad \text{on} \quad z = H + \eta. \quad (2.13)$$

$$w_1 = \frac{D}{Dt}(H - h) \quad \text{on} \quad z = H - h. \quad (2.14)$$

However because we wish to examine situations where $\eta \ll H$, we will approximate $H + \eta$ as H , imposing the *rigid lid approximation*. This effectively filters out all surface gravity waves, which are superinertial (and barotropic) in nature. Then (2.13) reduces to

$$w_1 = 0 \quad \text{on} \quad z = H. \quad (2.15)$$

We then integrate the continuity equation (2.4) in z (recall that $u_z = v_z = 0$) over the thickness of the upper layer, to obtain,

$$(u_{1x} + v_{1y})[H - (H - h)] + w_1(x, y, H, t) - w_1(x, y, H - h, t) = 0. \quad (2.16)$$

Exploiting (2.14) and (2.15).

$$(\nabla \cdot \mathbf{u}_1)h + h_t + \mathbf{u}_1 \cdot \nabla h = 0. \quad (2.17)$$

Simplifying,

$$h_t + \nabla \cdot (\mathbf{u}_1 h) = 0. \quad (2.18)$$

The kinematic condition for layer two on the interface is analogous to above. Meanwhile on the bottom, we require that the component of the flow perpendicular to the bottom is zero. For the purposes of this research, we will assume a linearly sloping bottom with slope s , as depicted in Figure 2.1. It should be emphasized however, that the model derivation can account for general bottom topography if that is desired. Defining \mathbf{n} to be the vector $(0, s, 1)$, normal to the bottom surface, we state these conditions as follows

$$\mathbf{n} \cdot \mathbf{u}_2 = 0 \quad \text{on} \quad z = -sy. \quad (2.19)$$

$$w_2 = \frac{D}{Dt}(H - h) \quad \text{on} \quad z = H - h. \quad (2.20)$$

Once again, integrating (2.4), this time over the thickness of the lower layer,

$$(u_{2x} + v_{2y})[H - h - (-sy)] + w_2(x, y, H - h, t) - w_2(x, y, -sy, t) = 0. \quad (2.21)$$

Substituting in (2.19) and (2.20),

$$(\nabla \cdot \mathbf{u}_2)(H - h + sy) - h_t - \mathbf{u}_2 \cdot \nabla h + sv_2 = 0. \quad (2.22)$$

Simplifying,

$$h_t + \nabla \cdot [\mathbf{u}_2(h - sy - H)] = 0. \quad (2.23)$$

Let us now write down all the equations we have derived. We will use asterisks here to emphasize that we are dealing with *dimensional* variables.

$$\mathbf{u}_{1t}^* + (\mathbf{u}_1^* \cdot \nabla^*) \mathbf{u}_1^* + f_o(\mathbf{k} \times \mathbf{u}_1^*) = -g \nabla^* \eta^*. \quad (2.24)$$

$$h_t^* + \nabla^* \cdot (\mathbf{u}_1^* h^*) = 0. \quad (2.25)$$

$$\mathbf{u}_{2t}^* + (\mathbf{u}_2^* \cdot \nabla^*) \mathbf{u}_2^* + f_o(\mathbf{k} \times \mathbf{u}_2^*) = -\frac{1}{\rho_2} \nabla^* \tilde{p}_2^*. \quad (2.26)$$

$$h_t^* + \nabla^* \cdot [\mathbf{u}_2^* (h^* - s^* y^* - H)] = 0. \quad (2.27)$$

where

$$\tilde{p}_2^* = \rho_1 g \eta^* - \rho_2 g' h^*. \quad (2.28)$$

and $g' = g(\rho_2 - \rho_1)/\rho_2$ is called the *reduced gravity*. We now have a closed system of seven equations (two of the above equations are in vector form) in seven unknowns $u_1^*, v_1^*, h^*, u_2^*, v_2^*, \tilde{p}_2^*$ and η^* .

2.3 Scalings for the variables

Our dimensional variables should now be scaled appropriately (see Swaters, 1993), so that all nondimensional variables are $O(1)$. While this step is not conceptually essential, it does make the derivation more straightforward. We first introduce a parameter δ , which will be of prime importance,

$$\delta = \frac{\bar{h}}{H}, \quad (2.29)$$

where the constant \bar{h} is a representative thickness of the upper layer and H is a scale for the total fluid depth.

Horizontal spatial coordinates will be scaled by

$$(x^*, y^*) = L(x, y). \quad (2.30)$$

where $L = \delta^{-\frac{1}{4}} R$, and $R = \sqrt{g' \bar{h}} / f_o$ is the *internal Rossby radius of deformation* for the upper layer. Typically, we expect $\delta^{-\frac{1}{4}}$ to be somewhat larger than unity, which implies that we are considering spatial scales slightly larger than the internal Rossby radius. This is not physically unreasonable, as was observed in lab experiments by Griffiths & Linden (1982). More importantly, this scaling ensures leading order geostrophy (i.e. a balance between Coriolis terms and the pressure gradient) in the final equations.

The scaling for time will be subinertial, i.e.

$$t^* = \frac{t}{f_o \delta}. \quad (2.31)$$

This means we are only concerned with processes which occur on longer time scales than the earth's rotation. Moreover, these time scales will become longer still, as the ratio δ decreases and the lower layer becomes less important. We scale the thickness of the upper layer according to

$$h^* = \bar{h} h, \quad (2.32)$$

where \bar{h} is simply δH .

To obtain a scaling for \mathbf{u}_2 we argue as follows. In this model the dynamics of the lower layer are driven through *vortex tube stretching* (and necessarily, *contraction*). Qualitatively, the strength of this process is measured by the parameter δ times the ambient vorticity f_o . We require that the relative vorticity of layer two, $v_x^* - u_y^*$, is roughly in balance with *vortex tube stretching*. Mathematically, the

scale of relative vorticity U/L must equal δf_o . Solving for the velocity scale U , we conclude that

$$\mathbf{u}_2^* = \delta f_o L \mathbf{u}_2. \quad (2.33)$$

The scaling for \mathbf{u}_1 is chosen in order that the model includes the advection of upper layer vorticity while filtering out higher frequency gravity waves,

$$\mathbf{u}_1^* = \delta^{\frac{1}{2}} f_o L \mathbf{u}_1. \quad (2.34)$$

Because we require that the flow be geostrophic to leading order, the scalings for η and p are necessarily

$$\eta^* = \delta^{\frac{1}{2}} \frac{(f_o L)^2}{g} \eta. \quad (2.35)$$

$$\bar{p}_2^* = \rho_2 \delta (f_o L)^2 p.$$

We also introduce a scaled slope parameter through

$$s^* = \frac{\bar{h}}{L} s. \quad (2.36)$$

The effect of this scaling may be easily verified *a posteriori*. by examining the final equation for the lower layer in its PV form (2.83). We shall see that the bottom slope term, sy , will be the same order of magnitude as the relative vorticity. This is indeed the situation we wish to study.

2.4 Governing Equations

Substituting the above scalings into the equations (2.24) through (2.28) we obtain

$$\delta \mathbf{u}_{1t} + \delta^{\frac{1}{2}}(\mathbf{u}_1 \cdot \nabla) \mathbf{u}_1 + \mathbf{k} \times \mathbf{u}_1 + \nabla \eta = 0. \quad (2.37)$$

$$\delta^{\frac{1}{2}} h_t + \nabla \cdot (\mathbf{u}_1 h) = 0. \quad (2.38)$$

$$\delta \mathbf{u}_{2t} + \delta(\mathbf{u}_2 \cdot \nabla) \mathbf{u}_2 + \mathbf{k} \times \mathbf{u}_2 + \nabla p_2 = 0. \quad (2.39)$$

$$\nabla \cdot \mathbf{u}_2 = \delta h_t + \delta \nabla \cdot [\mathbf{u}_2(h - sy)]. \quad (2.40)$$

$$\eta = h + \delta^{\frac{1}{2}} p. \quad (2.41)$$

where we neglected terms of $O(g'/g)$ in (2.41) since we assume that $(\rho_2 - \rho_1)$ is small in comparison to ρ_2 . This is the second part of our *rigid lid approximation*.

We now assume an asymptotic expansion of the form

$$(\mathbf{u}_1, \mathbf{u}_2, h, p, \eta) = (\mathbf{u}_1, \mathbf{u}_2, h, p, \eta)^{(0)} + \delta^{\frac{1}{2}}(\mathbf{u}_1, \mathbf{u}_2, h, p, \eta)^{(1)} + O(\delta). \quad (2.42)$$

and substitute into (2.37) through (2.41). We shall first discuss the lower layer equations since the details are more straightforward.

If the variables in (2.39) are expanded, then to leading order.

$$\mathbf{k} \times \mathbf{u}_2^{(0)} + \nabla p^{(0)} = 0, \quad (2.43)$$

or, taking $-\mathbf{k} \times$ (2.43),

$$\mathbf{u}_2^{(0)} = \mathbf{k} \times \nabla p^{(0)} = (-p_y^{(0)}, p_x^{(0)}). \quad (2.44)$$

Thus the leading order velocity in layer two is geostrophic, i.e. strictly determined

by a balance of the Coriolis terms and the pressure gradient, as we required.

To obtain an equation for the time evolution of p , we first write down (2.39) in component form.

$$\delta(u_{2t} + u_2 u_{2x} + v_2 u_{2y}) - v_2 + p_x = 0. \quad (2.45)$$

$$\delta(v_{2t} + u_2 v_{2x} + v_2 v_{2y}) + u_2 + p_y = 0. \quad (2.46)$$

Taking the curl (that is, $-\frac{\partial}{\partial y}$ (2.45) + $\frac{\partial}{\partial x}$ (2.46)) we obtain,

$$\begin{aligned} & \delta(v_{2x} - u_{2y})_t + \delta(u_{2x} v_{2x} + u_2 v_{2xx} - u_{2y} u_{2x} - u_2 u_{2xy} \\ & + v_{2x} v_{2y} + v_2 v_{2xy} - v_{2y} u_{2y} - v_2 u_{2yy}) + u_{2x} + v_{2y} = 0. \end{aligned} \quad (2.47)$$

or simply,

$$\delta \xi_t + \delta(u_2 \xi_x + v_2 \xi_y + u_{2x} \xi + v_{2y} \xi) + u_{2x} + v_{2y} = 0. \quad (2.48)$$

where we have defined $v_{2x} - u_{2y} = \xi$, the relative vorticity for the lower layer. We can rewrite the equation more compactly using the total derivative.

$$\delta \frac{D\xi}{Dt} + (1 + \delta \xi) \nabla \cdot \mathbf{u}_2 = 0. \quad (2.49)$$

Solving for the divergence of \mathbf{u}_2 in the mass conservation equation (2.40),

$$\nabla \cdot \mathbf{u}_2 = \delta h_t + \delta \nabla \cdot [\mathbf{u}_2(h - sy)], \quad (2.50)$$

and substituting this into (2.49), gives

$$\delta \frac{D\xi}{Dt} + (1 + \delta \xi) (\delta h_t + \delta \nabla \cdot [\mathbf{u}_2(h - sy)]) = 0. \quad (2.51)$$

Now expanding the variables as in (2.42). and dividing through by δ .

$$\frac{D\xi^{(0)}}{Dt} + (1 + \delta\xi^{(0)}) \left(h_t^{(0)} + \nabla \cdot \mathbf{u}_2^{(0)} h^{(0)} + \mathbf{u}_2^{(0)} \cdot \nabla (h^{(0)} - sy) \right) = 0. \quad (2.52)$$

where $\xi^{(0)} = v_{2x}^{(0)} - u_{2y}^{(0)}$, and since $(u_2^{(0)}, v_2^{(0)}) = (-p_y^{(0)}, p_x^{(0)})$.

$$\xi^{(0)} = \Delta p^{(0)}. \quad (2.53)$$

Here we have introduced the *Laplace operator*, $\Delta = \partial_{xx} + \partial_{yy}$. We have also written down just the first term of each expansion because the higher order terms will not be needed. as we will see shortly.

The leading order (that is $O(1)$) problem is given by

$$\frac{D}{Dt} \Delta p^{(0)} + h_t^{(0)} + \nabla \cdot \mathbf{u}_2^{(0)} h^{(0)} + \mathbf{u}_2^{(0)} \cdot \nabla (h^{(0)} - sy) = 0. \quad (2.54)$$

where $D/Dt = \partial_t + \mathbf{u}^{(0)} \cdot \nabla$. Now, the term $h_t^{(0)}$ may be written $(h^{(0)} - sy)_t$ since sy is independent of time. Also, the third term, $\nabla \cdot \mathbf{u}_2^{(0)} h^{(0)}$ vanishes, since $\nabla \cdot \mathbf{u}_2^{(0)} = -p_{yx}^{(0)} + p_{xy}^{(0)} = 0$. Therefore the above equation reduces to

$$\frac{D}{Dt} \Delta p^{(0)} + (h^{(0)} - sy)_t + \mathbf{u}_2^{(0)} \cdot \nabla (h^{(0)} - sy) = 0. \quad (2.55)$$

or simply

$$\frac{D}{Dt} (\Delta p^{(0)} + h^{(0)} - sy) = 0. \quad (2.56)$$

This is a statement of the conservation of leading order *Potential Vorticity*, a concept which will be discussed in the next section. Finally, let us rewrite the equation using the *Jacobian operator* defined by

$$J(A, B) = A_x B_y - A_y B_x. \quad (2.57)$$

Recalling the definition of the material derivative, and that $(u^{(0)}, v^{(0)}) = (-p_y^{(0)}, p_x^{(0)})$, our governing equation for layer 2 becomes

$$(\Delta p^{(0)} + h^{(0)})_t + J(p^{(0)}, \Delta p^{(0)} + h^{(0)} - sy) = 0. \quad (2.58)$$

Now we work with the upper layer. Expanding the variables in the momentum equation (2.37), we see immediately that the leading order velocity is geostrophic,

$$\mathbf{u}_1^{(0)} = \mathbf{k} \times \nabla h^{(0)}. \quad (2.59)$$

To determine the time evolution of h , we employ the same method as with the lower layer, by writing down the components of the momentum equation (2.37),

$$\delta u_{1t} + \delta^{\frac{1}{2}}(u_1 u_{1x} + v_1 u_{1y}) - v_1 + \eta_x = 0. \quad (2.60)$$

$$\delta v_{1t} + \delta^{\frac{1}{2}}(u_1 v_{1x} + v_1 v_{1y}) + u_1 + \eta_y = 0. \quad (2.61)$$

Taking the curl,

$$\delta(v_{1x} - u_{1y})_t + \delta^{\frac{1}{2}}(u_{1x} v_{1x} + u_1 v_{1xx} - u_{1y} u_{1x} - u_1 u_{1xy} \quad (2.62)$$

$$+ v_{1x} v_{1y} + v_1 v_{1xy} - v_{1y} u_{1y} - v_1 u_{1yy}) + u_{1x} + v_{1y} = 0.$$

or simply,

$$\delta \zeta_t + \delta^{\frac{1}{2}}(u_1 \zeta_x + v_1 \zeta_y + u_{1x} \zeta + v_{1y} \zeta) + u_{1x} + v_{1y} = 0, \quad (2.63)$$

where $\zeta = v_{1x} - u_{1y}$. More compactly,

$$\delta \zeta_t + \delta^{\frac{1}{2}} \mathbf{u}_1 \cdot \nabla \zeta + (1 + \delta^{\frac{1}{2}} \zeta) \nabla \cdot \mathbf{u}_1 = 0. \quad (2.64)$$

Now from the continuity equation (2.38), we find

$$\nabla \cdot \mathbf{u}_1 = -\delta^{\frac{1}{2}} \frac{h_t}{h} - \frac{1}{h} \mathbf{u}_1 \cdot \nabla h. \quad (2.65)$$

Substituting this into (2.64),

$$\delta \zeta_t + \delta^{\frac{1}{2}} \mathbf{u}_1 \cdot \nabla \zeta - (1 + \delta^{\frac{1}{2}} \zeta) \frac{1}{h} (\delta^{\frac{1}{2}} h_t + \mathbf{u}_1 \cdot \nabla h) = 0. \quad (2.66)$$

Expanding all variables as in (2.42), we arrive at the $O(1)$ problem:

$$\mathbf{u}_1^{(0)} \cdot \nabla h^{(0)} = 0. \quad (2.67)$$

However here we encounter a significant difference with the derivation of the lower layer governing equation. The leading order problem is in fact trivial. When (2.59) is substituted for $\mathbf{u}_1^{(0)}$, any sufficiently smooth $h^{(0)}$ will satisfy the relation. We still have the hydrostatic relation (2.41) and after expanding all variables in a series we obtain the following first order approximation:

$$\eta^{(0)} = h^{(0)}. \quad (2.68)$$

Unfortunately this still does not enable us to determine $h^{(0)}$. We therefore must consider the $O(\delta^{\frac{1}{2}})$ problem. But before we do, it is worth emphasizing at this point, that the leading order reduced pressure $\eta^{(0)}$ is decoupled from the lower layer pressure $p^{(0)}$. This is in marked contrast with a similar model, which describes bottom-dwelling density currents (Swaters & Flierl, 1991 and Swaters, 1991).

Continuing our analysis, we write down the next approximation ($O(\delta^{\frac{1}{2}})$ prob-

lem) for (2.37). (2.38) and (2.41).

$$\mathbf{k} \times \mathbf{u}_1^{(1)} + \nabla \eta^{(1)} = -(\mathbf{u}_1^{(0)} \cdot \nabla) \mathbf{u}_1^{(0)}. \quad (2.69)$$

$$h_t^{(0)} + \nabla \cdot [\mathbf{u}_1^{(0)} h^{(1)} + \mathbf{u}_1^{(1)} h^{(0)}] = 0. \quad (2.70)$$

$$\eta^{(1)} = h^{(1)} + p^{(0)}. \quad (2.71)$$

We obtain $\mathbf{u}_1^{(1)}$ and $h^{(1)}$ from (2.69) and (2.71) respectively.

$$\mathbf{u}_1^{(1)} = \mathbf{k} \times \nabla \eta^{(1)} + J(\nabla h^{(0)}, h^{(0)}). \quad (2.72)$$

$$h^{(1)} = \eta^{(1)} - p^{(0)}. \quad (2.73)$$

Next we expand (2.66). extract the $O(\delta^{\frac{1}{2}})$ problem. and substitute in (2.73).

$$-h_t^{(0)} + h^{(0)} \mathbf{u}_1^{(0)} \cdot \nabla \zeta^{(0)} - \zeta^{(0)} \mathbf{u}_1^{(0)} \cdot \nabla h^{(0)} \quad (2.74)$$

$$-\mathbf{u}_1^{(0)} \cdot \nabla (\eta^{(1)} - p^{(0)}) - \mathbf{u}_1^{(1)} \cdot \nabla h^{(0)} = 0.$$

Substituting (2.59) for $\mathbf{u}_1^{(0)}$, (2.72) for $\mathbf{u}_1^{(1)}$, and keeping in mind that $\zeta^{(0)} = \Delta h^{(0)}$,

$$h_t^{(0)} + h^{(0)} J(\Delta h^{(0)}, h^{(0)}) + \Delta h^{(0)} J(h^{(0)}, h^{(0)}) \quad (2.75)$$

$$+ (-h_y^{(0)} \cdot h_x^{(0)}) \cdot (\eta_x^{(1)}, \eta_y^{(1)}) + J(p^{(0)}, h^{(0)})$$

$$+ (-\eta_y^{(1)}, \eta_x^{(1)}) \cdot (h_x^{(0)}, h_y^{(0)}) + J(\nabla h^{(0)}, h^{(0)}) \cdot \nabla h^{(0)} = 0.$$

After simplification, we finally we arrive at the upper layer governing equation,

$$h_t^{(0)} + J\left(p^{(0)} + h^{(0)} \Delta h^{(0)} + \frac{1}{2} \nabla h^{(0)} \cdot \nabla h^{(0)}, h^{(0)}\right) = 0. \quad (2.76)$$

Like the lower layer equation, this too is a statement of *Potential Vorticity* conservation. However, it is not the leading order approximation, but rather the next order approximation.

2.5 Derivation from Potential Vorticity

One may derive the exact same equations (2.58) and (2.76) using the principle of *Potential Vorticity* conservation. For shallow water equations in the context of our problem, *Potential Vorticity* is defined as

$$PV = \frac{\text{relative} + \text{planetary vorticity}}{\text{thickness of layer}}, \quad (2.77)$$

and it is conserved following the flow, that is

$$\frac{D}{Dt} (PV) = 0. \quad (2.78)$$

For the lower layer, in *dimensional* variables,

$$\frac{D^*}{Dt} \left(\frac{v_{2x}^* - u_{2y}^* + f_o}{H - h^* + s^* y^*} \right) = 0. \quad (2.79)$$

where D^*/Dt denotes the *dimensional* total derivative. Employing the scalings introduced in Section 2.3,

$$(\delta f_o \partial_t + \delta f_o \mathbf{u}_2 \cdot \nabla) \left(\frac{\delta f_o (v_{2x} - u_{2y}) + f_o}{H - \delta H h + \delta H s y} \right) = 0. \quad (2.80)$$

Dividing by $\delta f_o/H$ and invoking the quotient rule for derivatives,

$$(1 - \delta h + \delta s y) \frac{D}{Dt} (\delta (v_{2x} - u_{2y}) + 1) \quad (2.81)$$

$$-(\delta(v_{2x} - u_{2y}) + 1) \frac{D}{Dt}(1 - \delta h + \delta sy) = 0.$$

Expanding the variables in a series, we obtain the $O(1)$ problem, given by

$$\frac{D}{Dt} (v_{2x}^{(0)} - u_{2y}^{(0)}) + \frac{D}{Dt} (h^{(0)} - sy) = 0. \quad (2.82)$$

which may be written

$$\frac{D}{Dt} (v_{2x}^{(0)} - u_{2y}^{(0)} + h^{(0)} - sy) = 0. \quad (2.83)$$

or simply.

$$(\Delta p^{(0)} + h^{(0)})_t + J(p^{(0)}, \Delta p^{(0)} + h^{(0)} - sy) = 0. \quad (2.84)$$

which is identical to (2.58).

Now we derive the upper layer governing equation, in a similar fashion. Again we start with conservation of *Potential Vorticity*,

$$\frac{D^*}{Dt} \left(\frac{v_{1x}^* - u_{1y}^* + f_o}{h^*} \right) = 0. \quad (2.85)$$

We apply the scalings (2.30) through (2.36).

$$(\delta f_o \partial_t + \delta^{\frac{1}{2}} f_o \mathbf{u}_1 \cdot \nabla) \left(\frac{\delta^{\frac{1}{2}} f_o (v_{1x} - u_{1y}) + f_o}{H - \delta H + \delta H sy} \right) = 0. \quad (2.86)$$

Then we divide through by $\delta^{\frac{1}{2}} f_o / H$ and invoke the quotient rule for derivatives,

$$\delta h (v_{1x} - u_{1y})_t + \delta^{\frac{1}{2}} h \mathbf{u}_1 \cdot \nabla (v_{1x} - u_{1y}) - [\delta^{\frac{1}{2}} (v_{1x} - u_{1y}) + 1] [\delta^{\frac{1}{2}} h_t + \mathbf{u}_1 \cdot \nabla h] = 0. \quad (2.87)$$

Expanding the variables in a series, we obtain the $O(1)$ problem. given by

$$\mathbf{u}_1^{(0)} \cdot \nabla h^{(0)} = 0. \quad (2.88)$$

Again, this is trivial and we must examine the next order problem.

$$h^{(0)} \mathbf{u}_1^{(0)} \cdot \nabla (\Delta h^{(0)}) - \Delta h^{(0)} \mathbf{u}_1^{(0)} \cdot \nabla h^{(0)} - h_t^{(0)} - \mathbf{u}_1^{(0)} \cdot \nabla h^{(1)} - \mathbf{u}_1^{(1)} \cdot \nabla h^{(0)} = 0. \quad (2.89)$$

Expanding and substituting in for $h^{(1)}$ and $\mathbf{u}_1^{(1)}$, we obtain

$$\begin{aligned} h_t^{(0)} + \Delta h^{(0)} (\mathbf{k} \times \nabla h^{(0)}) \cdot \nabla h^{(0)} - h^{(0)} (\mathbf{k} \times \nabla h^{(0)}) \cdot \nabla (\Delta h^{(0)}) \\ + (\mathbf{k} \times \nabla h^{(0)}) \cdot \nabla (\eta^{(1)} - p^{(0)}) + (\mathbf{k} \times \nabla \eta^{(1)}) \cdot \nabla h^{(0)} \\ + J(\nabla h^{(0)}, h^{(0)}) \cdot \nabla h^{(0)} = 0. \end{aligned} \quad (2.90)$$

which reduces to

$$h_t^{(0)} + J \left(p^{(0)} + h^{(0)} \Delta h^{(0)} + \frac{1}{2} \nabla h^{(0)} \cdot \nabla h^{(0)}, h^{(0)} \right) = 0. \quad (2.91)$$

This is the same equation as (2.76) which we derived in Section 2.4.

As the final step in this chapter, we write down both equations of motion.

$$h_t + J \left(p + h \Delta h + \frac{1}{2} \nabla h \cdot \nabla h, h \right) = 0. \quad (2.92)$$

$$(\Delta p + h)_t + J(p, \Delta p + h - sy) = 0, \quad (2.93)$$

for easy reference in the future. Here we have dropped the superscript notation for a cleaner appearance, but it must be stressed that we are still dealing with the leading order variables $h^{(0)}$ and $p^{(0)}$. For a discussion of general boundary

conditions appropriate for the model, we refer the reader to Swaters (1993). In this thesis we will utilize a simpler set of boundary conditions. better suited to the theory about to be presented. These will be discussed as necessary.

Chapter 3

The Linear Stability Problem

3.1 The Linear Stability Equations

There is much evidence to support the claim that large scale time-dependent motions in the world's oceans (or, for that matter, in the atmosphere) are simply waves, which start out as small perturbations to some unstable mean state. If circumstances allow such a perturbation to extract energy from the mean flow, then the wave amplifies. Eventually it may grow to a size which completely distorts the mean flow itself, and other processes come into play. If we are to understand this cycle of events, then a mean state appropriate for the physical system under study must be found, upon which a perturbation is to be superimposed.

It is usually very difficult to determine what the correct mean state is (Pedlosky, 1987), however we can find out a great deal about the instability of the flow by considering some intuitively reasonable steady state. Since a perturbation is assumed to be initially small, all terms in the governing equations which are quadratic in the perturbation may be considered infinitesimally small, and can be neglected. That is, the perturbation will, at least initially, be governed by linear dynamics. Fortunately, this greatly simplifies the first steps in the analysis.

We begin, therefore, by linearizing the governing equations about some known, steady solution and look for conditions which will make the flow stable or unstable with respect to small perturbations. For the purpose of this thesis, we will take our spatial domain to be a channel of width L , with periodic boundary conditions in the along-channel direction. To derive the linear stability equations, we introduce

$$h = h_o(y) + h'(x, y, t), \quad (3.1)$$

$$p = p_o(y) + p'(x, y, t), \quad (3.2)$$

where $h_o(y)$ and $p_o(y)$ are exact, time independent solutions to (2.92), (2.93), and h' and p' are small perturbation quantities.

Since any function of y will satisfy the nonlinear equations, and such a flow is not unreasonable physically, this is an obvious choice for the steady state. We substitute (3.1) and (3.2) into (2.92) and (2.93), and neglect all terms where primed terms are multiplied together. As previously mentioned, such terms are initially very small compared with all other terms in the equations and will not make any significant contribution for some time. Dropping the primes, we obtain

$$h_t + h_{oy}p_x + [U_o + h_{oy}h_o\Delta + (h_{oy})^2\partial_y - (h_o h_{oyy})_y]h_x = 0. \quad (3.3)$$

$$(\partial_t + U_o\partial_x)(\Delta p + h) + (h_{oy} - U_{oy} - s)p_x = 0. \quad (3.4)$$

in a channel $0 < y < L$, where $U_o = -p_{oy}$ is the lower layer mean flow.

We assume that the steady solution for the upper layer thickness takes the form of a simple wedge,

$$h_o(y) = 1 + \alpha(y - \frac{L}{2}). \quad (3.5)$$

Here α is the slope in the cross-channel direction of the interface between the two layers. For example, with α positive, the minimum and maximum thickness of the upper layer is given by $1 - \alpha \frac{L}{2} > 0$ and $1 + \alpha \frac{L}{2} > 0$, respectively. The dimensional slope is given by

$$\alpha^* = \frac{\bar{h}}{L} \alpha. \quad (3.6)$$

By setting the mean flow in the lower layer, $U_o \equiv 0$ we prevent shear instabilities, and are able to focus on the pure baroclinic problem (Swaters, 1993). We now obtain the linear stability equations for our model,

$$h_t + \alpha p_x + \alpha(1 + \alpha(y - \frac{L}{2}))\Delta h_x + \alpha^2 h_{xy} = 0. \quad (3.7)$$

$$(\Delta p + h)_t + (\alpha - s)p_x = 0. \quad (3.8)$$

3.2 Perturbation Energetics

It is possible to obtain a stability result from the averaged-energy form of the linearized equation for the upper layer. Here, we follow the work of Swaters (1993). Much of the derivation is actually possible for the more general problem (3.3), (3.4), having set $U_o = 0$, and we choose to present it here. We will invoke the special wedge-front solution in the last step. Let us assume that the interface does not actually outcrop on the fluid surface, and therefore the cross-channel width of the upper layer is simply the width of the channel itself, L . We multiply (3.3) by the perturbation amplitude $h(x, y, t)$, integrate over y from 0 to L , and over the length of the channel from $-X$ to X (X constant), defining the operator

$$\langle (...) \rangle = \int_{-X}^X (...) dx. \quad (3.9)$$

Since we are interested in baroclinic instability, we set $U_o = 0$, and obtain the following

$$\int_0^L \left\langle hh_t + h_{oy}hp_x + h_{oy}h_o h\Delta h_x + (h_{oy})^2 hh_{xy} - (h_o h_{oyy})_y hh_x \right\rangle dy = 0. \quad (3.10)$$

Since h_o has no x dependence, we may rewrite this as

$$\int_0^L \left([1] + h_{oy}h_o[2] + h_{oy}h_o[3] + (h_{oy})^2[4] + (h_o h_{oyy})_y[5] \right) dy = 0, \quad (3.11)$$

where $[1] = \left\langle \frac{1}{2}(h^2)_t + h_{oy}hp_x \right\rangle$, $[2] = \langle hh_{xx} \rangle$, $[3] = \langle hh_{xy} \rangle$, $[4] = \langle hh_{xy} \rangle$ and $[5] = \langle hh_x \rangle$. Integrating by parts, we see that the second integral $[2]$ vanishes, as does the last integral $[5]$, since

$$\begin{aligned} \int_{-X}^X hh_{xx} dx &= [h_x h_{xx}]_{-X}^X - \frac{1}{2} \int_{-X}^X (h_x^2)_x dx \\ &= 0 - \frac{1}{2} [h_x^2]_{-X}^X \\ &= 0. \end{aligned} \quad (3.12)$$

$$\begin{aligned} \int_{-X}^X hh_x dx &= \frac{1}{2} \int_{-X}^X (h^2)_x dx \\ &= \frac{1}{2} [h^2]_{-X}^X \\ &= 0. \end{aligned} \quad (3.13)$$

where we have used the periodicity condition at X and $-X$. The third and fourth integrals then combine to form

$$h_{oy}h_o[3] + (h_{oy})^2[4] = \langle h_{oy}h(h_o h_{xyy}) + h_{oy}h(h_{oy}h_{xy}) \rangle. \quad (3.14)$$

Factoring out $h_{oy}h$ and using the product rule for derivatives in reverse, this simplifies to

$$h_{oy}h_o[3] + (h_{oy})^2[4] = \langle h_{oy}h(h_o h_{xy})_y \rangle. \quad (3.15)$$

which we must integrate by parts several times.

$$\begin{aligned} & \int_0^L \langle h_{oy}h(h_o h_{xy})_y \rangle dy \\ &= \int_{-X}^X [h_o h_{oy} h h_{xy}]_0^L dx - \int_{-X}^X \int_0^L h_o h_{xy} (h_{oy} h)_y dy dx \\ &= \left[[h_o h_{oy} h h_y]_0^L \right]_{-X}^X - \int_{-X}^X [h_o h_{oy} h_x h_y]_0^L dx \\ & \quad - \int_{-X}^X \int_0^L h_o h_{xy} (h_{oyy} h + h_{oy} h_y) dy dx. \end{aligned} \quad (3.16)$$

Now, in the above result, the first integral vanishes due to periodicity in x , and the second one vanishes because $h_x = 0$ at $y = 0, L$ (no normal flow at boundaries). Only the third integral remains, and we can perform further simplifications on it, as follows.

$$\begin{aligned} & - \int_{-X}^X \int_0^L h_o h_{xy} (h_{oyy} h + h_{oy} h_y) dy dx \\ &= - \int_0^L \int_{-X}^X h_o h_{oyy} h h_{xy} dx dy - \int_0^L \frac{1}{2} \int_{-X}^X h_o h_{oy} (h_y^2)_x dx dy \\ &= - \int_0^L [h_o h_{oyy} h h_y]_{-X}^X dy + \int_0^L \int_{-X}^X h_o h_{oyy} h_x h_y dx dy \\ & \quad - \int_0^L \frac{1}{2} [h_o h_{oy} h_y^2]_{-X}^X dy \\ &= \int_{-X}^X \int_0^L h_o h_{oyy} h_x h_y dy dx. \end{aligned} \quad (3.17)$$

Here again, we have used the fact that both h and h_y are periodic in x . Now, if we substitute in the wedge front (3.5) for h_o , clearly $h_{oyy} = 0$ and so the above

integral also vanishes. In effect, (3.10) reduces to

$$\frac{\partial}{\partial t} \int_0^L \frac{1}{2} \langle h^2 \rangle dy = - \int_0^L \langle \alpha h p_x \rangle dy. \quad (3.18)$$

Therefore, a necessary condition for the growth of the perturbation is that the product $\alpha h p_x$ is negative somewhere. Conversely, if $\alpha h p_x$ is positive for all (x, y) in the domain, then this is sufficient to prevent the growth of the initial disturbance.

Heuristically, we can gain a physical appreciation of the above result in the following way. The flow is geostrophic to leading order, so p_x may be thought of as simply the cross channel perturbation velocity of the lower layer. Because h represents small variations in the upper layer thickness, a region where $h > 0$ corresponds to a warm anomaly in the slope water (and conversely, a region with $h < 0$ corresponds to a cold anomaly). For clarity, let us deal with an upper layer profile such that $\alpha > 0$. Since α is a constant, we may take it outside the integral. Then from (3.18) we can see that growth of the instability will occur if the transport of warm anomalies, averaged over the domain, is toward the shore, i.e. $\int_0^L \langle h p_x \rangle dy < 0$. Similarly, when $\alpha < 0$, the instability will grow if the area-averaged transport of warm anomalies is in the off-shore direction, i.e. $\int_0^L \langle h p_x \rangle dy > 0$.

3.3 Normal Mode Analysis

It is reasonable to assume that each perturbation field will be a superposition of waves. We therefore introduce instabilities of the form

$$p = \tilde{p}(y) \exp[ik(x - ct)] + c.c., \quad (3.19)$$

$$h = \tilde{h}(y) \exp[ik(x - ct)] + c.c., \quad (3.20)$$

where *c.c.* refers to the complex conjugate. *k* is the real-valued along-channel wavenumber, and *c* is the along-channel complex phase speed. We note that, with the above definitions, *p* and *h* are real. An instability of the basic flow arises when a perturbation begins to grow in time. In this section we will determine under what conditions this can or cannot happen.

As can be seen from (3.19) and (3.20), *p* and *h* will grow in time (and do so exponentially) if the imaginary part of the phase speed is positive. Substituting these expressions into (3.7) and (3.8),

$$[1 + \alpha(y - \frac{L}{2})][\partial_{yy} - k^2]\tilde{h} + \alpha\tilde{h}_y - \frac{c}{\alpha}\tilde{h} + \tilde{p} = 0. \quad (3.21)$$

$$[\partial_{yy} - k^2]\tilde{p} + \frac{s - \alpha}{c}\tilde{p} + \tilde{h} = 0. \quad (3.22)$$

The fluid must also satisfy the condition of no normal flow on the channel walls. Thus h_x and p_x must vanish on $y = 0, L$. However, because of the form we have assumed for *h* and *p*, the boundary conditions, in general, reduce to

$$\tilde{p} = \tilde{h} = 0 \quad \text{on} \quad y = 0, L. \quad (3.23)$$

Examining (3.21) and (3.22), we encounter an immediate difficulty. As far as we have been able to determine, the presence of the α terms makes this problem

analytically intractable. Let us assume therefore that α is small, and that s , the bottom slope, is $O(\alpha)$. As we will see later, c will then also be $O(\alpha)$, so we will neglect all $O(\alpha)$ terms in the above equations, but retain terms of $O(\frac{c}{\alpha})$ and $O(\frac{s}{c})$. In effect, we are considering a gently sloping wedge front. Dropping the tildes, this leads to a pair of ordinary differential equations

$$h'' - (\frac{c}{\alpha} + k^2)h + p = 0, \quad (3.24)$$

$$p'' - (\frac{\alpha - s}{c} + k^2)p + h = 0, \quad (3.25)$$

where the primes refer to derivatives with respect to y , and the boundary conditions on the channel walls are given by

$$p(0) = p(L) = h(0) = h(L) = 0. \quad (3.26)$$

The normal-mode solutions are necessarily of the form

$$p(y) = A \sin(ly) \quad , \quad h(y) = B \sin(ly). \quad (3.27)$$

where A and B are constants, and l , the quantized cross-channel wavenumber is given by

$$l = \frac{n\pi}{L}, \quad n \in \{1, 2, 3, \dots\}. \quad (3.28)$$

We now have the general form of the normal mode perturbation solutions, i.e.

$$p(x, y, t) = A \sin(ly) \exp[ik(x - ct)] + c.c., \quad (3.29)$$

$$h(x, y, t) = B \sin(ly) \exp[ik(x - ct)] + c.c. \quad (3.30)$$

Using these solutions, we can write (3.24) and (3.25) in matrix form,

$$\begin{bmatrix} K^2 + \frac{\alpha-s}{c} & -1 \\ -1 & K^2 + \frac{c}{\alpha} \end{bmatrix} \begin{bmatrix} A \\ B \end{bmatrix} = \begin{bmatrix} 0 \\ 0 \end{bmatrix}. \quad (3.31)$$

where $K^2 = k^2 + l^2$ is the *total wavenumber squared*. We remark that the above system puts a constraint on A and B , so that we can express one in terms of the other. Only one of the constants is free. For the problem to allow nontrivial solutions we require that the determinant of the coefficient matrix is identically zero:

$$(cK^2 + \alpha - s)(\alpha K^2 + c) - \alpha c = 0. \quad (3.32)$$

which gives a second-degree polynomial in c . Using the quadratic formula, we obtain the following *dispersion relation*

$$c = \frac{s - \alpha K^4 \pm [(\alpha K^4 - s)^2 - 4\alpha(\alpha - s)K^4]^{\frac{1}{2}}}{2K^2}. \quad (3.33)$$

We note that, as long as $K^2 \sim O(1)$ then $c \sim O(\alpha)$, as we required. Now, c can become complex if the expression in the square brackets (the discriminant) is negative. This gives two complex phase speeds, which are of course conjugates of each other. Here we point out that an instability takes place when two neutral modes (i.e. waves whose phase speed is real) coalesce, giving one real phase speed and two growth rates. Now, if we decompose c into

$$c = c_R + ic_I. \quad (3.34)$$

then as long as $c_I \neq 0$, we are guaranteed that $c_I > 0$ for one of the two conjugates, i.e. we have an instability.

Moreover, whenever the discriminant is positive, c is strictly real, ensuring that the system is stable to perturbations. This happens whenever $(\alpha K^4 - s)^2 -$

$4\alpha(\alpha - s)K^4 > 0$, and one way to ensure this is to make α positive and $(\alpha - s)$ negative. Thus, we can easily see that

$$0 < \alpha < s, \quad (3.35)$$

is a sufficient condition for stability, that is, whenever the slope of the interface is positive but less than the bottom slope (Swaters, 1993). Conversely, one of the conditions

$$\begin{aligned} \alpha < 0 \quad \text{or} \quad \alpha > s. \quad & \text{for } s > 0. \\ \alpha > 0 \quad \text{or} \quad \alpha < s. \quad & \text{for } s < 0. \end{aligned} \quad (3.36)$$

is necessary for instability.

The boundary between stability and instability may be examined by setting the discriminant equal to zero,

$$(\alpha K^4 - s)^2 = 4\alpha(\alpha - s)K^4. \quad (3.37)$$

Simplifying, we obtain the *Marginal Stability Curves* (MSC), given by

$$\frac{s}{\alpha} = K^2(2 - K^2) \quad (3.38)$$

and

$$\frac{s}{\alpha} = -K^2(2 + K^2). \quad (3.39)$$

Figure 3.1 shows the *Marginal Stability Curves*, with stable and unstable regions of the parameter space labeled. From here on we will call (3.38) the Upper Branch of the MSC and (3.39) the Lower Branch of the MSC. The point of marginal stability occurs at (1, 1) on the Upper Branch, i.e. $K^2 = 1$, $\frac{s}{\alpha} = 1$. Thus,

whenever the ratio $\frac{s}{\alpha}$ is less than unity, we can find wavenumbers for which the flow is unstable. There is also a high-frequency cutoff, defined simply by the Upper Branch of the MSC for $K^2 > 1$. Treating (3.38) as a polynomial in K^2 , we find the cutoff by taking the rightmost root, i.e.

$$K_{cutoff}^2 = 1 + \sqrt{1 - \frac{s}{\alpha}} \quad \text{whenever } \frac{s}{\alpha} < 1. \quad (3.40)$$

This means that as long as the ratio $\frac{s}{\alpha}$ is not too big (negatively), the flow is stable for all wavenumbers above some critical wavenumber. In the context of this analysis, $\frac{s}{\alpha}$ must be an $O(1)$ quantity, since we assumed that s is $O(\alpha)$.

The existence of a high-frequency cutoff ensures that the model is not subject to ultraviolet catastrophe. In models which are prone to this kind of instability, particularly Planetary Geostrophic models, c_i is nonzero for all k as $k \rightarrow \infty$, and so the growth rate, kc_i , grows with k (de Verdière, 1981). This is problematic, both theoretically and computationally, in that the shorter the wavelength of a perturbation, the faster it grows. A given flow has the potential of degenerating into a turbulent wavefield of small-scale noise, whose amplitude becomes unbounded and therefore unphysical.

For a given s , we define α_c to be the critical slope which satisfies one of (3.38) and (3.39). It was mentioned before that there exists a relationship between A and B . If we write down this relationship for points on the MSC, we find that on the Upper Branch $A = B$, while on the Lower Branch, $A = -B$. We call the first case, where the two solutions are in phase, the *barotropic mode*. The other case, where h and p are 180 degrees out of phase, the *baroclinic mode*.

Figure 3.2 is also a graph of the relations (3.38) and (3.39), but this time the ordinate axis is $\frac{\alpha}{s}$. The graph looks somewhat more complicated, and the region of instability has split in two. Therefore we will not refer to it later in

the thesis. It is worth pointing out however, that the plot is very reminiscent of the *Marginal Stability Curves* for the *Phillips model* (Pedlosky, 1987), where the *critical shear velocity* is graphed versus the *total wavenumber*. Introduced by Phillips in 1954, this was a simple two-layer Quasigeostrophic model. One further comment about the MSC may prove instructive at this point, relating our wedge-profile linear theory with that of Mooney & Swaters (1996). Their analysis was for a two-layer, non-quasigeostrophic model appropriate for gravity currents and bottom-dwelling cold domes derived by Swaters (1991). Mooney & Swaters showed that the associated linear problem becomes singular at the point of marginal stability (where $K^2 = 1$), in that it cannot be described as a limit of the $K \neq 1$ modes. In our model however, the linear system (3.31) does not become degenerate at the point of marginal stability.

Solving for α in terms of s and K in the relations (3.38) and (3.39), we can substitute the results into the dispersion relationship (3.33). This provides the real phase speed for the Upper and Lower branches of the MSC respectively, given by

$$c_1 = \frac{s(1 - K^2)}{K^2(2 - K^2)}, \quad (3.41)$$

$$c_2 = \frac{s(K^2 + 1)}{K^2(K^2 + 2)}. \quad (3.42)$$

These speeds (normalized by the parameter s) are plotted in Figures 3.3 and 3.4 versus K^2 .

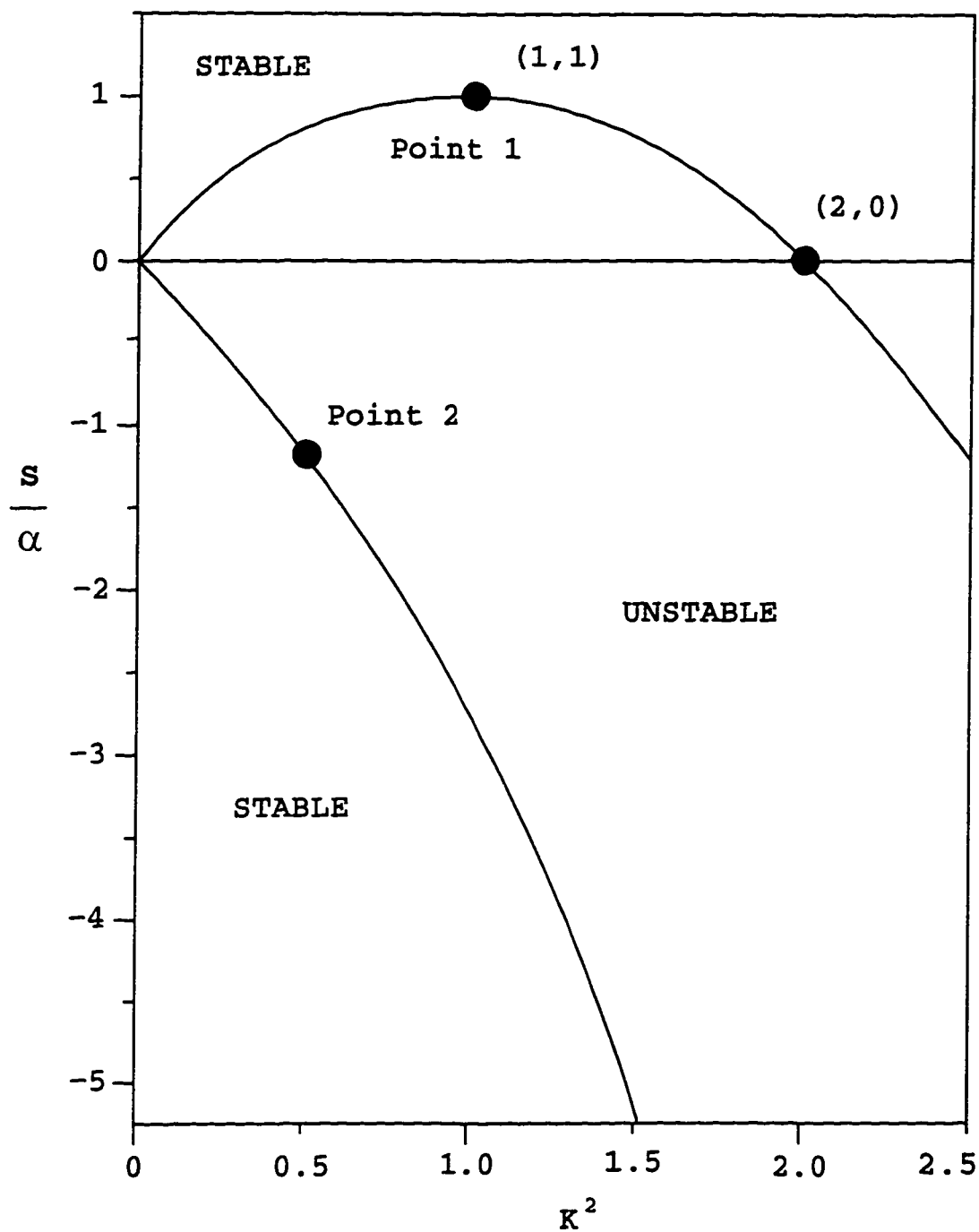


Figure 3.1: Marginal Stability Curves (MSC) for gently sloping wedge-front

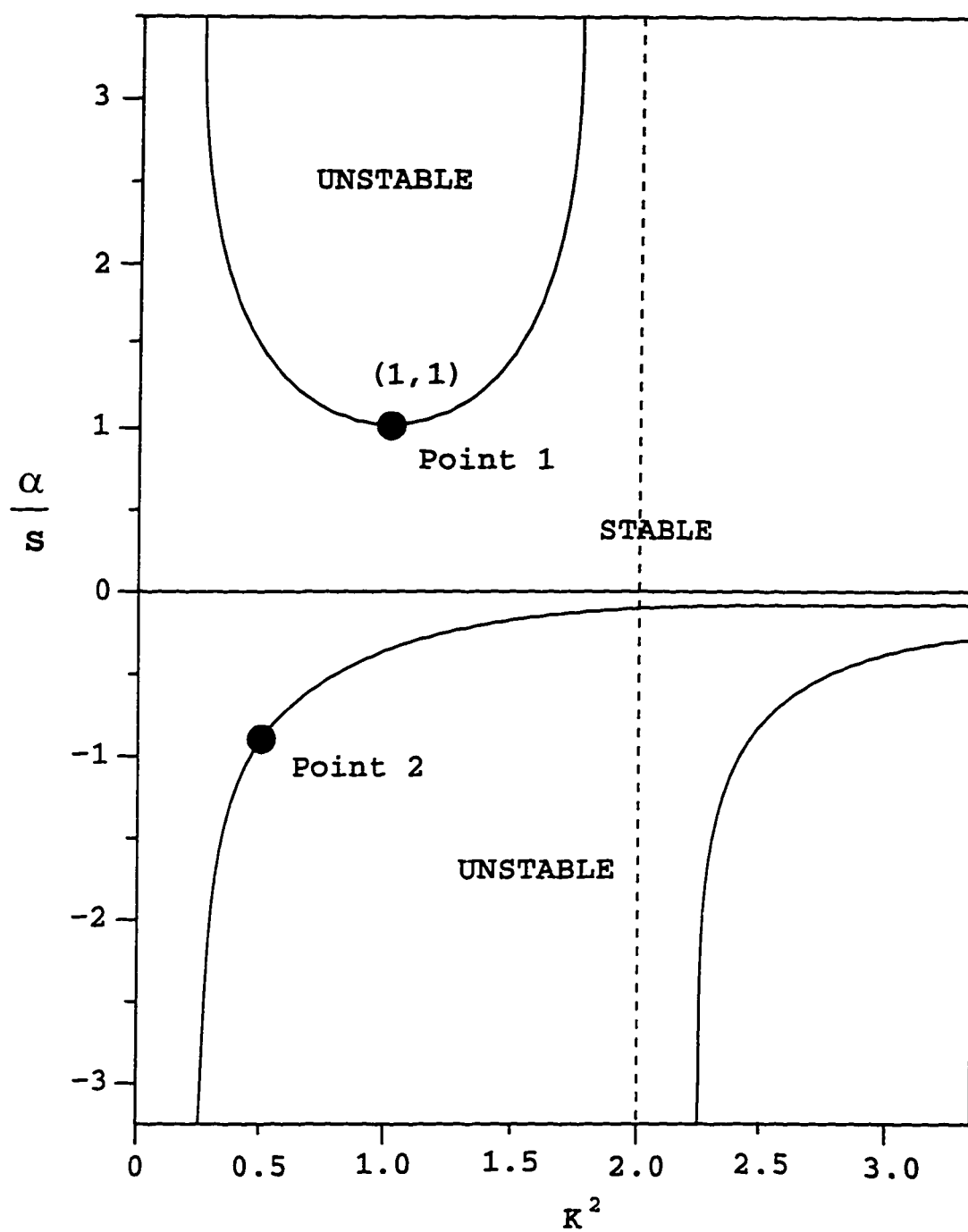


Figure 3.2: Marginal Stability Curves (MSC) for gently sloping wedge-front (alternate plot)

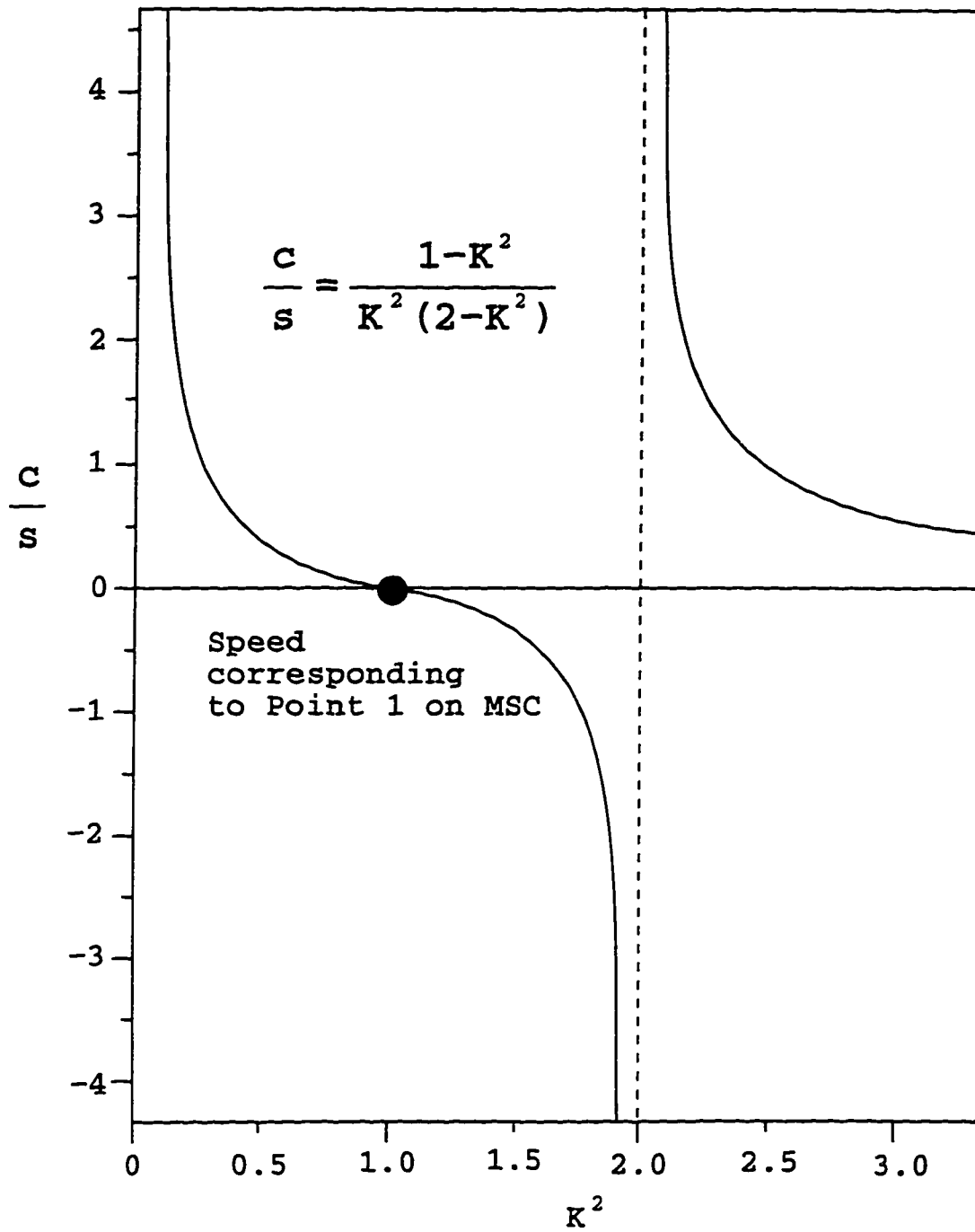


Figure 3.3: Real phase speed (normalized by s) on Upper Branch of Marginal Stability Curve

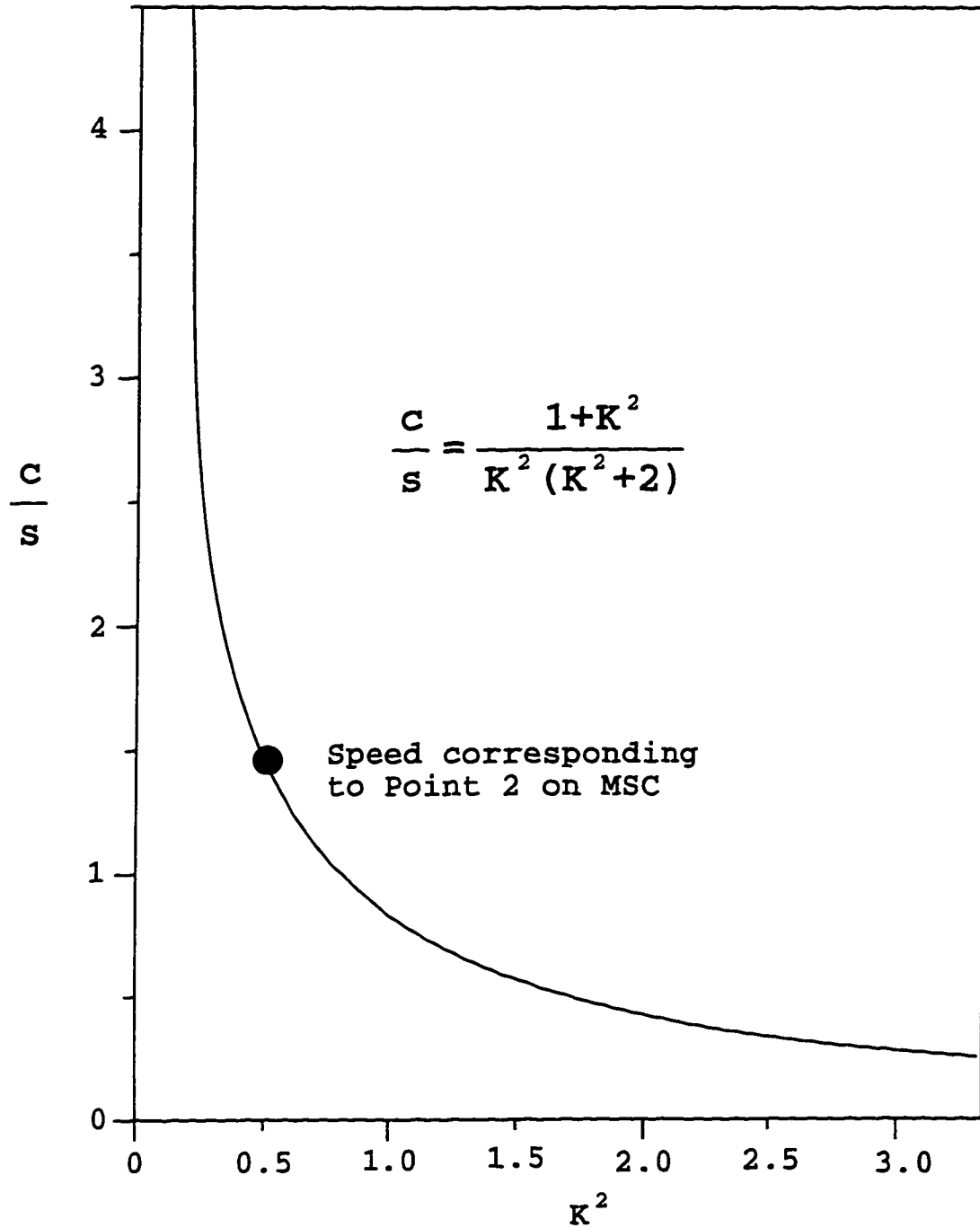


Figure 3.4: Real phase speed (normalized by s) on Lower Branch of Marginal Stability Curve

Chapter 4

Weakly Nonlinear Analysis

4.1 Introduction

Linear theory has provided us with the Curves of *Marginal Stability*, and solutions for the perturbations h and p , which are valid whenever the nonlinear terms are small. However, as a perturbation grows, the nonlinear terms which we neglected start to become more and more important. Even though we cannot solve the fully nonlinear equations, we can study the evolution of a wedge front which is *weakly unstable*, that is the nonlinear terms are small but significant. We assume the initial perturbation is small, and utilize the asymptotic methods introduced in the derivation of the governing equations (Section 2.4). This will enable us to find the Amplitude Equation, which governs the slow time evolution of the perturbation.

Although a wedge profile without isopycnal outcroppings is rather idealized, it does allow us to study available potential energy release and nonlinear interactions which will (hopefully) halt the growth predicted by linear theory. Griffiths & Linden (1981) were confident that their theory, which made use of such a profile, explained many of the instability characteristics observed in their laboratory

experiments. The derivation of an amplitude equation for even this simple front is rather involved, but the procedure itself is a standard one. and here we follow Pedlosky (1987). More in-depth studies may be found in a series of papers by Pedlosky (1970, 1972, 1982 and 1983).

4.2 The nonlinear problem

4.2.1 Nonlinear Perturbation Equations

Introducing the perturbed quantities (3.1) and (3.2) into the governing equations (2.92) and (2.93). we arrive at the Nonlinear Perturbation Equations

$$\begin{aligned}
 & h_t + h_{oy}h_o\Delta h_x + (h_{oy})^2h_{xy} - (h_o h_{oyy})_y + h_{oy}p_x \\
 & + h_o J(\Delta h, h) + h_{oy} [h\Delta h_x + 2h_y h_{xy} - h_x h_{yy} + h_x h_{xx}] \\
 & - h_{oyy}h_x h_y - h_{oyyy}h h_x + J(p, h) = 0.
 \end{aligned} \tag{4.1}$$

$$(\Delta p + h)_t + (h_{oy} - s)p_x + J(p, \Delta p + h) = 0. \tag{4.2}$$

where U_o has been set to zero and we have again dropped the primes for cleaner notation.

Unlike in the previous chapter. here we did not neglect the nonlinear terms. Again we choose the gently-sloping wedge front $h_o = 1 + \alpha(y - \frac{L}{2})$, $\alpha \ll 1$. Now we rescale via

$$\alpha = s\tilde{\alpha} \quad \text{and} \quad t = \tilde{t}/s, \tag{4.3}$$

which forces a scaling on the phase velocity,

$$c = s\tilde{c}. \quad (4.4)$$

From now on we will drop the tildes when referring to these new quantities. For clarity, let us write down the new critical slope α_c and phase speed c ,

$$\alpha_c = \frac{-1}{K^2(K^2 + 2)}, \quad c = \frac{K^2 + 1}{K^2(K^2 + 2)}, \quad \text{on the Lower Branch.} \quad (4.5)$$

$$\alpha_c = \frac{1}{K^2(2 - K^2)}, \quad c = \frac{1 - K^2}{K^2(2 - K^2)}, \quad \text{on the Upper Branch.} \quad (4.6)$$

In order to push the nonlinear interaction into a higher order problem, we also rescale the perturbation quantities.

$$h = s^2\tilde{h}, \quad p = s^2\tilde{p}. \quad (4.7)$$

Substituting into (4.1) and (4.2), and dropping the tildes,

$$h_t + \alpha\Delta h_x + \alpha p_x = -s\alpha^2 h_{xy} - s\alpha^2(y - \frac{L}{2})\Delta h_x \quad (4.8)$$

$$\begin{aligned} & -sJ(\Delta h + p, h) - s^2\alpha(y - \frac{L}{2})J(\Delta h, h) \\ & -s^2\alpha[h\Delta h_x + 2h_y h_{xy} - h_x h_{yy} + h_x h_{xx}] + O(s^3). \end{aligned}$$

$$(\Delta p + h)_t + (\alpha - 1)p_x = sJ(\Delta p + h, p). \quad (4.9)$$

where we have neglected terms of $O(s^3)$ and higher, since they do not appear in our subsequent analysis.

4.2.2 Scaling for slow time

We must now find an appropriate scaling for the slow time T , during which nonlinear interaction will become significant. We begin by introducing a supercriticality in α ,

$$\alpha = \alpha_c - \Delta, \quad (4.10)$$

where Δ is some small, positive quantity. This corresponds to a shift from the Lower Branch of the MSC slightly into the unstable region (see Figure 4.1). We are assured that c_I is non-zero, and can recast it in terms of the new (scaled) parameter α :

$$c_I = \frac{[4\alpha(\alpha - 1)K^4 - (\alpha K^4 - 1)^2]^{\frac{1}{2}}}{2K^2}, \quad (4.11)$$

where we have chosen the positive root. Substituting the perturbed α into (4.11), as well as the expression (4.5) for the critical α_c , we arrive at

$$c_I = \frac{\Delta^{\frac{1}{2}}}{2K^2} \left[K^2(K^2 + 2) \left(\frac{4}{K^2 + 2} - K^2(K^2 - 2)\Delta \right) \right]^{\frac{1}{2}}. \quad (4.12)$$

Since all terms in the square brackets are assumed to be $O(1)$, this tells us that the growth rate kc_I will be on the order $\Delta^{\frac{1}{2}}$.

The small parameter, s , is intimately tied to the stability of the linear system as shown in (3.35) and (3.36). Moreover, we would like to study the instability as it is influenced by small changes to the bottom slope (which will affect the stretching of vortex tubes). We therefore want the growth rate to be dependent on s , and we define $\Delta = \delta^2 s^2$. Here s is squared to prevent numerous square roots from appearing in future calculations, and δ is an $O(1)$ free parameter which will give us precise control over the size of the supercriticality. Now, if the growth rate

is an $O(s)$ quantity, then this implies slow time should be scaled as

$$T = st \quad (\text{i.e. } \partial_t \longrightarrow \partial_t + s\partial_T). \quad (4.13)$$

The above argument is similar for the Upper Branch of the MSC (except that α must be increased, rather than decreased) and the scaling for time is the same.

For convenience, we introduce a parameter μ , which will facilitate discussion of both branches of the MSC at the same time. In all future calculations, we will assume $\mu = 1$ on the Upper Branch and $\mu = -1$ on the Lower Branch. Accordingly, our scaled slope takes the form

$$\alpha = \alpha_c + \mu\delta^2 s^2. \quad (4.14)$$

while the critical slope and phase speed may be written as, respectively,

$$\alpha_c = \frac{\mu}{K^2(2 - \mu K^2)}, \quad c = \frac{1 - \mu K^2}{K^2(2 - \mu K^2)}. \quad (4.15)$$

The resulting equations are

$$\begin{aligned} h_t + \alpha_c \Delta h_x + \alpha_c p_x &= -s\alpha_c^2 h_{xy} - s\alpha_c^2 \left(y - \frac{L}{2}\right) \Delta h_x \\ -sh_T - sJ(\Delta h + p, h) - s^2\alpha_c \left(y - \frac{L}{2}\right) J(\Delta h, h) \\ -\mu\delta^2 s^2 (\Delta h + p)_x - s^2\alpha_c [h\Delta h_x + 2h_y h_{xy} - h_x h_{yy} + h_x h_{xx}], \end{aligned} \quad (4.16)$$

$$(\Delta p + h)_t + (\alpha_c - 1)p_x = -sJ(p, \Delta p + h) - s(\Delta p + h)_T - \mu\delta^2 s^2 p_x. \quad (4.17)$$

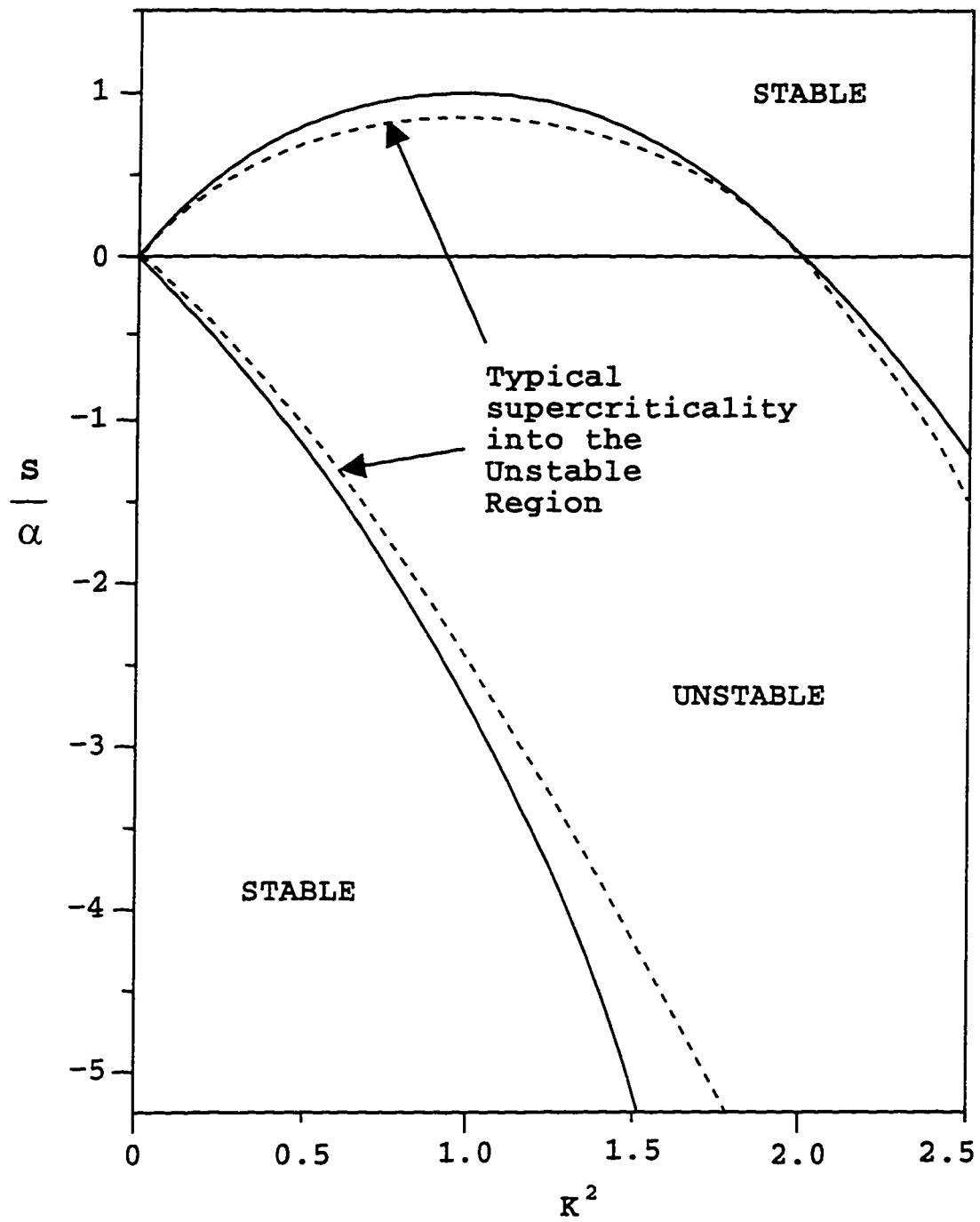


Figure 4.1: MSC for gently sloping wedge-front and supercriticality curves

4.2.3 $O(1)$ Problem

Now we expand h and p in the small parameter s .

$$p(x, y, t; T) = p^{(0)}(x, y, t; T) + sp^{(1)}(x, y, t; T) + s^2p^{(2)}(x, y, t; T) + \dots \quad (4.18)$$

$$h(x, y, t; T) = h^{(0)}(x, y, t; T) + sh^{(1)}(x, y, t; T) + s^2h^{(2)}(x, y, t; T) + \dots \quad (4.19)$$

with the implicit requirement that $p^{(0)}, h^{(0)}, p^{(1)}, h^{(1)}$, etc. are all $O(1)$ quantities. Substituting into (4.16) and (4.17), the $O(1)$ problem becomes.

$$h_t^{(0)} + \alpha_c \Delta h_x^{(0)} + \alpha_c p_x^{(0)} = 0. \quad (4.20)$$

$$(\Delta p^{(0)} + h^{(0)})_t + (\alpha_c - 1)p_x^{(0)} = 0. \quad (4.21)$$

Assuming normal mode expressions for $p^{(0)}$ and $h^{(0)}$, the problem turns out to be equivalent to (3.24), (3.25), so that the $O(1)$ solutions are simply the linear solutions.

$$p^{(0)} = A(T) \exp[ik\theta] \sin(ly) + c.c.. \quad (4.22)$$

$$h^{(0)} = B(T) \exp[ik\theta] \sin(ly) + c.c.. \quad (4.23)$$

where we have defined the phase $\theta = x - ct$ for convenience. The amplitude coefficients A and B are now assumed to be functions of the slow time T . In this section we want to find an equation for the evolution of $A(T)$, realizing that the relation $B(T) = \mu A(T)$ holds as before.

4.2.4 $O(s)$ Problem

The $O(s)$ problem is

$$h_t^{(1)} + \alpha_c \Delta h_x^{(1)} + \alpha_c p_x^{(1)} = -\alpha_c^2 (y - \frac{L}{2}) \Delta h_x^{(0)} - \alpha_c^2 h_{xy}^{(0)} - h_T^{(0)}. \quad (4.24)$$

$$(\Delta p^{(1)} + h^{(1)})_t + (\alpha_c - 1)p_x^{(1)} = -(\Delta p^{(0)} + h^{(0)})_T. \quad (4.25)$$

The solutions are assumed to be of the form

$$p^{(1)} = \tilde{p}(y, T) \exp[ik\theta] + c.c. + \Psi(y, T), \quad (4.26)$$

$$h^{(1)} = \tilde{h}(y, T) \exp[ik\theta] + c.c. + \Phi(y, T), \quad (4.27)$$

where we have introduced the mean-flow correction terms Ψ and Φ . These are needed to account for changes to the mean flow caused by interaction of nonlinear terms. as will be evident in the $O(s^2)$ problem (Pedlosky, 1987). Ψ and Φ have no fast-phase oscillation and, being modifications to the $O(s)$ streamfunction, they are streamfunctions themselves.

Substituting (4.26) and (4.27) into (4.24) and (4.25), and dividing through by $i\alpha_c k$ and $-ick$ respectively, we obtain

$$\left[\partial_{yy} - k^2 - \frac{c}{\alpha_c} \right] \tilde{h} + \tilde{p} = -\alpha_c \mu A \cos(ly) \quad (4.28)$$

$$+ \alpha_c (y - \frac{L}{2}) K^2 \mu A \sin(ly) + \frac{i\mu}{\alpha_c k} A_T \sin(ly).$$

$$\left[\partial_{yy} - k^2 - \frac{\alpha_c - 1}{c} \right] \tilde{p} + \tilde{h} = \frac{i}{kc} (K^2 A - \mu A)_T \sin(ly). \quad (4.29)$$

To establish the existence of the solutions \tilde{h} and \tilde{p} , we first consider the associated

homogeneous problem.

$$\begin{bmatrix} \partial_{yy} - k^2 - \frac{c}{\alpha_c} & 1 \\ 1 & \partial_{yy} - k^2 - \frac{\alpha_c - 1}{c} \end{bmatrix} \begin{bmatrix} \tilde{h} \\ \tilde{p} \end{bmatrix} = \begin{bmatrix} 0 \\ 0 \end{bmatrix}. \quad (4.30)$$

with the boundary conditions.

$$\tilde{h}(L) = \tilde{h}(0) = \tilde{p}(L) = \tilde{p}(0) = 0. \quad (4.31)$$

This selfadjoint Boundary Value Problem is identical to the $O(1)$ problem so that the two-tuple $[\mu A \sin(ly), A \sin(ly)]$ is clearly a solution.

Integrating by parts, it can be verified that the inner product of $[\mu A \sin(ly), A \sin(ly)]$ with the left-hand side of (4.28) and (4.29) is zero, that is

$$\int_0^L A \sin(ly) [\mu, 1] \cdot \begin{bmatrix} \partial_{yy} - k^2 - \frac{c}{\alpha_c} & 1 \\ 1 & \partial_{yy} - k^2 - \frac{\alpha_c - 1}{c} \end{bmatrix} \begin{bmatrix} \tilde{h} \\ \tilde{p} \end{bmatrix} dy = 0. \quad (4.32)$$

It follows, by the *Fredholm Alternative* (Nagle & Saff, 1993), that the inhomogeneous problem (4.28) and (4.29) has solutions if and only if

$$\begin{aligned} & \int_0^L \left[-\alpha_c \mu l A \cos(ly) + \alpha_c K^2 (y - \frac{L}{2}) \mu A \sin(ly) \right. \\ & \quad \left. + \frac{i\mu}{\alpha_c k} A_T \sin(ly) \right] \mu A \sin(ly) dy \\ & + \int_0^L \left[\frac{i}{kc} (K^2 A - \mu A)_T \sin(ly) \right] A \sin(ly) dy = 0. \end{aligned} \quad (4.33)$$

We integrate term by term. Clearly,

$$-\alpha_c l \int_0^L A^2 \cos(ly) \sin(ly) dy = 0. \quad (4.34)$$

Next, using integration by parts, we obtain

$$\alpha_c K^2 \int_0^L (y - \frac{L}{2}) A^2 \sin^2(ly) dy = 0. \quad (4.35)$$

Finally, the remaining expressions yield

$$\frac{i}{k} \int_0^L (\frac{1}{\alpha_c} + \frac{K^2 - \mu}{c}) A A_T \sin^2(ly) dy = 0. \quad (4.36)$$

where we had to make use of the respective expressions for α_c , c and μ appropriate for the Upper and Lower branches. The integral in (4.33) trivially vanishes. Thus, the $O(s)$ problem is degenerate in the sense it gives us no new condition on A .

We are forced to examine the next order problem, but first we have to determine the solutions \bar{h} , \bar{p} . Solving for \bar{h} in (4.29) gives

$$\bar{h} = -[\partial_{yy} - k^2 - \frac{\alpha_c - 1}{c}] \bar{p} + \frac{i}{kc} (K^2 A \sin(ly) - \mu A \sin(ly))_T. \quad (4.37)$$

Before we determine \bar{p} , we simplify the operator on \bar{h} in (4.28), and the operator on \bar{p} in (4.29) as follows.

$$\left[\partial_{yy} - k^2 - \frac{c}{\alpha_c} \right] = \left[\partial_{yy} + l^2 - \mu \right]. \quad (4.38)$$

$$\left[\partial_{yy} - k^2 - \frac{\alpha_c - 1}{c} \right] = \left[\partial_{yy} + l^2 - \mu \right]. \quad (4.39)$$

Substitution of (4.37) through (4.39) into (4.28) allows us to write

$$\begin{aligned} \{ [\partial_{yy} + l^2 - \mu]^2 - 1 \} \bar{p} &= \frac{i}{kc} [\partial_{yy} + l^2 - \mu] \\ &\times (K^2 A \sin(ly) - \mu A \sin(ly))_T + \alpha_c l \mu A \cos(ly) \end{aligned} \quad (4.40)$$

$$-\alpha_c(y - \frac{L}{2})K^2\mu A \sin(ly) - \frac{i}{k\alpha_c}\mu A_T \sin(ly).$$

Substituting in for $h^{(0)}$ and $p^{(0)}$, simplifying the right hand side, and writing the left hand side operator (a difference of squares) as a product of two operators yields the system

$$[\partial_{yy} + l^2 - 2\mu]\bar{p} = \xi, \quad (4.41)$$

$$[\partial_{yy} + l^2]\xi = \alpha_c l \mu A \cos(ly) - \alpha_c(y - \frac{L}{2})K^2\mu A \sin(ly). \quad (4.42)$$

where we have introduced the intermediate solution, ξ . The particular solution ξ_{P1} , associated with $\alpha_c l \mu A \cos(ly)$ in (4.42) may be written down immediately.

$$\xi_{P1} = \frac{1}{2}\mu\alpha_c(y - \frac{L}{2})A \sin(ly). \quad (4.43)$$

The other particular solution, ξ_{P2} , satisfies

$$[\partial_{yy} + l^2]\xi_{P2} = -\mu\alpha_c K^2 A(y - \frac{L}{2}) \sin(ly). \quad (4.44)$$

We assume the solution has the form

$$\xi_{P2} = \beta(y - \frac{L}{2}) \sin(ly) + \gamma(y - \frac{L}{2})^2 \cos(ly). \quad (4.45)$$

and determine β and γ by substitution into (4.42),

$$2\beta l \cos(ly) + 2\gamma \cos(ly) - 4\gamma(y - \frac{L}{2})l \sin(ly) = -\mu\alpha_c K^2 A(y - \frac{L}{2}) \sin(ly). \quad (4.46)$$

Exploiting the linear independence of $\sin(ly)$ and $\cos(ly)$, we obtain

$$\beta = -\mu\alpha_c A(\frac{K}{2l})^2, \quad \gamma = \frac{\mu\alpha_c K^2 A}{2}. \quad (4.47)$$

The general solution ξ is given by

$$\xi = \xi_{P1} + \xi_{P2} + \Gamma \cos(ly). \quad (4.48)$$

where $\Gamma \cos(ly)$ is the homogeneous solution. The sum $\xi_{P1} + \xi_{P2}$ cannot satisfy the boundary conditions by itself, but it is possible to choose Γ so that $\tilde{p}(0) = \tilde{p}(L) = 0$. We remark that the homogeneous solution does not need a $\sin(ly)$ term, because any such term may just be absorbed into the $O(1)$ solution. For convenience, we will write

$$\xi = \Gamma_1(y - \frac{L}{2}) \sin(ly) + \Gamma_2(y - \frac{L}{2})^2 \cos(ly) + \Gamma \cos(ly). \quad (4.49)$$

where

$$\Gamma_1 = \frac{\mu\alpha_c K^2 A}{2}, \quad \Gamma_2 = \frac{\mu\alpha_c A}{2} - \mu\alpha_c A \left(\frac{K}{2l}\right)^2. \quad (4.50)$$

and Γ is still to be determined.

Now we must determine \tilde{p} from (4.41). The following form for the particular solution is assumed.

$$\tilde{p}_p = \gamma_1(y - \frac{L}{2})^2 \cos(ly) + \gamma_2(y - \frac{L}{2}) \sin(ly) + \gamma_3 \cos(ly). \quad (4.51)$$

Substitution into (4.41) gives

$$[\partial_{yy} + l^2 - 2\mu]\tilde{p}_p = 2(\gamma_1 + \gamma_2 l) \cos(ly) \quad (4.52)$$

$$\begin{aligned} & -2(2\gamma_1 l + \mu\gamma_2)(y - \frac{L}{2}) \sin(ly) \\ & -2\mu\gamma_1(y - \frac{L}{2})^2 \cos(ly) - 2\mu\gamma_3 \cos(ly), \end{aligned}$$

where the right-hand side must also equal ξ . Exploiting linear independence of

the functions involved, we obtain

$$\gamma_1 = \frac{\Gamma_2}{2}, \quad \gamma_2 = \frac{\Gamma_1}{2} + l\Gamma_2, \quad \Gamma = 2\gamma_1 + 2l\gamma_2 + 2\gamma_3. \quad (4.53)$$

where γ_3 is still free. All other constants are determined, at least up to γ_3 .

The homogeneous part of \tilde{p} depends on the sign of $l^2 - 2\mu$.

Case 1: $l^2 - 2\mu > 0$

We remark that this is always true for the Lower Branch (since $\mu = -1$), and can be true for the Upper Branch if l is large enough. In this case the homogeneous part is

$$\tilde{p}_h = \gamma_4 \sin(ry) + \gamma_5 \sin(r(y - L)). \quad (4.54)$$

where $r^2 = l^2 - 2\mu > 0$.

The new constants γ_4 and γ_5 are determined using the boundary conditions.

$$\tilde{p}(0) = 0 = \frac{\gamma_1 L^2}{4} + \gamma_3 - \gamma_5 \sin(rL). \quad (4.55)$$

$$\tilde{p}(L) = 0 = (-1)^n \frac{\gamma_1 L^2}{4} + (-1)^n \gamma_3 + \gamma_4 \sin(rL). \quad (4.56)$$

so that

$$\gamma_4 = (-1)^{n+1} \frac{\gamma_1 L^2 + 4\gamma_3}{4 \sin(rL)}, \quad \gamma_5 = \frac{\gamma_1 L^2 + 4\gamma_3}{4 \sin(rL)}. \quad (4.57)$$

We now simplify (4.37) to obtain an expression for \tilde{h} .

$$\tilde{h} = -[\partial_{yy} + l^2 - \mu]\tilde{p} + \frac{i}{kc}(K^2 - \mu)A_T \sin(ly). \quad (4.58)$$

When the boundary condition is applied to \tilde{h} , we obtain

$$[\partial_{yy} + l^2 - \mu]\tilde{p} = 0 \quad \text{on} \quad y = 0, L, \quad (4.59)$$

i.e.

$$\begin{aligned}
& (2\gamma_1 + 2\gamma_2 l - \mu\gamma_3) \cos(ly) - (4l\gamma_1 + \mu\gamma_2)(y - \frac{L}{2}) \sin(ly) \\
& - \mu\gamma_1(y - \frac{L}{2})^2 \cos(ly) + \mu\gamma_4 \sin(ry) \\
& + \mu\gamma_5 \sin(r(y - L)) = 0 \quad \text{on} \quad y = 0, L.
\end{aligned} \tag{4.60}$$

which simplifies to

$$(2 - \mu \frac{L^2}{4})\gamma_1 + 2l\gamma_2 - \mu\gamma_3 - \mu\gamma_5 \sin(rL) = 0, \tag{4.61}$$

$$(-1)^n(2 - \mu \frac{L^2}{4})\gamma_1 + 2(-1)^n l\gamma_2 - (-1)^n \mu\gamma_3 + \mu\gamma_4 \sin(rL) = 0. \tag{4.62}$$

These two conditions in fact reduce to one. and this determines γ_3 .

$$\gamma_3 = (\mu - \frac{L^2}{4})\gamma_1 + \mu l\gamma_2. \tag{4.63}$$

All constants are now defined. and so are the solutions \tilde{p} and \tilde{h} . To summarize, for the case where $l^2 - 2\mu > 0$. the $O(s)$ tilde solutions are

$$\begin{aligned}
\tilde{p}(y, T) = & \gamma_1(y - \frac{L}{2})^2 \cos(ly) + \gamma_2(y - \frac{L}{2}) \sin(ly) \\
& + \gamma_3 \cos(ly) + \gamma_4 \sin(ry) + \gamma_5 \sin(r(y - L)).
\end{aligned} \tag{4.64}$$

$$\tilde{h}(y, T) = -[\partial_{yy} + l^2 - \mu]\tilde{p} + \frac{i}{kc}(K^2 - \mu) \sin(ly) A_T. \tag{4.65}$$

with

$$\begin{aligned}
\gamma_1 = & -\frac{K^2}{8l} \alpha_c A, \quad \gamma_2 = \left[\frac{\mu K^2 - 1}{4} + \frac{1}{2} \left(\frac{K}{2l} \right)^2 \right] \alpha_c A. \\
\gamma_3 = & \left[\frac{K^2 L^2}{32l} + \frac{l(K^2 - \mu)}{4} \right] \alpha_c A, \quad \gamma_4 = \frac{l(K^2 - \mu)(-1)^{n+1}}{4 \sin(rL)} \alpha_c A,
\end{aligned} \tag{4.66}$$

$$\gamma_5 = \frac{l(K^2 - \mu)}{4 \sin(rL)} \alpha_c A, \quad r = \sqrt{l^2 - 2\mu}.$$

Case 2: $l^2 - 2\mu < 0$

We remark that this can only be true on the Upper Branch (where $\mu = 1$). We will thus set $\mu = 1$ without loss of generality. In this case the homogeneous part of \bar{p} must be of the form

$$\bar{p}_h = \bar{\gamma}_4 \exp(-\bar{r}y) + \bar{\gamma}_5 \exp(\bar{r}(y - L)), \quad (4.67)$$

where $\bar{r}^2 = 2 - l^2 > 0$.

As before, the new constants $\bar{\gamma}_4$ and $\bar{\gamma}_5$ are determined using the boundary conditions on \bar{p} .

$$\bar{p}(0) = 0 = \frac{\gamma_1 L^2}{4} + \gamma_3 + \bar{\gamma}_4 - \bar{\gamma}_5 \exp(-\bar{r}L). \quad (4.68)$$

$$\bar{p}(L) = 0 = (-1)^n \frac{\gamma_1 L^2}{4} + (-1)^n \gamma_3 + \bar{\gamma}_4 \exp(-\bar{r}L) + \bar{\gamma}_5. \quad (4.69)$$

so that

$$\begin{aligned} \bar{\gamma}_4 &= -\gamma_1 \frac{L^2}{4} - \gamma_3 - \bar{\gamma}_5 \exp(-\bar{r}L), \\ \bar{\gamma}_5 &= \frac{(\gamma_1 L^2 + 4\gamma_3) \exp(-\bar{r}L) - (-1)^n (\gamma_1 L^2 + 4\gamma_3)}{4(1 - \exp(-2\bar{r}L))}. \end{aligned} \quad (4.70)$$

We apply the boundary conditions to \bar{h} ,

$$[\partial_{yy} + l^2 - 1]\bar{p} = 0 \quad \text{on} \quad y = 0, L, \quad (4.71)$$

i.e.

$$(2\gamma_1 + 2\gamma_2 l - \gamma_3) \cos(ly) - (4l\gamma_1 + \gamma_2)(y - \frac{L}{2}) \sin(ly) \quad (4.72)$$

$$\begin{aligned}
& -\gamma_1(y - \frac{L}{2})^2 \cos(ly) + \bar{\gamma}_4 \exp(-\bar{r}y) \\
& + \bar{\gamma}_5 \exp(\bar{r}(y - L)) = 0 \quad \text{on} \quad y = 0, L.
\end{aligned}$$

which simplifies to

$$(2 - \frac{L^2}{4})\gamma_1 + 2l\gamma_2 - \gamma_3 - \bar{\gamma}_5 \exp(\bar{r}L) = 0, \quad (4.73)$$

$$(-1)^n(2 - \frac{L^2}{4})\gamma_1 + 2(-1)^nl\gamma_2 - (-1)^n\gamma_3 + \bar{\gamma}_4 \exp(\bar{r}L) = 0. \quad (4.74)$$

These two conditions again reduce to one, resulting in

$$\gamma_3 = (1 - \frac{L^2}{4})\gamma_1 + l\gamma_2, \quad (4.75)$$

which is the same as γ_3 in Case 1 with $\mu = 1$. All constants are now defined, and so are the solutions \bar{p} and \bar{h} .

To summarize, for the case where $l^2 - 2 < 0$, the $O(s)$ tilde solutions are

$$\begin{aligned}
\bar{p}(y, T) = & \gamma_1(y - \frac{L}{2})^2 \cos(ly) + \gamma_2(y - \frac{L}{2}) \sin(ly) \\
& + \gamma_3 \cos(ly) + \bar{\gamma}_4 \exp(-\bar{r}y) + \bar{\gamma}_5 \exp(\bar{r}(y - L)).
\end{aligned} \quad (4.76)$$

$$\bar{h}(y, T) = -[\partial_{yy} + l^2 - \mu]\bar{p} + \frac{i}{kc}(K^2 - \mu) \sin(ly) A_T. \quad (4.77)$$

with γ_1 , γ_2 and γ_3 as before, and

$$\begin{aligned}
\bar{\gamma}_4 = & \frac{((-1)^n \exp(-\bar{r}L) - 1)(K^2 - 1)l}{4(1 - \exp(-2\bar{r}L))} \alpha_c A, \\
\bar{\gamma}_5 = & \frac{(\exp(-\bar{r}L) - (-1)^n)(K^2 - 1)l}{4(1 - \exp(-2\bar{r}L))} \alpha_c A, \quad \bar{r} = \sqrt{2 - l^2}.
\end{aligned} \quad (4.78)$$

4.2.5 $O(s^2)$ Problem

The $O(s^2)$ problem is given by

$$h_t^{(2)} + \alpha_c \Delta h_x^{(2)} + \alpha_c p_x^{(2)} = -\alpha_c^2 \left(y - \frac{L}{2}\right) \Delta h_x^{(1)} - \alpha_c^2 h_{xy}^{(1)} \quad (4.79)$$

$$\begin{aligned} & -J(\Delta h^{(1)}, h^{(0)}) - J(\Delta h^{(0)}, h^{(1)}) \\ & -J(p^{(0)}, h^{(1)}) - J(p^{(1)}, h^{(0)}) - h_T^{(1)} - \mu \delta^2 (\Delta h^{(0)} + p^{(0)})_x \\ & -\alpha_c [h^{(0)} \Delta h_x^{(0)} + 2h_y^{(0)} h_{xy}^{(0)} - h_x^{(0)} h_{yy}^{(0)} + h_x^{(0)} h_{xx}^{(0)}]. \end{aligned}$$

$$(\Delta p^{(2)} + h^{(2)})_t + (\alpha_c - 1)p_x^{(2)} = -(\Delta p^{(1)} + h^{(1)})_T \quad (4.80)$$

$$-J(p^{(0)}, \Delta p^{(1)} + h^{(1)}) - J(p^{(1)}, \Delta p^{(0)} + h^{(0)}) - \mu \delta^2 p_x^{(0)}.$$

Substituting in our expressions for the solutions to the $O(1)$ and $O(s)$ problems.

$$h_t^{(2)} + \alpha_c \Delta h_x^{(2)} + \alpha_c p_x^{(2)} = \quad (4.81)$$

$$\begin{aligned} & \exp(ik\theta) \left[ik^3 \alpha_c^2 \left(y - \frac{L}{2}\right) \bar{h} - ik \alpha_c^2 \bar{h}_y \right. \\ & \left. - ik \alpha_c^2 \left(y - \frac{L}{2}\right) \bar{h}_{yy} - \bar{h}_T + ik \delta^2 (K^2 - \mu) \sin(ly) A \right. \\ & \left. + ik \mu \sin(ly) A (\Phi_{yyy} + \Psi_y) + ik (\mu K^2 - 1) \sin(ly) A \Phi_y \right] + c.c. \\ & - 2 \frac{l}{c} (K^2 + 1) \sin(ly) \cos(ly) (A A_T^* + A^* A_T) - \Phi_T, \end{aligned}$$

$$(\Delta p^{(2)} + h^{(2)})_t + (\alpha_c - 1)p_x^{(2)} = \quad (4.82)$$

$$\exp(ik\theta) \left[k^2 \bar{p}_T - \bar{p}_{yyT} - \bar{h}_T - ik \delta^2 \mu \sin(ly) A \right]$$

$$\begin{aligned}
& -ik \sin(ly) A(\Psi_{yyy} + \Phi_y) - ik(K^2 - \mu) \sin(ly) A \Psi_y \Big] \\
& + ik \exp(2ik\theta) \Big[-l\mu \cos(ly) A(l^2 \bar{h} + \bar{h}_{yy}) + \mu \sin(ly) A(l^2 \bar{h}_y + \bar{h}_{yyy}) \\
& \quad - l \cos(ly) A(l^2 \bar{p} + \bar{p}_{yy}) - \sin(ly) A(l^2 \bar{p}_y + \bar{p}_{yyy}) \\
& \quad + K^2 \alpha_c \sin^2(ly) A^2 - 2l^2 \alpha_c A^2 \Big] + c.c. \\
& - 2 \frac{l}{c} (K^2 - \mu) \sin(ly) \cos(ly) (A A_T^* + A^* A_T) - \Psi_{yyT} - \Phi_T.
\end{aligned}$$

Terms on the right hand side without fast-phase oscillation lead to particular solutions which will grow linearly in t . so to avoid this secular growth, the sum of these terms must be set equal to zero. Employing the identity $A A_T^* + A^* A_T = (|A|^2)_T$, we obtain

$$\Phi_T + 2 \frac{l}{c} (K^2 - \mu) \sin(ly) \cos(ly) (|A|^2)_T = 0. \quad (4.83)$$

$$\Psi_{yyT} + \Phi_T + 2 \frac{l}{c} (K^2 - \mu) \sin(ly) \cos(ly) (|A|^2)_T = 0. \quad (4.84)$$

Forming (4.84) - (4.83), and making use of the identity $2 \sin(ly) \cos(ly) = \sin(2ly)$, results in

$$\Psi_{yyT} = 0. \quad (4.85)$$

$$\Phi_T = - \frac{l}{c} (K^2 - \mu) \sin(2ly) (|A|^2)_T. \quad (4.86)$$

We integrate both equations,

$$\Psi(y, T) = a(T)y + b(T) + d(y), \quad (4.87)$$

$$\Phi(y, T) = - \frac{l}{d} (K^2 - \mu) \sin(2ly) (|A|^2 - |A_o|^2), \quad (4.88)$$

where $a(T)$, $b(T)$ and $d(y)$ are as yet unknown, and $A_o = A(T = 0)$.

We now derive a boundary condition on Ψ_{yT} at $y = 0, L$ as follows. On either of the two boundaries, the no-normal-flow condition requires that $v \equiv 0$. Recalling that the domain is periodic in x , Kelvin's Circulation Theorem (Pedlosky, 1987) takes the form

$$\frac{d}{dt} \int_{-X}^X u_2 dx = 0 \quad \text{on } y = 0, L, \quad (4.89)$$

where the integral is over a closed curve of length $2X$. We can write this in terms of the lower layer streamfunction,

$$\frac{d}{dt} \int_{-X}^X p_y^{(0)} dx + O(\delta^{\frac{1}{2}}) = 0 \quad \text{on } y = 0, L, \quad (4.90)$$

where $p^{(0)}$ refers to the leading order term in the original expansion (2.42). This, together with the asymptotic expansion (4.18), the solutions (4.22) and (4.26), and the time scaling (4.13), yields

$$(\partial_t + s\partial_T) \int_{-X}^X \left\{ (A \sin(l y) + s\bar{p})_y \exp[ik(x - ct)] + s\Psi_y \right\} dx = 0 \quad \text{on } y = 0, L. \quad (4.91)$$

if we consider terms up to $O(s)$ in (4.18). Now, all terms associated with $\exp[ik(x - ct)]$ integrate to zero, and since Ψ has no x or t dependence, we conclude that, to leading order,

$$\Psi_{yT} = 0 \quad \text{on } y = 0, L. \quad (4.92)$$

Upon application of this condition to (4.87), we obtain $a'(T) = 0$, i.e. $a(T) = a$ is a constant for all T . Since the mean flow correction is zero when the perturbation is first introduced at $T = 0$ (Pedlosky, 1987), we find that $ay + d(y) = -b(0)$. Indeed, $ay + d(y)$ retains this value for all T , being dependent on y only, so that $\Psi = b(T) - b(0)$. Finally, since Ψ is a streamfunction, and a streamfunction is

only defined up to a constant (with respect to x and y), we can write

$$\Psi \equiv 0. \quad (4.93)$$

without loss of generality.

Upon substituting Φ and Ψ into the $O(s^2)$ problem, we consider all the terms associated with $\exp(\pm ik\theta)$. Assuming the $O(s^2)$ solutions are of the form

$$p^{(2)} = \hat{p}(y; T) \exp[ik\theta] + c.c.. \quad (4.94)$$

$$h^{(2)} = \hat{h}(y; T) \exp[ik\theta] + c.c.. \quad (4.95)$$

then dividing (4.81) by $ik\alpha_c$ and (4.82) by $-ikc$, the equations become

$$[\partial_{yy} - k^2 - \frac{c}{\alpha_c}] \hat{h} + \hat{p} = \alpha_c k^2 (y - \frac{L}{2}) \bar{\hat{h}} - \alpha_c \bar{\hat{h}}_y \quad (4.96)$$

$$\begin{aligned} & -\alpha_c (y - \frac{L}{2}) \bar{\hat{h}}_{yy} + \frac{i}{k\alpha_c} \bar{\hat{h}}_T + \frac{\delta^2}{\alpha_c} (K^2 - \mu) \sin(ly) A \\ & + 2 \frac{l^2}{\alpha_c c} (K^2 - \mu)^2 \sin(ly) \cos(2ly) A (|A|^2 - |A_o|^2) \\ & - 8 \frac{l^4}{\alpha_c c} (K^2 - \mu) \sin(ly) \cos(2ly) A (|A|^2 - |A_o|^2), \end{aligned}$$

$$\begin{aligned} & [\partial_{yy} - k^2 - \frac{\alpha_c - 1}{c}] \hat{p} + \hat{h} = \frac{i}{kc} (k^2 \bar{\hat{p}}_T - \bar{\hat{p}}_{yyT}) - \frac{i}{kc} \bar{\hat{h}}_T \\ & + \mu \frac{\delta^2}{c} \sin(ly) A - 2 \frac{l^2}{c^2} (K^2 - \mu) \sin(ly) \cos(2ly) A (|A|^2 - |A_o|^2). \end{aligned} \quad (4.97)$$

As in the $O(s)$ problem, the solvability condition is that the homogeneous solution

to (4.96) and (4.97) must be orthogonal to the inhomogeneity.

$$\begin{aligned}
& \int_0^L \left\{ \mu \alpha_c k^2 \left(y - \frac{L}{2} \right) \bar{h} - \mu \alpha_c \bar{h}_y - \mu \alpha_c \left(y - \frac{L}{2} \right) \bar{h}_{yy} + \mu \frac{i}{k \alpha_c} \bar{h}_T \right. \\
& + \mu \frac{\delta^2}{\alpha_c} (K^2 - \mu) \sin(ly) A + \frac{ik}{c} \bar{p}_T - \frac{i}{kc} \bar{p}_{yyT} - \frac{i}{kc} \bar{h}_T + \mu \frac{\delta^2}{c} \sin(ly) A \\
& \left. - 2l^2 K^4 \frac{(K^2 - 2\mu)^2}{K^2 - \mu} [4l^2 (K^2 - \mu) - K^2 (K^2 - 2\mu)] \right. \\
& \left. \times \sin(ly) \cos(2ly) A (|A|^2 - |A_o|^2) \right\} \sin(ly) A dy = 0.
\end{aligned} \tag{4.98}$$

By the *Fredholm Alternative*, this a sufficient (as well as necessary) condition for the existence of solutions to the inhomogeneous problem (4.96) and (4.97).

Now we must substitute in the following expressions: α_c and c from (4.15), as well as \bar{p} and \bar{h} from (4.64) and (4.65) (or (4.76) and (4.77), as appropriate). Having performed the integration in y , we divide through by the coefficient of A_{TT} and, after rearranging, we obtain the Amplitude Equation.

$$A_{TT} = \sigma A - N A (|A|^2 - |A_o|^2). \tag{4.99}$$

The coefficients σ and N depend on the wavenumbers k and l , and the parameter μ (in addition, σ involves the parameter δ). The expression for the nonlinear coefficient, N , may be written down easily. Substituting in the appropriate value of μ ,

$$N = k^2 l^2 \left[2 + K^2 - 4 \frac{l^2}{K^2} (K^2 + 1) \right] \quad \text{on the Lower Branch,} \tag{4.100}$$

$$N = k^2 l^2 \left[2 - K^2 + 4 \frac{l^2}{K^2} (K^2 - 1) \right] \quad \text{on the Upper Branch.} \tag{4.101}$$

Analogous expressions for the linear coefficient σ were computed symbolically

using the software package *Maple*, and may be found in Appendix B. They contain very many terms, and are more readily examined in the form of a graph. The coefficients σ and N are plotted in Figures 4.2 and 4.3 for the Lower and Upper branches respectively, with typical values of the flow parameters ($n = 1$, $L = 4$, $\delta = 1$). It is evident from both plots, that the growth rate σ is of the form prescribed by linear theory.

At this point we want to make sure that in the limit of a very small amplitude, we recover the growth rate predicted by linear theory (Chapter 3). According (4.12), which is a direct result of the dispersion relation (3.33), the growth rate kc_I should be $O(s\Delta^{\frac{1}{2}}/K^2)$, where $\Delta = \delta^2 s^2$. We see that in terms of slow time T , taking into account the scaling (4.13), $kc_I \simeq O(\delta k/K)$. Now, neglecting the nonlinear term, the amplitude equation (4.99) reduces to $A_{TT} = \sigma A$. If we also neglect all terms of $O(\alpha_c)$, then σ simplifies to $\delta^2 k^2/K^2$. This implies an exponential growth rate of $\delta k/K$, and we have recovered the linear result.

A word of explanation is also required for the vertical asymptote in the plot of σ , in Figure 4.3. The region where σ becomes unbounded corresponds to the point (2.0) on the Upper Branch of the MSC. A value of zero for the ratio s/α implies that $s \rightarrow 0$ (for α bounded) or $\alpha \rightarrow \infty$ (for s bounded), either of which clearly violates our assumption that $s \simeq O(\alpha)$. Therefore we should avoid referring to this area of the plot, since our analysis is not meaningful there. We also note, that in each graph, there is a region where $N < 0$. This has important ramifications for the behavior of the Amplitude Equation.

When $N > 0$, the nonlinear term serves to damp exponential growth. Thus, the amplitude obeys the following cycle. When the amplitude is small, the nonlinear term is negligible, and $\sigma > 0$ causes exponential growth. After a time, the nonlinear term is large enough that it begins to damp the growth of the disturbance, eventually reversing the growth altogether. The amplitude then becomes

small again, and the process repeats. On the other hand, if $N < 0$, then there is nothing to counteract the linear term, and the disturbance exhibits explosive growth. Both types of behavior will be discussed in the next section.

It is also interesting to investigate what happens when we relax the condition that terms involving α_c are very small. The effect on the coefficients σ and N is dramatic, as Figures 4.4 and 4.5 illustrate. If we let the channel width L slowly increase, this causes the growth rate σ to dip down below the k axis. This yields two new regimes, i.e. one which is linearly stable and nonlinearly unstable, and one which is stable both in the linear and nonlinear sense.

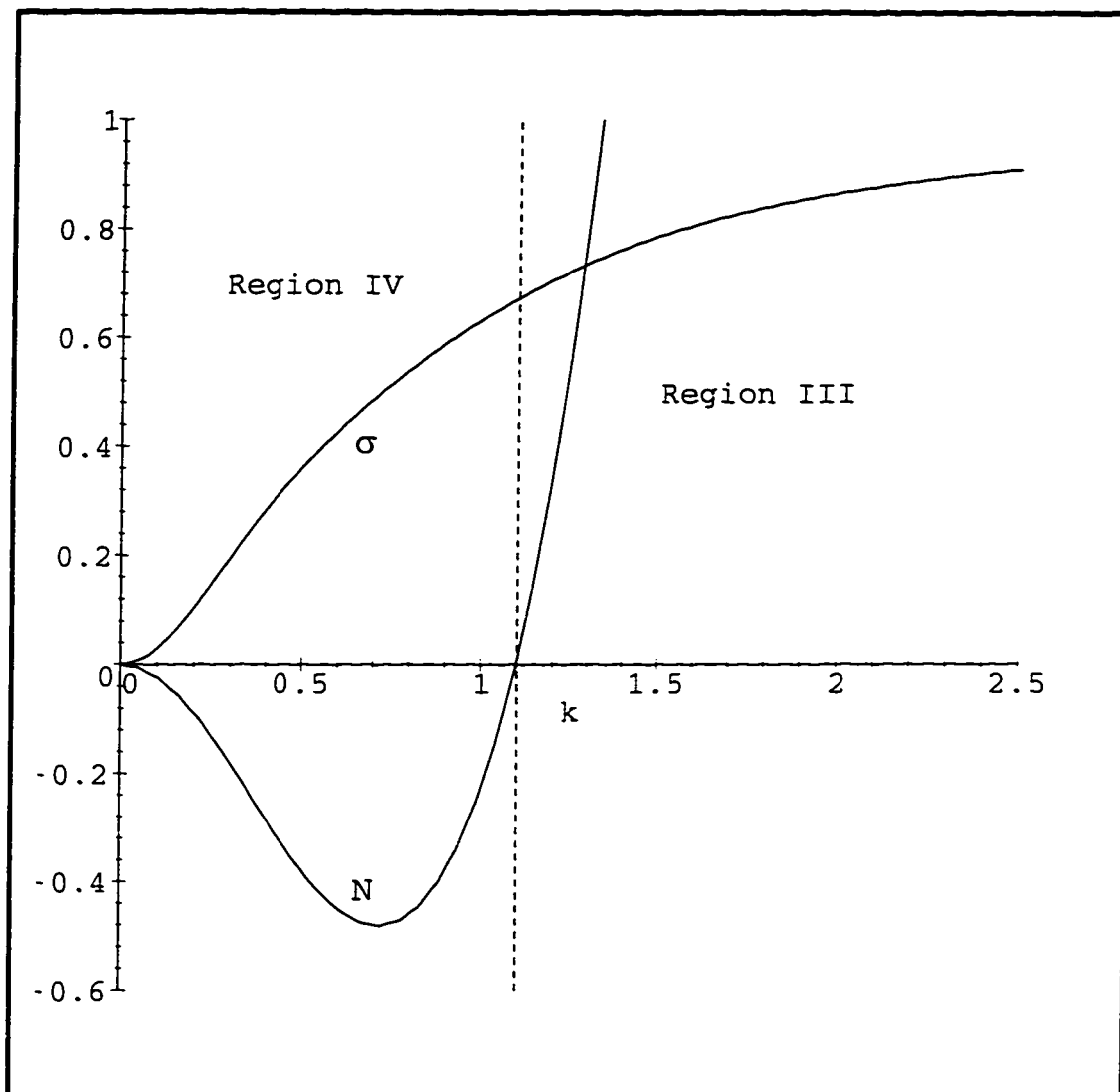


Figure 4.2: Plot of σ and N for Lower Branch of MSC, with $n = 1$, $L = 4$, $\delta = 1$.

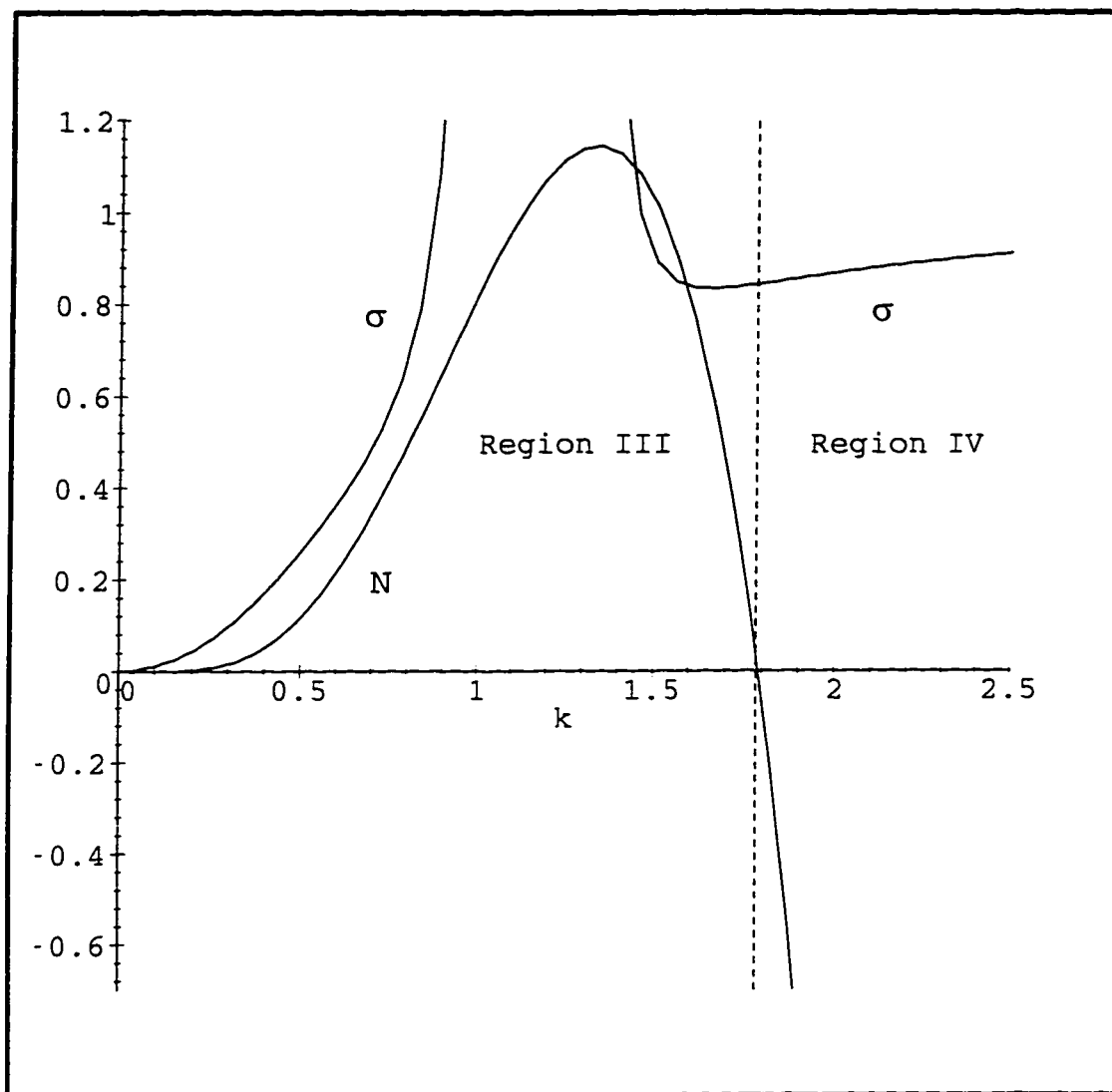


Figure 4.3: Plot of σ and N for Upper Branch of MSC, with $n = 1$, $L = 4$, $\delta = 1$.

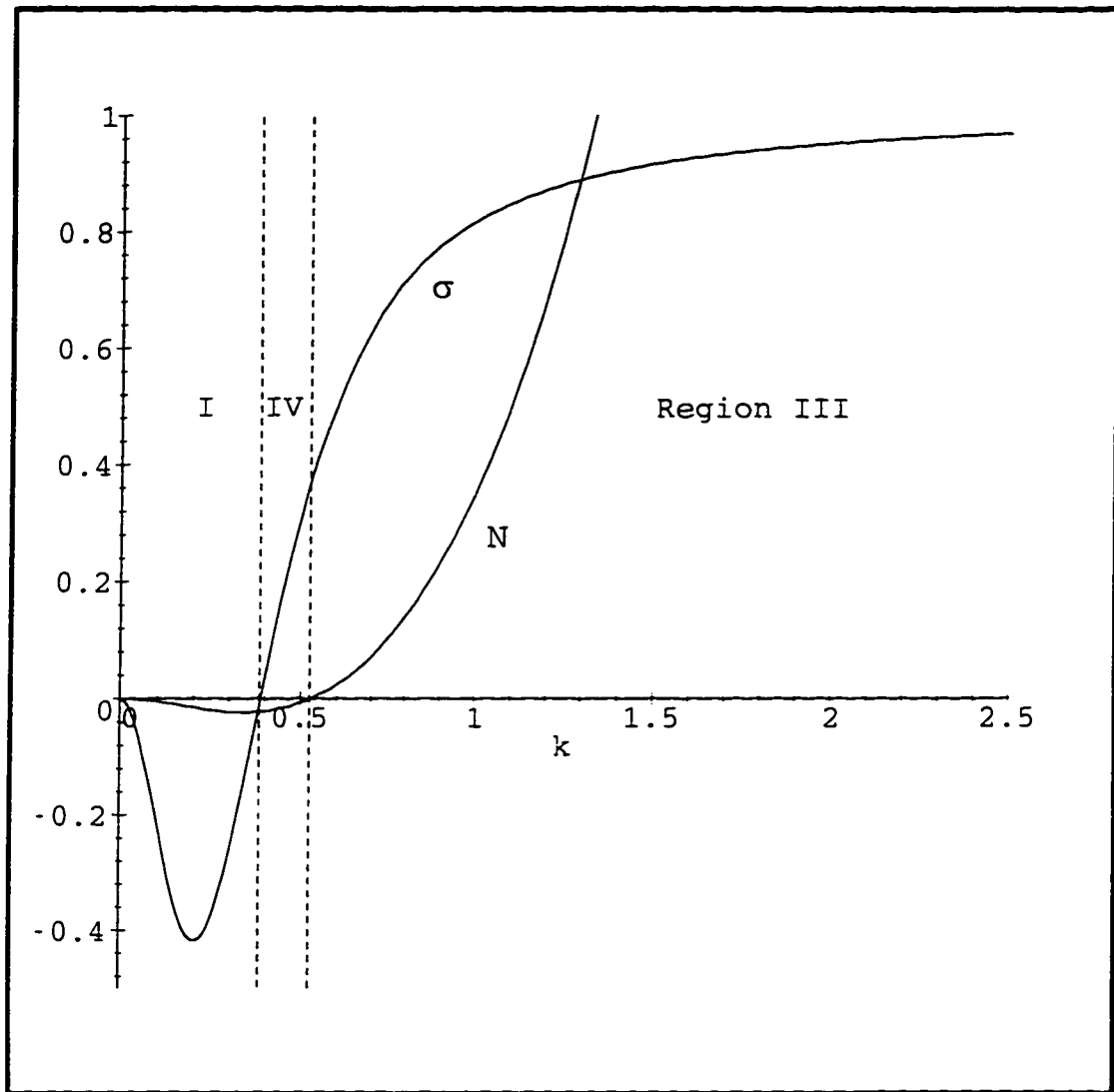


Figure 4.4: Plot of σ and N for Lower Branch of MSC, with $n = 1$, $L = 7$, $\delta = 1$.

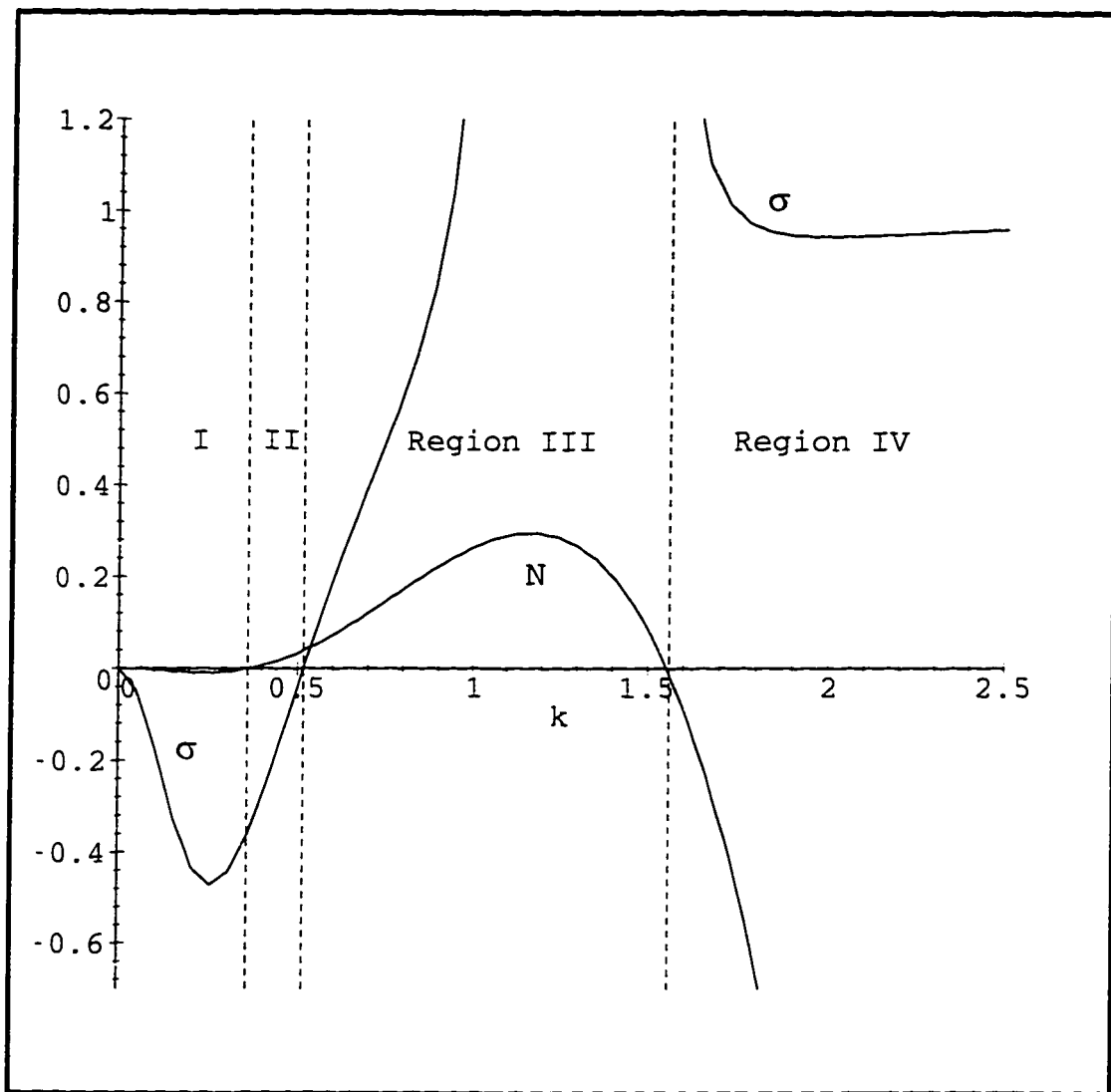


Figure 4.5: Plot of σ and N for Upper Branch of MSC, with $n = 1$, $L = 6$, $\delta = 1$.

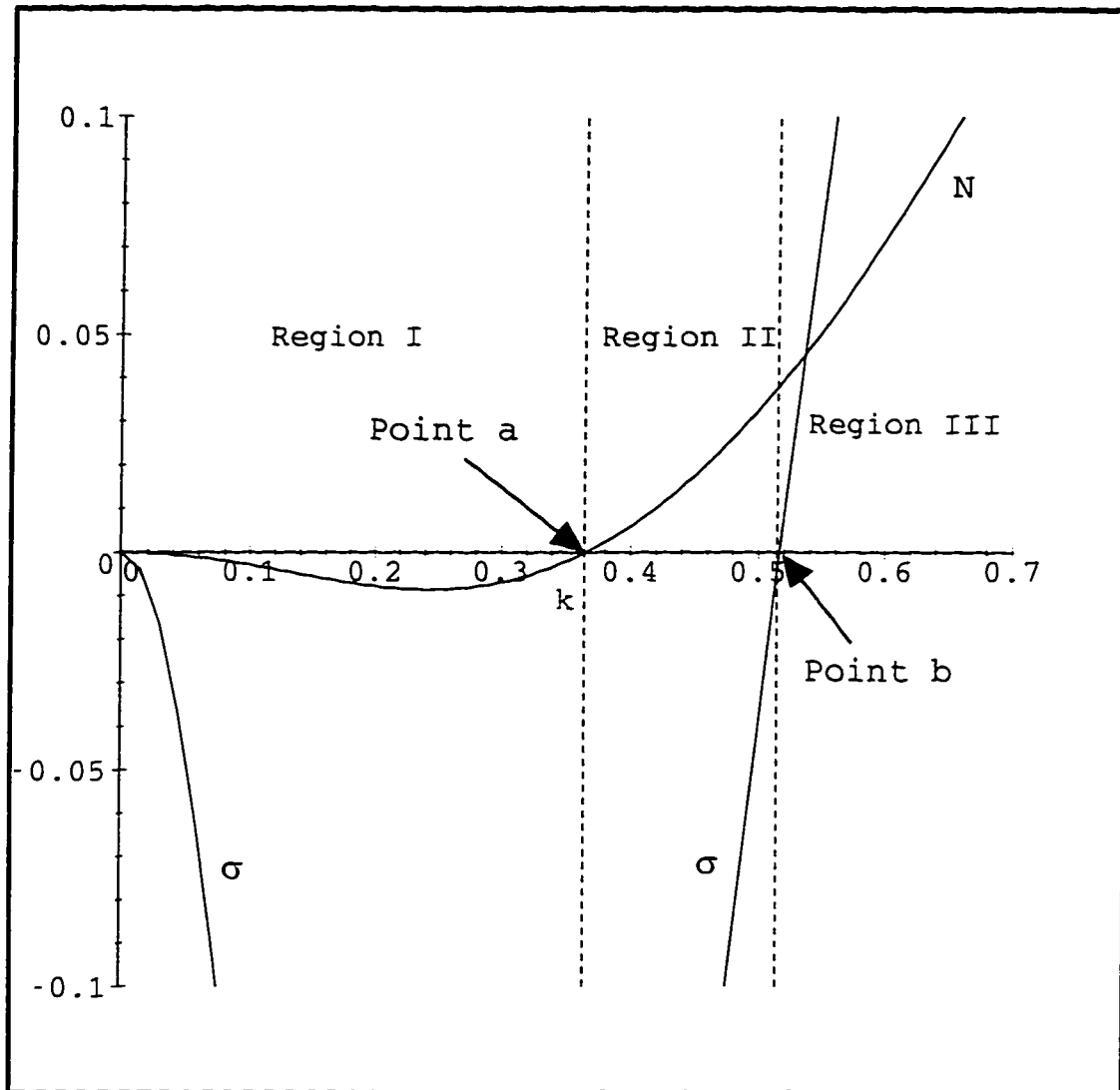


Figure 4.6: Zoom-in of Figure 4.5, with points a and b labeled.

4.3 Solutions to the Amplitude Equation

To obtain solutions to (4.99), we follow Pedlosky (1987). The amplitude A is written in the form

$$A(T) = R(T) \exp[i\Theta(T)], \quad (4.102)$$

where R is real and Θ is the phase in slow time T . Substituting this into (4.99) and separating real and imaginary parts,

$$\Theta_T = \frac{M}{R^2}, \quad (4.103)$$

$$R_{TT} - \frac{M}{R^3} = \sigma R - NR(R^2 - R_o^2). \quad (4.104)$$

where M is constant and $R_o = R(0)$. If we assume that Θ does not vary with time, then necessarily $M = 0$ and (4.104) reduces to

$$R_{TT} = \sigma R - NR(R^2 - R_o^2). \quad (4.105)$$

We will also make use of the initial condition

$$\frac{dR}{dT}(0) = \sqrt{|\sigma|} R_o. \quad (4.106)$$

which means that initially the amplitude grows at the linear growth rate. Multiplying equation (4.105) by R_T and integrating, we may rewrite it as

$$R_T^2 = \sigma R^2 + (|\sigma| - \sigma) R_o^2 - \frac{N}{2} (R^2 - R_o^2)^2. \quad (4.107)$$

4.3.1 Region I

We now discuss the cases when the α_c terms are not negligible. according to Figure 4.5. In Region I. $\sigma < 0$ and $N < 0$, so that, after a little algebra. equation (4.107) becomes

$$R_\tau^2 = -\frac{N}{2}(R^2 - R_o^2 - \frac{\sigma}{N})^2 - \sigma(R_o^2 - \frac{\sigma}{2N}). \quad (4.108)$$

We define the following transformation.

$$R = \sqrt{\frac{2\sigma}{N}}P, \quad R_o = \sqrt{\frac{2\sigma}{N}}P_o, \quad T = \frac{\tau}{\sqrt{-\sigma}}, \quad (4.109)$$

and after simplification. (4.108) can be written

$$P_\tau^2 = (P^2 - P_o^2 - \frac{1}{2})^2 + P_o^2 - \frac{1}{4}. \quad (4.110)$$

This problem splits up into three cases. i.e. $P_o^2 = \frac{1}{4}$. $P_o^2 < \frac{1}{4}$ and $P_o^2 > \frac{1}{4}$.

Case 1: $P_o^2 = \frac{1}{4}$

Equation (4.110) reduces to

$$P_\tau^2 = (P^2 - \frac{3}{4})^2. \quad (4.111)$$

First let us assume that $P_o = \frac{1}{2}$. Then $P_\tau(0) = \frac{1}{2} > 0$. We will show *a posteriori* that $|P| \leq \frac{\sqrt{3}}{2}$, which allows us to conclude

$$P_\tau = \left| P^2 - \frac{3}{4} \right| = -(P^2 - \frac{3}{4}). \quad (4.112)$$

Using separation of variables,

$$\int_{P_o}^P \frac{d\xi}{\xi^2 - \frac{3}{4}} = - \int_0^\tau d\tau, \quad (4.113)$$

then integrating both sides and substituting $P_o = \frac{1}{2}$, we obtain

$$\tau = \frac{1}{\sqrt{3}} \ln \left| \frac{\sqrt{3} + 2P}{\sqrt{3} - 2P} \frac{\sqrt{3} - 1}{\sqrt{3} + 1} \right|. \quad (4.114)$$

It is now possible to solve for $P(\tau)$

$$P(\tau) = \left(\frac{\sqrt{3}}{2} \right) \frac{1 - \sqrt{3} + (1 + \sqrt{3}) \exp[\sqrt{3}\tau]}{\sqrt{3} - 1 + (1 + \sqrt{3}) \exp[\sqrt{3}\tau]}. \quad (4.115)$$

We note that $P(0) = \frac{1}{2}$ as we required and $|P| \leq \frac{\sqrt{3}}{2}$ as we assumed. Also, it is interesting to point out that this solution monotonically approaches the constant value $\frac{\sqrt{3}}{2}$ as $\tau \rightarrow \infty$.

The argument is almost exactly the same for $P_o = -\frac{1}{2}$ and the solution is found to be

$$P(\tau) = - \left(\frac{\sqrt{3}}{2} \right) \frac{1 - \sqrt{3} + (1 + \sqrt{3}) \exp[\sqrt{3}\tau]}{\sqrt{3} - 1 + (1 + \sqrt{3}) \exp[\sqrt{3}\tau]}. \quad (4.116)$$

which approaches $-\frac{\sqrt{3}}{2}$ as $\tau \rightarrow \infty$.

Case2: $P_o^2 < \frac{1}{4}$

In this case the constant term $P_o^2 - \frac{1}{4}$ is negative, and (4.110) may be viewed as a difference of squares. Decomposing the right hand side into two factors,

$$P_\tau^2 = (\beta^2 - P^2)(\zeta^2 - P^2), \quad (4.117)$$

where

$$\beta^2 = P_o^2 + \frac{1}{2} + \sqrt{\frac{1}{4} - P_o^2} > 0, \quad (4.118)$$

and

$$\zeta^2 = P_o^2 + \frac{1}{2} - \sqrt{\frac{1}{4} - P_o^2} > 0. \quad (4.119)$$

For convenience, let us take β and ζ (without loss of generality) to be positive

quantities and define

$$P = \beta Q, \quad P_o = \beta Q_o. \quad (4.120)$$

Then (4.117) becomes

$$Q_\tau^2 = \beta^2(1 - Q^2)(m^2 - Q^2), \quad (4.121)$$

with

$$m = \frac{\zeta}{\beta}, \quad (4.122)$$

and $0 < m < 1$.

Let us first deal with the possibility that $P_o > 0$, i.e. that $P_\tau(0) > 0$. It is evident from (4.121) that $|Q| \leq m$ always holds, so that

$$Q_\tau = \beta \sqrt{(1 - Q^2)(m^2 - Q^2)}. \quad (4.123)$$

which we rewrite as

$$\int_{Q_o}^Q \frac{d\xi}{\sqrt{(1 - \xi^2)(m^2 - \xi^2)}} = \beta \int_0^\tau d\tau. \quad (4.124)$$

This elliptic integral yields the solution (Milne-Thomson, 1950),

$$Q = m \operatorname{sn}(\beta(\tau - \tau_o) | m^2), \quad (4.125)$$

where $\operatorname{sn}(\)$ refers to the Jacobi elliptic snoidal function and τ_o is given by

$$\tau_o = -\frac{1}{\beta} \int_0^{Q_o} \frac{d\xi}{\sqrt{(1 - \xi^2)(m^2 - \xi^2)}}. \quad (4.126)$$

If $P_o < 0$, a similar argument produces the solution

$$Q = -m \operatorname{sn} (\beta(\tau - \tau_o)|m^2), \quad (4.127)$$

with

$$\tau_o = \frac{1}{\beta} \int_0^{Q_o} \frac{d\xi}{\sqrt{(1 - \xi^2)(m^2 - \xi^2)}}. \quad (4.128)$$

The solution (4.125) is plotted, for typical values of the parameters, in Figure 4.7 versus slow time T . We see that this snoidal wave oscillates in a sinusoidal manner about zero, with a short period (about 0.2) and $O(1)$ maximum amplitude.

Case 3: $P_o^2 > \frac{1}{4}$

This third case introduces the possibility of explosive growth of the disturbance. We will first show that the solution is unbounded, and then show that the solution becomes arbitrarily large in a finite time. Since $P_o^2 - \frac{1}{4}$ is a positive quantity bounded away from zero, so is the right hand side of (4.110). Taking the square root of both sides leads to the conclusion that P monotonically tends to ∞ or $-\infty$, depending on the value of $P_\tau(0)$. In the following proof we assume that $P_\tau(0) > 0$. The argument is similar for $P_\tau(0) < 0$.

Claim: P becomes arbitrarily large in finite time, if $P_o^2 > \frac{1}{4}$.

Proof: P grows monotonically, without bound. We may express the time required for $P \rightarrow \infty$ as the integral

$$\tau^* = \int_{P_o}^{\infty} \frac{dP}{\sqrt{(P^2 - P_o^2 - \frac{1}{2})^2 + P_o^2 - \frac{1}{4}}}. \quad (4.129)$$

Now, τ^* satisfies

$$\tau^* = \int_{P_o}^{P^*} \frac{dP}{\sqrt{(P^2 - P_o^2 - \frac{1}{2})^2 + P_o^2 - \frac{1}{4}}} + \int_{P^*}^{\infty} \frac{dP}{\sqrt{(P^2 - P_o^2 - \frac{1}{2})^2 + P_o^2 - \frac{1}{4}}}. \quad (4.130)$$

for some $P^* > \sqrt{P_o^2 + \frac{1}{2}}$. Therefore.

$$\tau^* < I_1 + I_2, \quad (4.131)$$

where

$$I_1 = \int_{P_o}^{P^*} \frac{dP}{\sqrt{(P^2 - P_o^2 - \frac{1}{2})^2 + P_o^2 - \frac{1}{4}}} \quad (4.132)$$

is finite, since the radicand is never zero, and

$$I_2 = \int_{P^*}^{\infty} \frac{dP}{|P^2 - P_o^2 - \frac{1}{2}|}. \quad (4.133)$$

Because $P^2 - P_o^2 - \frac{1}{2} > 0$ for all $P \geq P^*$, we can remove the absolute value signs and easily integrate I_2 :

$$\begin{aligned} I_2 &= \lim_{l \rightarrow \infty} \int_{P^*}^l \frac{dP}{P^2 - a^2} \quad \text{where } a^2 = P_o^2 + \frac{1}{2} \\ &= \lim_{l \rightarrow \infty} \frac{1}{2a} \ln \left| \frac{l-a}{l+a} \right| - \frac{1}{2a} \ln \left| \frac{P^*-a}{P^*+a} \right| \\ &= \frac{1}{2a} \ln(1) - \frac{1}{2a} \ln \left| \frac{P^*-a}{P^*+a} \right| \\ &= \frac{1}{2a} \ln \left| \frac{P^*+a}{P^*-a} \right| < \infty. \end{aligned} \quad (4.134)$$

Now, since I_1 and I_2 are finite, this implies that τ^* is finite. **QED**

A similar result was found by Meacham (1988) in his analysis of a resonant triad of neutral Rossby waves in a marginally unstable, baroclinic flow. This finite amplitude study was done in the context of the Phillips (Pedlosky, 1987) model. Unbounded growth in finite time is clearly unphysical, and we may ask what are the implications of such a finding. One of two possibilities arises. The first is that an assumption of weakly nonlinear theory no longer holds, and the explosive growth is a spurious result. The second possibility is that the rapid

growth is real, but after the perturbation amplitude is no longer small (as we assumed) weakly nonlinear analysis breaks down and other effects may come into play. Fully nonlinear interactions may halt the growth, but this is beyond the small-amplitude regime we are studying.

The latter possibility seems very likely in this case. For unbounded growth to occur, the initial scaled amplitude must be greater than some threshold value, i.e. $P_o^2 > \frac{1}{4}$. Since, by (4.106), the initial kinetic energy $\frac{1}{2}R_T(0)$ is directly related to the initial unscaled amplitude R_o , it is reasonable that with a high enough input of energy the system would enter a more nonlinear state. At that point, the methodology described here can no longer provide a sensible picture of flow development. However, the onset of unbounded growth in the weakly nonlinear sense is noteworthy, because it pinpoints conditions under which the flow can deform dramatically in a very short time. This behavior will again be discussed in relation to Region IV. We present two plots of τ^* versus P_o in Figure 4.8.

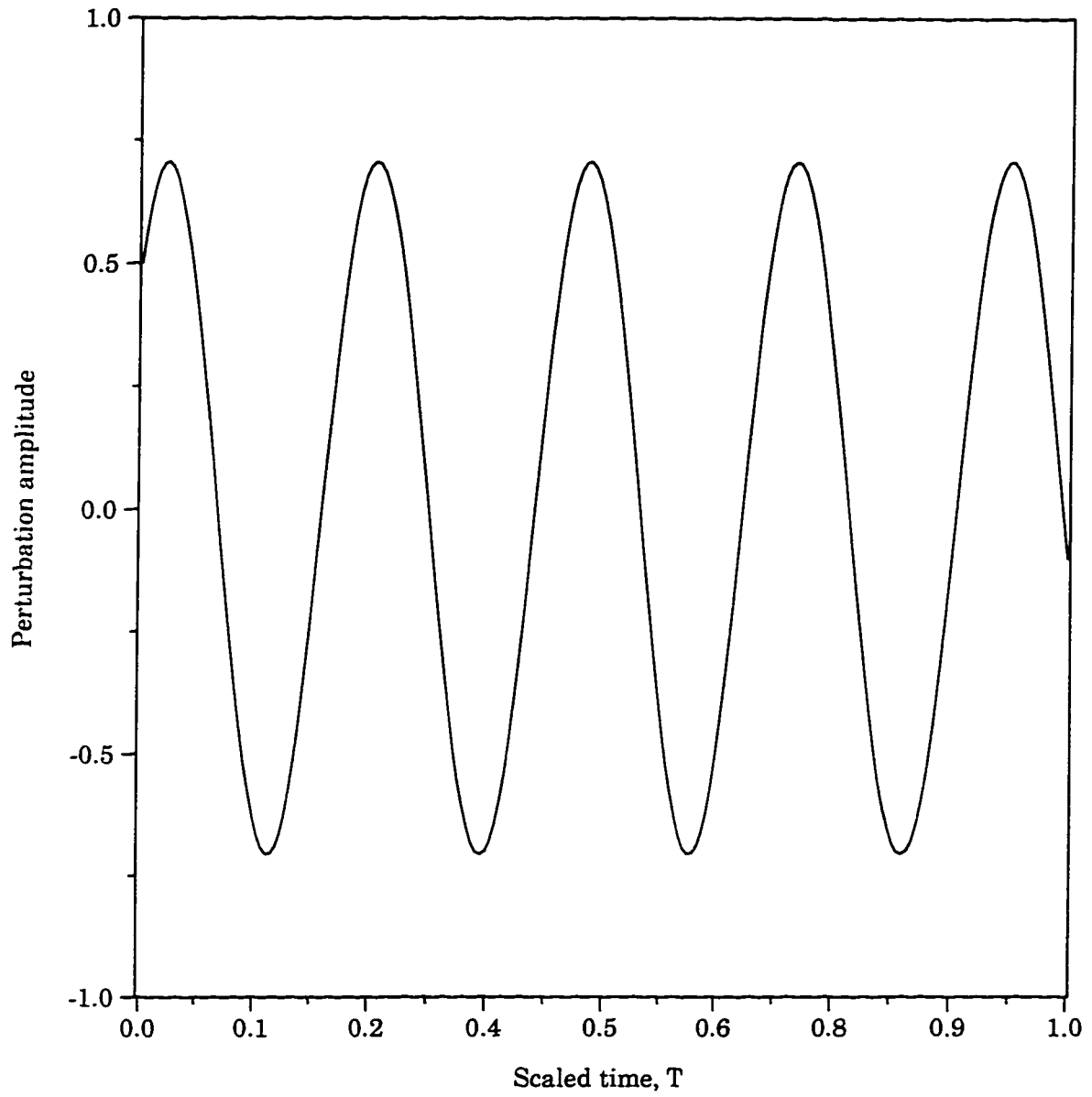


Figure 4.7: Snoidal wave solution at $k=0.1$ in Region I, corresponding to Lower Branch of MSC with $n=1$, $\delta=1$, $L=8$.

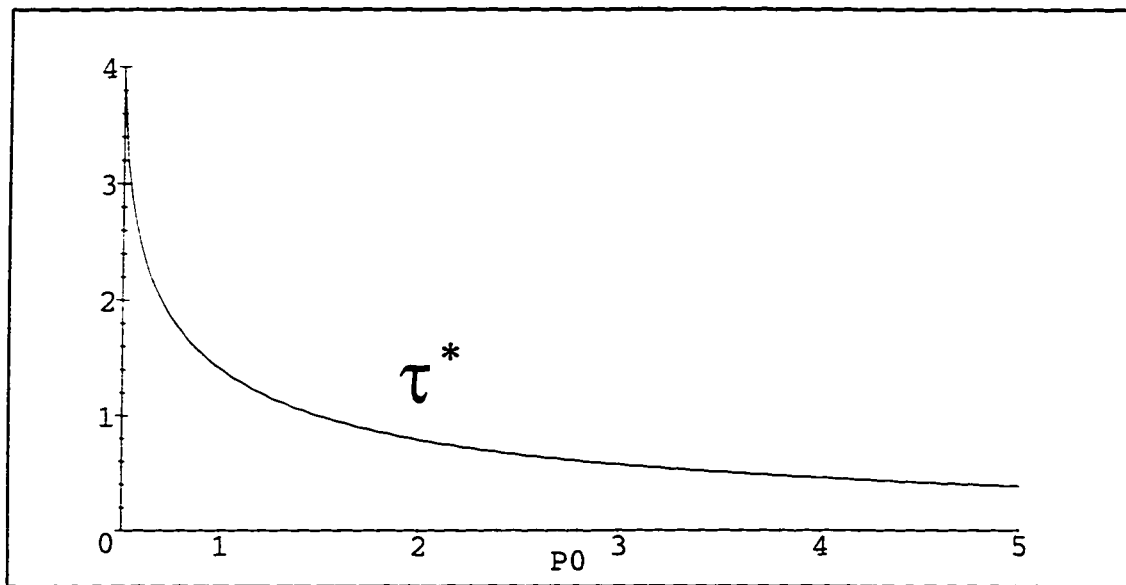
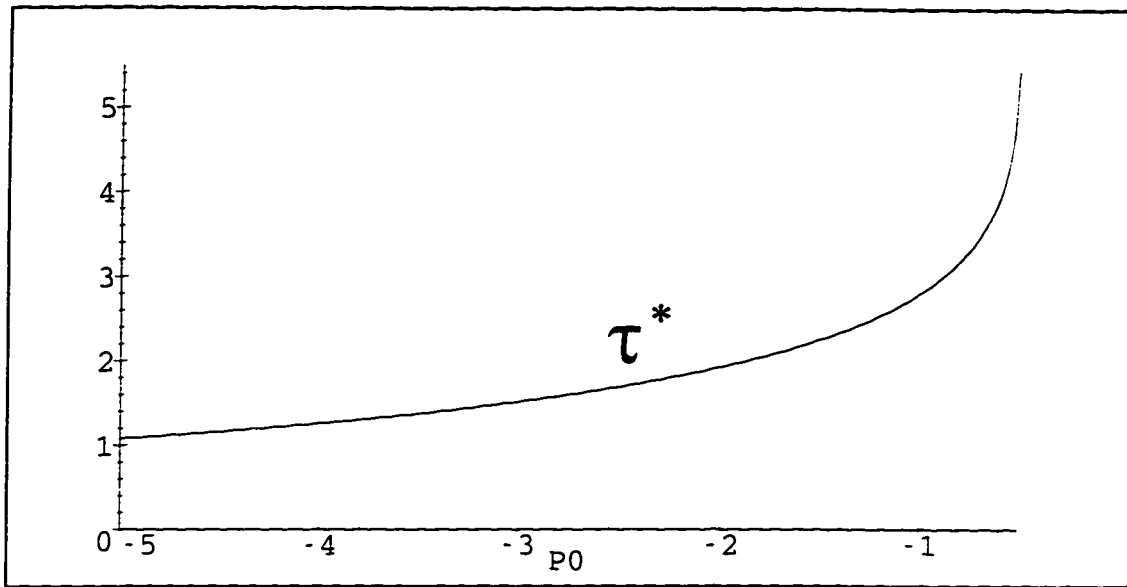


Figure 4.8: Time required for blow-up of solution in Region I.

4.3.2 Region II

Here $\sigma < 0$, $N > 0$. Equation (4.107) becomes

$$R_T^2 = -\frac{N}{2}(R^2 - R_o^2 - \frac{\sigma}{N})^2 - \sigma(R_o^2 - \frac{\sigma}{2N}). \quad (4.135)$$

We define the following transformation,

$$R = \sqrt{-\frac{2\sigma}{N}}P, \quad R_o = \sqrt{-\frac{2\sigma}{N}}P_o, \quad T = \frac{\tau}{\sqrt{-\sigma}}. \quad (4.136)$$

and after simplification, (4.135) can be written

$$P_\tau^2 = P_o^2 + \frac{1}{4} - (P^2 - P_o^2 + \frac{1}{2})^2. \quad (4.137)$$

Since $P_o^2 + \frac{1}{4}$ is strictly positive, we can immediately write the right hand side in factored form

$$P_\tau^2 = (P^2 + \sqrt{P_o^2 + \frac{1}{4}} - P_o^2 + \frac{1}{2})(\sqrt{P_o^2 + \frac{1}{4}} + P_o^2 - \frac{1}{2} - P^2). \quad (4.138)$$

Because $\sqrt{P_o^2 + \frac{1}{4}} + P_o^2 - \frac{1}{2} > 0$, the problem now hinges on the sign of $\sqrt{P_o^2 + \frac{1}{4}} - P_o^2 + \frac{1}{2}$, i.e. whether $P_o^2 = 2$, $P_o^2 < 2$ or $P_o^2 > 2$.

Case 1: $P_o^2 = 2$

Equation (4.137) reduces to

$$\begin{aligned} P_\tau^2 &= \frac{9}{4} - (P^2 - \frac{3}{2})^2 \\ &= P^2(3 - P^2). \end{aligned} \quad (4.139)$$

Defining

$$P = \sqrt{3}Q, \quad P_o = \sqrt{3}Q_o, \quad (4.140)$$

and using separation of variables, we find that

$$\int_{Q_o}^Q \frac{d\xi}{\sqrt{\xi^2(1-\xi^2)}} = \sqrt{3} \int_0^\tau d\tau. \quad (4.141)$$

We make the change of variable

$$\xi = \sin \theta, \quad d\xi = \cos \theta d\theta, \quad (4.142)$$

and obtain

$$\begin{aligned} \tau &= -\frac{1}{\sqrt{3}} \ln |\csc \theta - \cot \theta| + \text{const} \\ &= -\frac{1}{\sqrt{3}} \ln \left| \frac{1 + \sqrt{1 - \xi^2}}{\xi} \right|_{Q_o}^Q. \end{aligned} \quad (4.143)$$

but since

$$Q_o = \frac{1}{\sqrt{3}} P_o = \sqrt{\frac{2}{3}}. \quad (4.144)$$

we can write

$$\exp[-\sqrt{3}\tau] = \frac{1 + \sqrt{1 - Q^2}}{Q} \frac{\sqrt{2}/\sqrt{3}}{1 + \sqrt{1 - 2/3}}. \quad (4.145)$$

where we have taken the exponential of both sides. After some algebra, it is possible to solve for Q

$$Q = \sqrt{2} \left(\left(\frac{\sqrt{3} - 1}{2} \right) \exp[\sqrt{3}\tau] + \left(\frac{\sqrt{3} + 1}{2} \right) \exp[-\sqrt{3}\tau] \right)^{-1}. \quad (4.146)$$

and $P(\tau)$ is given by (4.140).

Case2: $P_o^2 < 2$

In this case the decomposition of the right hand side of (4.137) takes the form

$$P_\tau^2 = (P^2 + \zeta^2)(\beta^2 - P^2). \quad (4.147)$$

where

$$\beta^2 = P_o^2 - \frac{1}{2} + \sqrt{P_o^2 + \frac{1}{4}} > 0, \quad (4.148)$$

and

$$\zeta^2 = -P_o^2 + \frac{1}{2} + \sqrt{P_o^2 + \frac{1}{4}} > 0. \quad (4.149)$$

If we substitute the transformation

$$P = \beta Q, \quad P_o = \beta Q_o. \quad (4.150)$$

then (4.147) becomes

$$Q_\tau^2 = \beta^2(Q^2 + m^2)(1 - Q^2), \quad (4.151)$$

with

$$m = \frac{\zeta}{\beta}. \quad (4.152)$$

and $0 < m < 1$.

We take the square root of both sides, and write (4.151) as the integral

$$\int_{Q_o}^Q \frac{d\xi}{\sqrt{(\xi^2 + m^2)(1 - \xi^2)}} = \beta \int_0^\tau d\tau. \quad (4.153)$$

This elliptic integral yields the solution (Milne-Thomson, 1950),

$$Q = \text{cn} \left(\sqrt{m^2 + 1} \beta (\tau - \tau_o) \middle| \frac{1}{m^2 + 1} \right). \quad (4.154)$$

where $\text{cn}(\cdot)$ refers to the Jacobi elliptic cnoidal function and τ_o is given by

$$\tau_o = \frac{1}{\beta\sqrt{m^2+1}} \int_{Q_o}^1 \frac{d\xi}{\sqrt{(\xi^2+m^2)(1-\xi^2)}}. \quad (4.155)$$

A graph of the solution (4.154) versus slow time T can be seen in Figure 4.9. As in the case of the snoidal wave, this cnoidal function oscillates about zero. Its period and amplitude are both $O(1)$ quantities.

Case 3: $P_o > 2$

In this third case we write

$$P_\tau^2 = (P^2 - \zeta^2)(\beta^2 - P^2), \quad (4.156)$$

where

$$\beta^2 = P_o^2 - \frac{1}{2} + \sqrt{P_o^2 + \frac{1}{4}} > 0. \quad (4.157)$$

and

$$\zeta^2 = P_o^2 - \frac{1}{2} - \sqrt{P_o^2 + \frac{1}{4}} > 0. \quad (4.158)$$

If we substitute the transformation

$$P = \beta Q, \quad P_o = \beta Q_o, \quad (4.159)$$

then (4.156) becomes

$$Q_\tau^2 = \beta^2(Q^2 - m^2)(1 - Q^2), \quad (4.160)$$

with

$$m = \frac{\zeta}{\beta}, \quad (4.161)$$

and $0 < m < 1$.

We take the square root of both sides, and write (4.160) as the integral

$$\int_{Q_o}^Q \frac{d\xi}{\sqrt{(\xi^2 - m^2)(1 - \xi^2)}} = \beta \int_0^\tau d\tau. \quad (4.162)$$

This elliptic integral yields the solution (Milne-Thomson, 1950),

$$Q = \mathbf{dn}(\beta(\tau - \tau_o)|1 - m^2), \quad (4.163)$$

where $\mathbf{dn}(\)$ refers to the Jacobi elliptic dnoidal function and τ_o is given by

$$\tau_o = \frac{1}{\beta} \int_{Q_o}^1 \frac{d\xi}{\sqrt{(\xi^2 - m^2)(1 - \xi^2)}}. \quad (4.164)$$

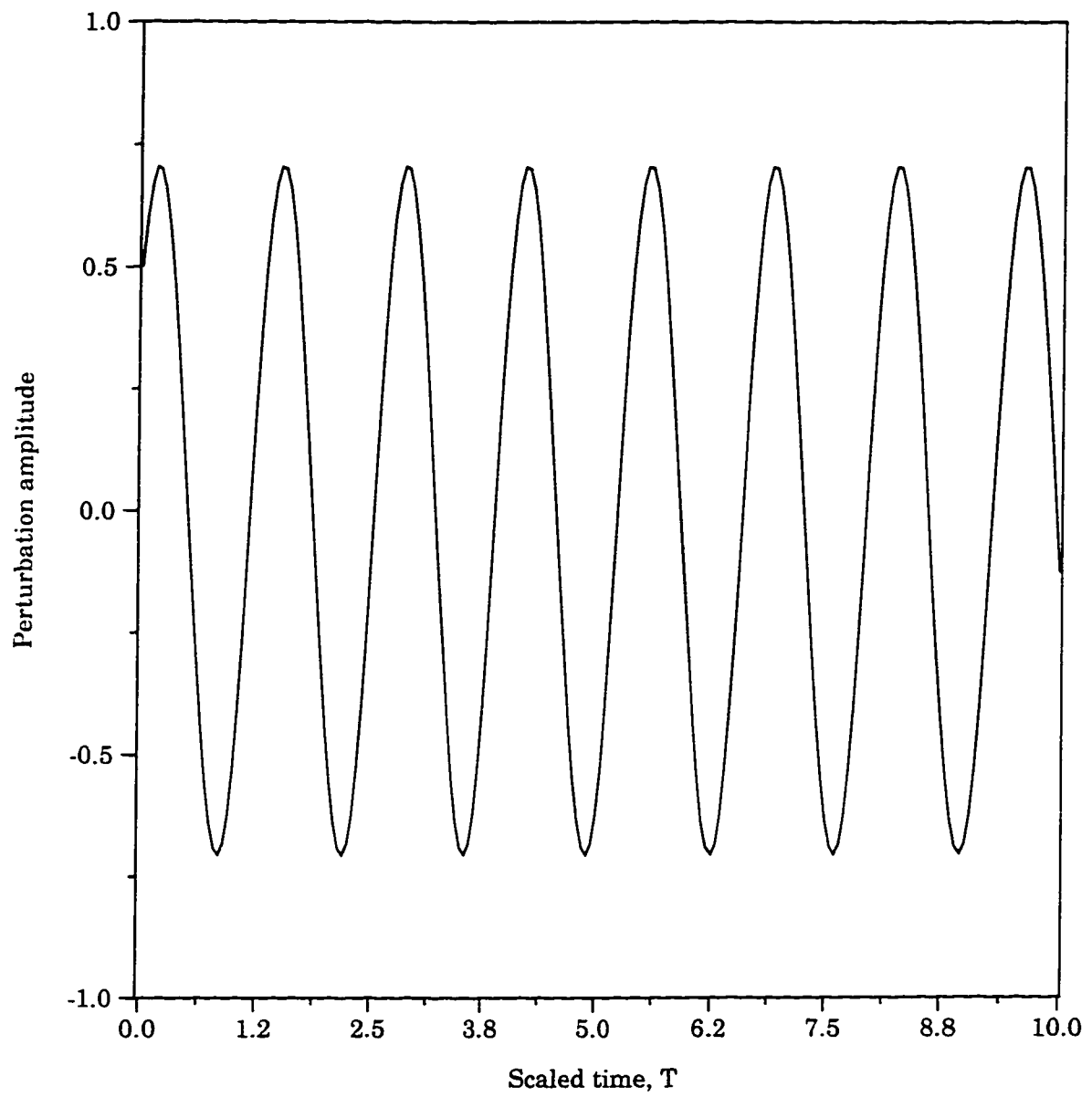


Figure 4.9: Cnoidal wave solution at $k=0.5$ in Region II, corresponding to Lower Branch of MSC with $n=1$, $\delta=1$, $L=8$.

4.3.3 Region III

Region III covers most of the wavenumber spectrum in Figure 4.3. Here both σ and N are positive. Let us first apply the transformation

$$R = \sqrt{\frac{2\sigma}{N}}P, \quad R_o = \sqrt{\frac{2\sigma}{N}}P_o, \quad T = \frac{\tau}{\sqrt{\sigma}}. \quad (4.165)$$

so that (4.107) becomes

$$P_\tau^2 = -P^4 + (2P_o^2 + 1)P^2 - P_o^4. \quad (4.166)$$

We can proceed toward the solution mechanically, as for previous regions, however at this point we choose to present a more physically meaningful argument. If R is thought of as displacement, then (4.105) is a special case of the equation governing the rectilinear motion of a particle under the action of a restoring force, which depends on displacement only (Ross, 1974). Then, it is possible to view the above equation as a decomposition of total energy, E , into kinetic energy, $\frac{1}{2}P_\tau^2$, and potential energy, $V(P)$.

$$E = \frac{1}{2}P_\tau^2 + V(P), \quad (4.167)$$

where $E = -\frac{1}{2}P_o^4$ is a constant and $V(P) = \frac{1}{2}P^4 - (P_o^2 + \frac{1}{2})P^2$.

To determine the maximum and minimum values of P for this harmonic oscillator, we demand that the total energy consist only of potential energy, or equivalently, we set the kinetic energy $\frac{1}{2}P_\tau^2$ equal to zero. By virtue of (4.166), this means that

$$-P^4 + (2P_o^2 + 1)P^2 - P_o^4 = 0. \quad (4.168)$$

By the quadratic formula,

$$P_{\max}^2, P_{\min}^2 = (P_o^2 + \frac{1}{2}) \pm \frac{1}{2} \sqrt{4P_o^2 + 1}, \quad (4.169)$$

which allows us to write (4.166) in the factored form,

$$P_{\tau}^2 = -(P^2 - P_{\max}^2)(P^2 - P_{\min}^2). \quad (4.170)$$

For convenience, we introduce the normalized amplitude

$$Q = \frac{P}{P_{\max}}. \quad (4.171)$$

a scaled time

$$\tau' = P_{\max} \tau. \quad (4.172)$$

and the quantity β , defined as

$$\beta = \frac{P_{\min}}{P_{\max}}. \quad (4.173)$$

so that (4.170) becomes

$$\left(\frac{dQ}{d\tau'}\right)^2 = (1 - Q^2)(Q^2 - \beta^2). \quad (4.174)$$

i.e.

$$d\tau' = \frac{dQ}{\sqrt{(1 - Q^2)(Q^2 - \beta^2)}}. \quad (4.175)$$

The problem is now posed in the form of an elliptic integral

$$\tau' - \tau'_o = \int_{Q_o}^Q \frac{dQ}{\sqrt{(1 - Q^2)(Q^2 - \beta^2)}}, \quad (4.176)$$

which yields the Jacobi elliptic dnoidal function (Milne-Thomson, 1950)

$$Q = \text{dn} (\tau' - \tau'_o | 1 - \beta^2), \quad (4.177)$$

where the phase shift τ'_o ensures that $P_o = P(0)$ and is given by

$$\tau'_o = \int_{Q_o}^1 \frac{dQ}{\sqrt{(1 - Q^2)(Q^2 - \beta^2)}}. \quad (4.178)$$

Finally, the solution to (4.107) is

$$R = \sqrt{\frac{2\sigma}{N}} P_{\max} \text{dn} (\tau' - \tau'_o | 1 - \beta^2). \quad (4.179)$$

with P_{\max} defined above.

The solution (4.177) is plotted, for typical values of the parameters, in Figure 4.10 versus slow time T . We see that, unlike snoidal and cnoidal wave solutions, the dnoidal wave oscillates about some positive quantity and never crosses zero. Also, the pattern of the oscillation is such that the peaks are fairly sharp and the troughs rather gentle. Finally, while the amplitude of the solution is $O(1)$, the period is markedly longer than in the previous two cases.

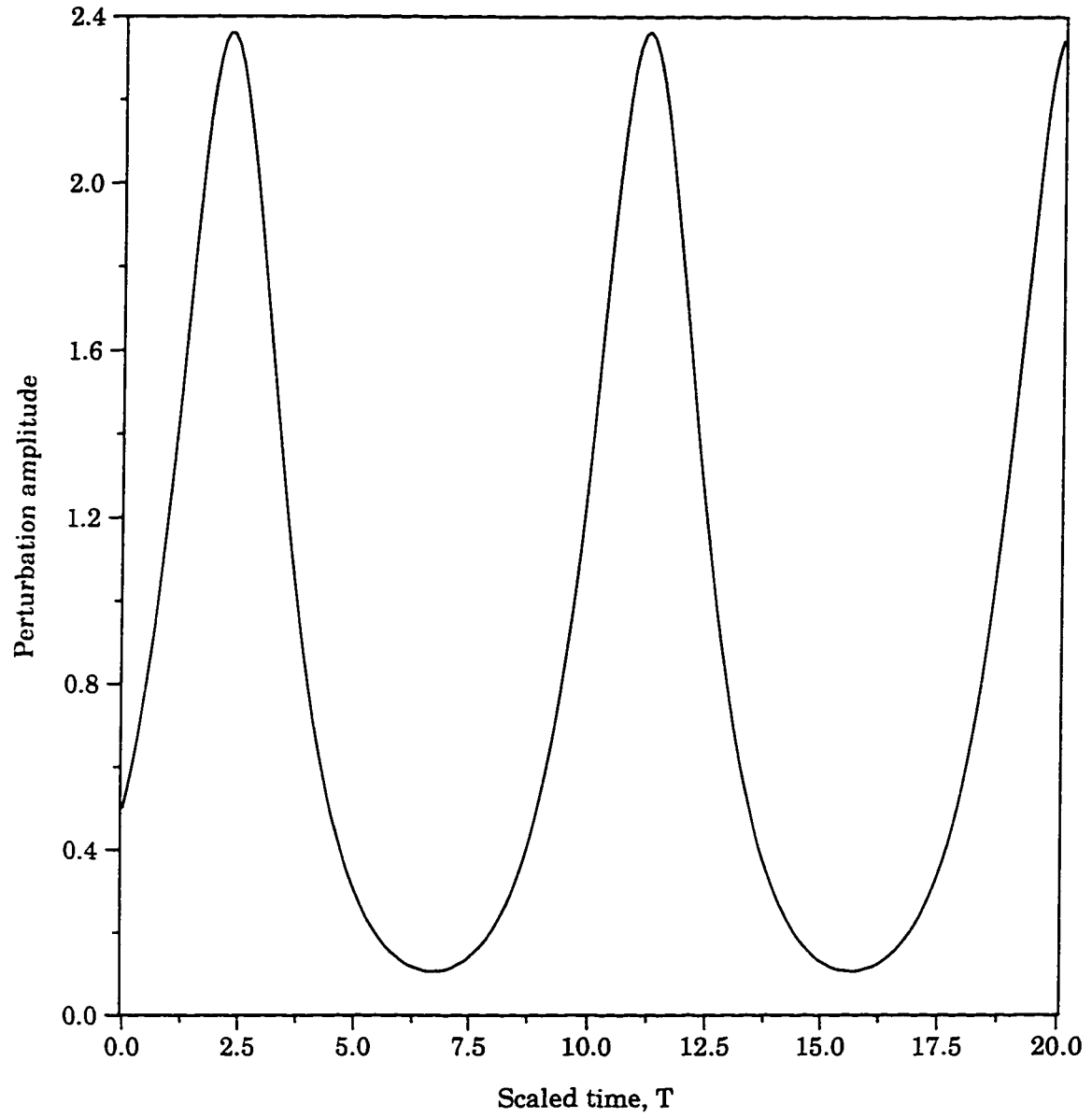


Figure 4.10: Dnoidal wave solution at $k=1.5$ in Region III, corresponding to Lower Branch of MSC with $n=1$, $\delta=1$, $L=8$.

4.3.4 Region IV:

This pathological case, which occurs for small k in Figure 4.2 and large k in Figure 4.3, yields explosive growth of the perturbation. Unlike in Region I, this growth does not require that the initial amplitude be above some threshold value. Since $\sigma > 0$ and $N < 0$, we define the transformation

$$R = \sqrt{-\frac{2\sigma}{N}}P, \quad R_o = \sqrt{-\frac{2\sigma}{N}}P_o, \quad T = \frac{\tau}{\sqrt{\sigma}}. \quad (4.180)$$

which allows (4.107) to be written

$$P_\tau^2 = (P^2 - P_o^2 + \frac{1}{2})^2 + P_o^2 - \frac{1}{4}. \quad (4.181)$$

If $P_o^2 > \frac{1}{4}$ then both terms on the right hand side are positive and their sum is never zero (the second term $P_o^2 - \frac{1}{4}$ is a strictly positive quantity). The equation may also be recast as

$$P_\tau^2 = P^4 + (1 - 2P_o^2)P^2 + P_o^4. \quad (4.182)$$

If $P_o^2 \leq \frac{1}{4}$ then the coefficient of P^2 is positive, and again P_τ^2 can never vanish. Indeed, a nonzero P_o ensures that the right hand side of (4.181) is bounded away from zero. Thus, we conclude that P (and therefore R) grows, positively or negatively, without bound. As in Region I, this occurs in a finite time, as we now demonstrate. For conciseness, we consider the case $P \rightarrow \infty$ (i.e. $P_\tau(0) > 0$) only. The case $P \rightarrow -\infty$ follows similarly.

Claim: P becomes arbitrarily large in finite time in Region IV.

Proof: P grows monotonically, without bound. Using separation of variables

in (4.182), we may express the time required for $P \rightarrow \infty$ as the integral

$$\tau^* = \int_{P_o}^{\infty} \frac{dP}{\sqrt{P^4 + (1 - 2P_o^2)P^2 + P_o^4}}. \quad (4.183)$$

If we first assume that $P_o^2 \leq \frac{1}{2}$, then $(1 - 2P_o^2)P^2$ is a positive quantity. Neglecting the uninteresting possibility that $P_o = 0$, P_o^4 is strictly positive. It is therefore true that

$$\tau^* < \int_{P_o}^{\infty} \frac{dP}{\sqrt{P^4}} = \int_{P_o}^{\infty} \frac{dP}{P^2}, \quad (4.184)$$

where the rightmost integral is clearly finite because the exponent on P is greater than 1.

If, on the other hand, $P_o^2 > \frac{1}{2}$, then we rewrite (4.183) in the form

$$\tau^* = \int_{P_o}^{\infty} \frac{dP}{\sqrt{(P^2 - P_o^2 + \frac{1}{2})^2 + P_o^2 - \frac{1}{4}}}. \quad (4.185)$$

Now, $P_o^2 - \frac{1}{4}$ is strictly greater than zero, which implies

$$\tau^* < \int_{P_o}^{\infty} \frac{dP}{\left|P^2 - P_o^2 + \frac{1}{2}\right|}. \quad (4.186)$$

Moreover, $P^2 - P_o^2 + \frac{1}{2}$ will be strictly positive for all time, so that the absolute value signs may be omitted. Integrating,

$$\begin{aligned} \int_{P_o}^{\infty} \frac{dP}{P^2 - P_o^2 + \frac{1}{2}} &= \int_{P_o}^{\infty} \frac{dP}{P^2 - a^2} \quad \text{with } a^2 = P_o^2 - \frac{1}{2} \\ &= \lim_{l \rightarrow \infty} \left[\frac{1}{2a} \ln \left| \frac{P - a}{P + a} \right| \right]_{P_o}^l \\ &= \frac{1}{2a} \left(\ln(1) - \ln \left| \frac{P_o - a}{P_o + a} \right| \right) \\ &= \frac{1}{2a} \ln \left| \frac{P_o + a}{P_o - a} \right| < \infty. \end{aligned} \quad (4.187)$$

Therefore τ^* is finite. **QED**

We present a plot of τ^* versus P_o in Figure 4.11. Since (4.183) contains only even powers of P_o , we only plot the blow-up time for $P_o > 0$. The above result requires some qualification. Let us first consider Region IV as it appears in Figure 4.3, that is, for the Upper Branch of the MSC. The region covers all wavenumbers above $k \simeq 1.8$, a value which at first glance does not seem unreasonably high. One must realize however, that our analysis is constrained by certain relationships between parameters, which were explicitly, or implicitly, assumed throughout. The plot in Figure 4.3 corresponds to a cross-channel wavenumber of $l = 0.79$, and if we take $k = 1.8$, then we obtain a value for the total wavenumber squared, $K^2 = 3.85$. The fundamental assumption of this chapter is that the perturbation is supercritical, i.e. close to the MSC.

Now, the plot of the MSC in Figure 3.1 shows that the Upper Branch decreases (becomes more negative) as $K \rightarrow \infty$. In fact, it is easy to estimate that for $K^2 = 3.85$, the Upper Branch requires $\frac{s}{\alpha} \simeq -7$. Clearly, the interfacial and bottom slopes differ by a factor of 7, which is no longer $O(1)$. This violates one of the assumptions of our Linear Analysis (Chapter 3), namely that $s \sim O(\alpha)$. In effect, this argument limits the range of wavenumbers where weakly nonlinear analysis can be trusted. Outside this range the results may still be true, but more evidence should be sought. Finally, we point out that for Region IV as it appears in Figure 4.2, no such inconsistencies were found and explosive growth seems intrinsic to the system.

Given a value of T , it is possible to demonstrate that adjacent solutions approach one another at the boundaries between regions. That is, the composite solution is continuous in wavenumber space. Figure 4.12 shows this solution, for a particular initial amplitude R_o and time T . For the parameter values specific to this solution, the cusp at $k \simeq 1$ corresponds to a change of sign for σ , that

is, σ becomes positive. For the physical system, this means a shift from linear stability to linear instability. It is not clear whether the same initial condition (4.106) should be used in both cases. In our research, we have tried to follow Pedlosky (1987) which, unfortunately, only considers a situation like Region III. The graph in Figure 4.12 is however, continuous. Analytically, we can show this by taking the limit of R , as N and σ approach 0 from the left and the right. Such calculations are tedious and can be found in Appendix A.

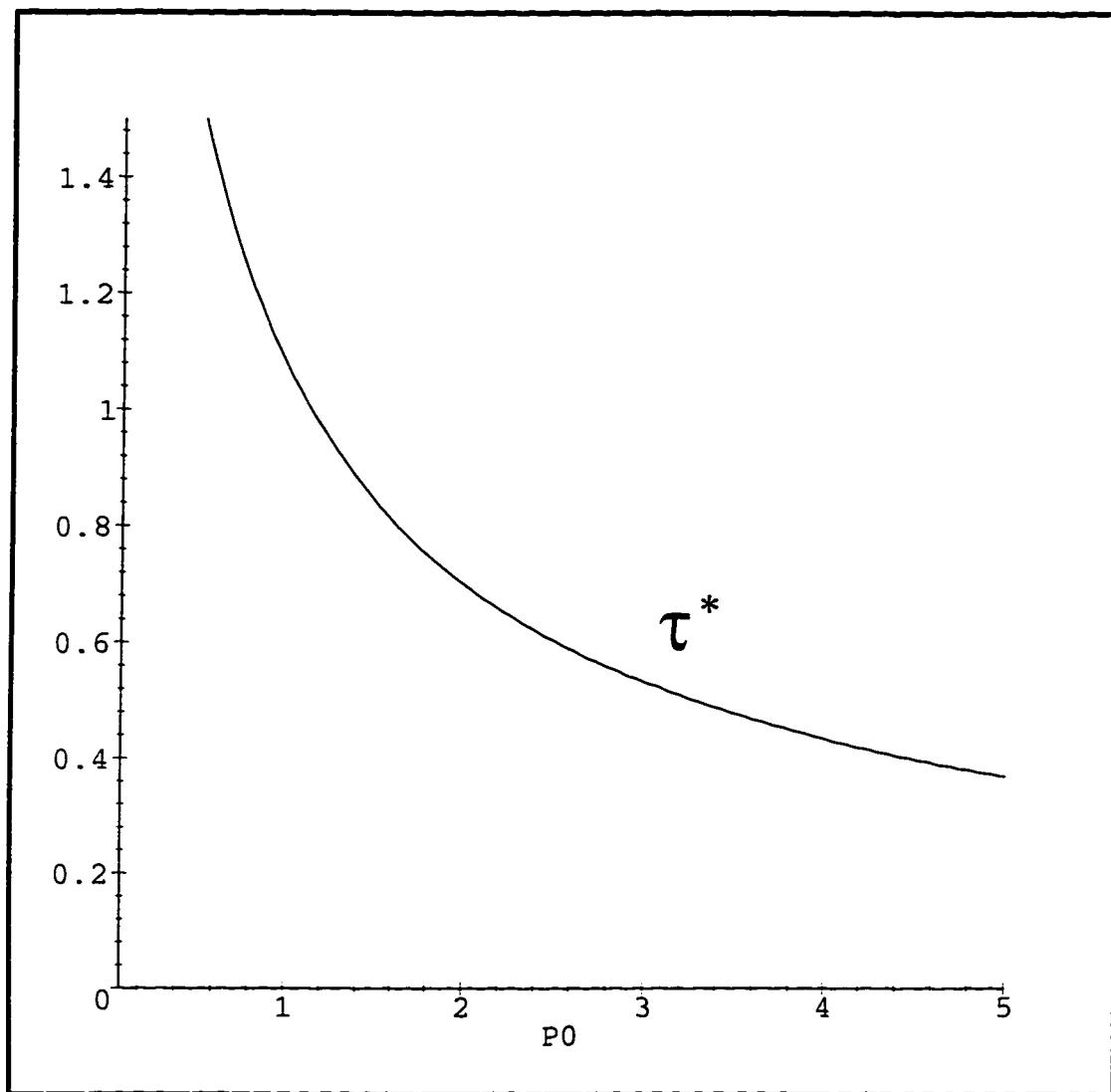


Figure 4.11: Time required for blow-up of solution in Region IV

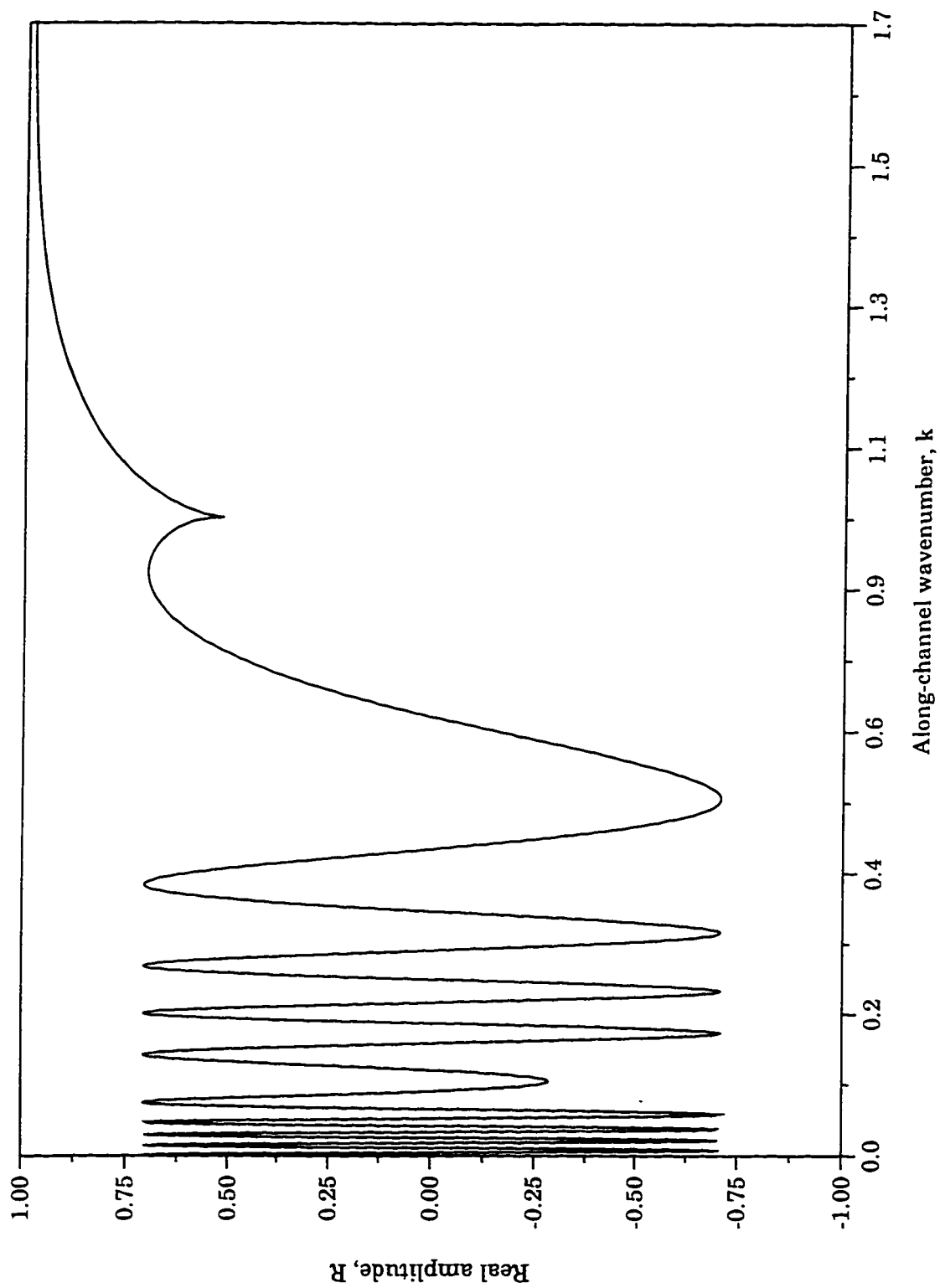


Figure 4.12: Amplitude structure in wavenumber space at $T=1$.

Chapter 5

Dependence on Spatial Scales

It would be useful to explore the along-channel spatial structure of the perturbation presented in the last chapter. We may also examine weakly nonlinear interactions on an even slower time scale than before. Here we derive a more general amplitude equation, which includes three new variables, X , χ and τ , corresponding to “large” space, “very large” space (both proportional to x) and “very slow” time, respectively. The calculations are a straightforward extension of the previous work, and we do not discuss them in detail. It will be found that the amplitude, A , has no dependence on X or τ but the new equation will admit soliton solutions in χ and T . Let us now introduce

$$X = sx, \quad \chi = s^2x, \quad \tau = s^2t. \quad (5.1)$$

These new scales modify spatial and time derivatives as follows,

$$\partial_t \longrightarrow \partial_t + s\partial_T + s^2\partial_\tau, \quad (5.2)$$

$$\partial_x \longrightarrow \partial_x + s\partial_X + s^2\partial_\chi. \quad (5.3)$$

Substituting into (2.92), (2.93), after a little algebra, we obtain

$$h_t + \alpha_c \Delta h_x + \alpha_c p_x = -s\alpha_c^2 h_{xy} - s\alpha_c^2 (y - \frac{L}{2}) \Delta h_x - sh_T - s\alpha_c p_X \quad (5.4)$$

$$\begin{aligned} & -sJ(\Delta h + p, h) - s\alpha_c \Delta h_X - 2s\alpha_c h_{xx} - \mu\delta^2 s^2 (\Delta h + p)_x - s^2 h_\tau \\ & -s^2 \alpha_c \Delta h_\chi - 3s^2 \alpha_c h_{xX} - 2s^2 \alpha_c h_{xx\chi} - s^2 \alpha_c p_\chi - s^2 \alpha_c h_{Xy} \\ & -s^2 \alpha_c (y - \frac{L}{2}) \Delta h_X - 2s^2 \alpha_c^2 (y - \frac{L}{2}) h_{xx} - 2s^2 J(h_{xX}, h) \\ & -s^2 \alpha_c [h \Delta h_x + 2h_y h_{xy} - h_x h_{yy} + h_x h_{xx}] - s^2 J_X(\Delta h + p, h) \\ & -s^2 \alpha_c (y - \frac{L}{2}) J(\Delta h, h) + O(s^3). \end{aligned}$$

$$(\Delta p + h)_t + (\alpha_c - 1)p_x = -sJ(p, \Delta p + h) - s(\Delta p + h)_T - 2sp_{xXt} \quad (5.5)$$

$$\begin{aligned} & -s(\alpha_c - 1)p_X - \mu\delta^2 s^2 p_x - s^2 J_X(p, \Delta p + h) - s^2 (\Delta p + h)_\tau \\ & -s^2 p_{XXt} - 2s^2 p_{x\chi t} - s^2 (\alpha_c - 1)p_\chi - 2s^2 p_{xXT} - 2s^2 J(p, p_{xX}) + O(s^3). \end{aligned}$$

where $J_X(A, B) = A_X B_y - A_y B_X$.

We expand h and p in an asymptotic series, as in Section 4.2.

$$(p, h) = (p^{(0)}, h^{(0)}) + s(p^{(1)}, h^{(1)}) + s^2(p^{(2)}, h^{(2)}) + \dots, \quad (5.6)$$

where now $p^{(0)}, h^{(0)}, p^{(1)}, h^{(1)}, p^{(2)}$ and $h^{(2)}$ are functions of x, y, t, X, χ, T and τ .

5.1 $O(1)$ Problem

The $O(1)$ problem is the same as before.

$$h_t^{(0)} + \alpha_c \Delta h_x^{(0)} + \alpha_c p_x^{(0)} = 0, \quad (5.7)$$

$$(\Delta p^{(0)} + h^{(0)})_t + (\alpha_c - 1)p_x^{(0)} = 0. \quad (5.8)$$

Recalling the definition $\theta = x - ct$, the $O(1)$ solutions are again,

$$(p^{(0)}, h^{(0)}) = (A, B) \exp[ik\theta] \sin(l y) + c.c., \quad (5.9)$$

with the one exception, that A and B are now formally functions of X , χ , T and τ .

5.2 $O(s)$ Problem

The $O(s)$ problem has five new terms on the right hand side,

$$\begin{aligned} h_t^{(1)} + \alpha_c \Delta h_x^{(1)} + \alpha_c p_x^{(1)} = & -\alpha_c^2 (y - \frac{L}{2}) \Delta h_x^{(0)} - \alpha_c^2 h_{xy}^{(0)} - h_T^{(0)} \\ & -\alpha_c \Delta h_X^{(0)} - 2\alpha_c h_{xxX}^{(0)} - \alpha_c p_X^{(0)}, \end{aligned} \quad (5.10)$$

$$\begin{aligned} (\Delta p^{(1)} + h^{(1)})_t + (\alpha_c - 1)p_x^{(1)} = & -(\Delta p^{(0)} + h^{(0)})_T \\ & -(\alpha_c - 1)p_X^{(0)} - 2p_{xXt}^{(0)}. \end{aligned} \quad (5.11)$$

The solutions are once again assumed to be of the form

$$(p^{(1)}, h^{(1)}) = (\bar{p}, \bar{h}) \exp[ik\theta] + c.c. + (\Psi, \Phi), \quad (5.12)$$

where, now, \bar{p} , \tilde{h} , Ψ and Φ are considered to be functions of y , X , χ , T and τ .

Substituting in and dividing through by $i\alpha_c k$ and $-ick$ respectively, we obtain

$$\begin{aligned} \left[\partial_{yy} - k^2 - \frac{c}{\alpha_c} \right] \tilde{h} + \bar{p} &= -\alpha_c \mu A \cos(ly) \\ + \alpha_c \left(y - \frac{L}{2} \right) K^2 \mu A \sin(ly) + \frac{i\mu}{\alpha_c k} A_T \sin(ly) \\ + \frac{i}{k} (A - l^2 \mu A)_X \sin(ly) - 3i\mu k A_X \sin(ly). \end{aligned} \quad (5.13)$$

$$\begin{aligned} \left[\partial_{yy} - k^2 - \frac{\alpha_c - 1}{c} \right] \bar{p} + \tilde{h} &= \frac{i}{kc} (K^2 A - \mu A)_T \\ - 2ik A_X \sin(ly) - \frac{i}{kc} (\alpha_c - 1) A_X \sin(ly). \end{aligned} \quad (5.14)$$

A necessary condition for the solvability for this pair of equations is

$$\int_0^L \left[h^{(0)}, p^{(0)} \right] \begin{bmatrix} \partial_{yy} - k^2 - \frac{c}{\alpha_c} & 1 \\ 1 & \partial_{yy} - k^2 - \frac{\alpha_c - 1}{c} \end{bmatrix} \begin{bmatrix} \tilde{h} \\ \bar{p} \end{bmatrix} dy = 0. \quad (5.15)$$

By the *Fredholm Alternative*, this is also a sufficient condition. Utilizing the right hand side of (5.13), (5.14), we obtain

$$\begin{aligned} \int_0^L & \left[-\alpha_c \mu l A \cos(ly) + \alpha_c K^2 \left(y - \frac{L}{2} \right) \mu A \sin(ly) + \frac{i\mu}{\alpha_c k} A_T \sin(ly) \right. \\ & + \frac{i}{k} (A - l^2 \mu A)_X \sin(ly) - 3i\mu k A_X \sin(ly) \left. \right] \mu A \sin(ly) dy \\ & + \int_0^L \left[\frac{i}{kc} (K^2 A - \mu A)_T \sin(ly) - 2ik A_X \sin(ly) \right. \\ & \left. - \frac{i}{kc} (\alpha_c - 1) A_X \sin(ly) \right] A \sin(ly) dy = 0. \end{aligned} \quad (5.16)$$

However, we can split this integral into a sum of two integrals, where the first is identical to the integral in (4.33), and the second consists of derivatives with respect to X . By the results of Section 4.2, the first integral vanishes, and we are left with

$$\begin{aligned} & \int_0^L \left[\frac{i}{k} (A - l^2 \mu A)_X \sin(ly) - 3i\mu k A_X \sin(ly) \right] \mu A \sin(ly) dy \\ & - \int_0^L \left[2ik A_X \sin(ly) + \frac{i}{kc} (\alpha_c - 1) A_X \sin(ly) \right] A \sin(ly) dy = 0. \end{aligned} \quad (5.17)$$

Simplifying, and substituting in for α_c and c , results in

$$\begin{aligned} & \frac{i}{k} [\mu A A_X - l^2 A A_X - 3k^2 A A_X - 2k^2 A A_X \\ & - \frac{K^2(2 - \mu K^2)}{1 - \mu K^2} \frac{\mu - K^2(2 - K^2)}{K^2(2 - \mu K^2)} A A_X] \int_0^L \sin^2(ly) dy = 0. \end{aligned} \quad (5.18)$$

Since the integral of $\sin^2(ly)$ cannot be equal to zero, we conclude that

$$(\mu - l^2 - 5k^2 + K^2 - \mu) A A_X = -4k^2 A A_X = 0. \quad (5.19)$$

Because we are not interested in the trivial case $A \equiv 0$, this implies in turn, that

$$A_X = 0. \quad (5.20)$$

Thus, the amplitude coefficients A and $B = \mu A$ are not dependent on the large spatial variable X . This being the case, our $O(s)$ problem reduces to (4.24), (4.25), and the solutions $p^{(1)}$ and $h^{(1)}$ are the same as in Chapter 4.

5.3 $O(s^2)$ Problem

First, we note that no new secular terms arise in the $O(s^2)$ problem due to the presence of the new variables. Therefore, we may define the mean flow corrections Ψ and Φ as in (4.85) and (4.86), which will make all secularities vanish. (It must be noted however, that both Ψ and Φ are now functions of y , χ , T and τ .) As another simplification, no derivatives of $p^{(0)}$ or $h^{(0)}$ with respect to X appear on the right hand side, since $A_X = B_X = 0$. Thus, we can state the $O(s^2)$ problem as follows,

$$h_t^{(2)} + \alpha_c \Delta h_x^{(2)} + \alpha_c p_x^{(2)} = -\alpha_c^2 \left(y - \frac{L}{2}\right) \Delta h_x^{(1)} - \alpha_c^2 h_{xy}^{(1)} \quad (5.21)$$

$$\begin{aligned} & -h_y^{(0)} \Delta h_x^{(1)} - h_y^{(1)} \Delta h_x^{(0)} + h_x^{(0)} \Delta h_y^{(1)} + h_x^{(1)} \Delta h_y^{(0)} \\ & -J(p^{(0)}, h^{(1)}) - J(p^{(1)}, h^{(0)}) - h_T^{(1)} - \mu \delta^2 \Delta h_x^{(0)} - \mu \delta^2 p \\ & -\alpha_c [h^{(0)} \Delta h_x^{(0)} + 2h_y^{(0)} h_{xy}^{(0)} - h_x^{(0)} h_{yy}^{(0)} + h_x^{(0)} h^{(0)} h_{xx}^{(0)}] \\ & -h_\tau^{(0)} - \alpha_c \Delta h_\chi^{(0)} - 2\alpha_c h_{xx\chi}^{(0)} - \alpha_c p_\chi^{(0)}. \end{aligned} \quad (5.22)$$

$$\begin{aligned} & (\Delta p^{(2)} + h^{(2)})_t + (\alpha_c - 1)p_x^{(2)} = -(\Delta p^{(1)} + h^{(1)})_T \\ & -2p_{x\chi t}^{(0)} - (\Delta p^{(0)} + h^{(0)})_\tau - (\alpha_c - 1)p_\chi^{(0)} \\ & -J(p^{(0)}, \Delta p^{(1)} + h^{(1)}) - J(p^{(1)}, \Delta p^{(0)} + h^{(0)}) - \mu \delta^2 p_x^{(0)}. \end{aligned}$$

We assume solutions of the form

$$(p^{(2)}, h^{(2)}) = (\hat{p}, \hat{h}) \exp[ik\theta] + c.c., \quad (5.23)$$

where \hat{p} and \hat{h} are functions of y , χ , T and τ , and consider only terms associated

with $\exp[\pm ik\theta]$. Dividing (5.21) by $ik\alpha_c$ and (5.22) by $-ikc$, the equations become

$$[\partial_{yy} - k^2 - \frac{c}{\alpha_c}] \hat{h} + \hat{p} = \alpha_c k^2 (y - \frac{L}{2}) \bar{h} - \alpha_c \bar{h}_y \quad (5.24)$$

$$\begin{aligned} & -\alpha_c (y - \frac{L}{2}) \bar{h}_{yy} + \frac{i}{k\alpha_c} \bar{h}_T + \frac{\delta^2}{\alpha_c} (K^2 - \mu) \sin(ly) A \\ & + 2 \frac{l^2}{\alpha_c c} (K^2 - \mu)^2 \sin(ly) \cos(2ly) A (|A|^2 - |A_o|^2) \\ & - 8 \frac{l^4}{\alpha_c c} (K^2 - \mu) \sin(ly) \cos(2ly) A (|A|^2 - |A_o|^2) \\ & + \frac{i}{k} (K^2 + 1)^2 \sin(ly) A_\chi + 2ik \sin(ly) A_\chi - \frac{i}{k\alpha_c} A_\tau \sin(ly). \end{aligned}$$

$$\begin{aligned} & [\partial_{yy} - k^2 - \frac{\alpha_c - 1}{c}] \hat{p} + \hat{h} = \frac{i}{kc} (k^2 \bar{p}_T - \bar{p}_{yyT}) - \frac{i}{kc} \bar{h}_T \quad (5.25) \\ & + \mu \frac{\delta^2}{c} \sin(ly) A - 2 \frac{l^2}{c^2} (K^2 - \mu) \sin(ly) \cos(2ly) A (|A|^2 - |A_o|^2) \\ & - 2ik \sin(ly) A_\chi - \frac{i}{kc} (\alpha_c - 1) \sin(ly) A_\chi + \frac{i}{kc} (K^2 + 1) \sin(ly) A_\tau. \end{aligned}$$

where $A_o = A(\chi, T = 0)$. The solvability condition is

$$\begin{aligned} & \int_0^L \{ \mu \alpha_c k^2 (y - \frac{L}{2}) \bar{h} - \mu \alpha_c \bar{h}_y - \mu \alpha_c (y - \frac{L}{2}) \bar{h}_{yy} + \mu \frac{i}{k\alpha_c} \bar{h}_T \quad (5.26) \\ & + \mu \frac{\delta^2}{\alpha_c} (K^2 - \mu) \sin(ly) A + \frac{ik}{c} \bar{p}_T - \frac{i}{kc} \bar{p}_{yyT} - \frac{i}{kc} \bar{h}_T + \mu \frac{\delta^2}{c} \sin(ly) A \\ & - 2l^2 K^4 \frac{(K^2 - 2\mu)^2}{K^2 - \mu} [4l^2 (K^2 - \mu) - K^2 (K^2 - 2\mu)] \\ & \times \sin(ly) \cos(2ly) A (|A|^2 - |A_o|^2) \\ & - \frac{i}{k} (K^2 - \mu) \sin(ly) A_\chi - 2ik \sin(ly) A_\chi + \frac{i}{k\alpha_c} \sin(ly) A_\tau - 2ik \sin(ly) A_\chi \end{aligned}$$

$$-\frac{i}{kc}(\alpha_c - 1) \sin(ly) A_\chi + \frac{i}{kc}(K^2 - \mu) \sin(ly) A_\tau \} \sin(ly) A dy = 0.$$

By the *Fredholm Alternative*, it is also a sufficient condition for the existence of solutions to (5.24) and (5.25).

Substituting in the expressions for α_c and c from (4.15) we encounter a simplification, i.e. terms which involve A_τ sum to zero. Now, the terms associated with the new variable χ are imaginary. Moreover, after replacing \tilde{p} and \tilde{h} by the expressions (4.64) and (4.65) (or (4.76) and (4.77) as appropriate), it becomes clear that these are the *only* imaginary terms in the equation. Therefore, carrying out the above integration results in an Amplitude Equation whose real components are exactly the same as (4.99), plus an imaginary term proportional to A_χ . Having divided through by the coefficient of A_{TT} and rearranged the terms, we obtain

$$A_{TT} = \sigma A + iPA_\chi - NA(|A|^2 - |A_o|^2). \quad (5.27)$$

where

$$P = 4\mu \frac{k^3(K^2 - \mu)}{K^6(K^2 - 2\mu)^2}. \quad (5.28)$$

and the coefficients σ and N are defined in Subsection 4.2.5.

The remainder of this chapter will follow the study by Tan & Liu (1995). First, we introduce

$$\bar{\sigma}(\chi) = -(\sigma + N|A_o|^2),$$

with $A_o(\chi) = A(\chi, T = 0)$, and rearrange (5.27) to obtain

$$A_{TT} + \bar{\sigma}A - iPA_\chi + NA|A|^2 = 0. \quad (5.29)$$

This is known as the Unstable Nonlinear Schrödinger (UNS) equation, and is a special case of the Ginzburg-Landau Equation. If T and χ are interchanged, (5.29)

becomes the conventional Nonlinear Schrödinger equation.

The UNS equation may be cast in standard form by eliminating all terms proportional to A . Imposing the transformation

$$A(\chi, T) = \exp\left(-\frac{i}{P} \int_0^\chi \bar{\sigma}(\xi) d\xi\right) C(\chi, T), \quad (5.30)$$

substituting in. and dividing through by $\exp\left(-\frac{i}{P} \int_0^\chi \bar{\sigma}(\xi) d\xi\right)$, yields

$$C_{TT} + \bar{\sigma}C + iP\frac{i\bar{\sigma}}{P}C - iPC_\chi + NC|C|^2 = 0. \quad (5.31)$$

After simplification, we obtain the standard form of the UNS equation.

$$C_{TT} - iPC_\chi + NC|C|^2 = 0. \quad (5.32)$$

Equation (5.32) may be solved by the Inverse Scattering Transform, and it admits soliton solutions.

5.4 Steadily Travelling Solitons

Presently, we demonstrate that the steadily travelling solitary wave is a possible solution to (5.32). The function C is assumed to be the product of a wave field dependent on χ and T , and an unknown function Z , dependent on $\chi - UT$ only, where U is the speed of the soliton. We define

$$C = \exp[i r \chi - i s T] \times Z(\Theta), \quad (5.33)$$

where $\Theta = \chi - UT$, while r and s are constant parameters. Both parameters will be related to other constants shortly.

Upon substitution of (5.33) into (5.32) we obtain the ordinary differential equation

$$U^2 Z'' + i(2sU - P)Z' + (rP - s^2)Z + NZ|Z|^2 = 0. \quad (5.34)$$

Defining s as

$$s = \frac{P}{2U}. \quad (5.35)$$

eliminates the Z' term from the equation. As there are no longer any imaginary coefficients, we now assume that Z is real. For convenience, we also define r in terms of a new quantity η ,

$$r = \frac{s^2 - \eta^2}{P}. \quad (5.36)$$

to obtain

$$U^2 Z'' - \eta^2 Z + NZ^3 = 0. \quad (5.37)$$

Multiplying by Z' and integrating once, yields

$$\frac{2U^2}{N}(Z')^2 = -Z^4 + \frac{2\eta^2}{N}Z^2 - Z^*, \quad (5.38)$$

where Z^* is a constant of integration. Taking the square root of both sides and rearranging, gives

$$\sqrt{\frac{2}{N}}U \frac{dZ}{d\Theta} = \left((\beta^2 - Z^2)(Z^2 - \zeta^2) \right)^{\frac{1}{2}}, \quad (5.39)$$

with

$$\beta^2 = \frac{\eta^2}{N} + \sqrt{\frac{\eta^4}{N^2} - Z^*}, \quad (5.40)$$

$$\zeta^2 = \frac{\eta^2}{N} - \sqrt{\frac{\eta^4}{N^2} - Z^*}. \quad (5.41)$$

Equation (5.39) can be written in terms of an elliptic integral.

$$\int_Z^\beta \frac{d\xi}{\sqrt{(\beta^2 - \xi^2)(\xi^2 - \zeta^2)}} = \frac{1}{U} \sqrt{\frac{N}{2}} \int d\Theta, \quad (5.42)$$

and we will show, *a posteriori*, that $\zeta < Z < \beta$.

After integration of (5.42) (Milne-Thomson, 1950) and a little algebra, we find that

$$Z = \beta \operatorname{dn} \left(\sqrt{\frac{N}{2}} \frac{\beta}{U} (\Theta - \Theta^*) \middle| \frac{\beta^2 - \zeta^2}{\beta^2} \right), \quad (5.43)$$

for some constant of integration, Θ^* . We now argue that, for a soliton solution, Z and its derivatives should vanish for $\chi \rightarrow \pm\infty$ (holding T fixed). Therefore, equation (5.38) implies that the constant Z^* must in fact be zero (Pedlosky, 1972). In this limiting case, one may easily verify that $\beta \rightarrow \sqrt{\frac{2}{N}}\eta$, $\zeta \rightarrow 0$ and the limit of the solution is

$$Z = \sqrt{\frac{2}{N}}\eta \operatorname{sech} \left[\frac{\eta}{U} (\chi - UT - \Theta^*) \right], \quad (5.44)$$

since $\operatorname{dn}(u|1) = \operatorname{sech}(u)$ (Milne-Thomson, 1950). We note that Z is a non-negative function with a maximum amplitude of $\sqrt{\frac{2}{N}}\eta$, so that it oscillates between ζ and β as we required.

Setting $\Theta^* = 0$ for clarity, the amplitude function can now be expressed as

$$\begin{aligned} A(\chi, T) = & \sqrt{\frac{2}{N}}\eta \exp \left[i \left(\frac{\sigma}{P} + r \right) \chi - i \frac{P}{2U} T \right] \\ & \times \exp \left[i \frac{N}{P} \int_0^\chi |A_o(\xi)|^2 d\xi \right] \times \operatorname{sech} \left[\frac{\eta}{U} (\chi - UT) \right], \end{aligned} \quad (5.45)$$

where U and η are free parameters, while σ , N , P and r have been defined previously. This may be simplified in the following manner. We first write down

the expression for $A(\chi, 0)$

$$A(\chi, 0) = \sqrt{\frac{2}{N}}\eta \exp[i \left\{ \left(\frac{\sigma}{P} + r \right) \chi + \frac{N}{P} \int_0^\chi |A_o(\xi)|^2 d\xi \right\}] \quad (5.46)$$

$$\times \text{sech} \left[\frac{\eta}{U} \chi \right],$$

and take the modulus of both sides,

$$|A_o| = \sqrt{\frac{2}{N}}\eta \text{sech} \left[\frac{\eta}{U} \chi \right], \quad (5.47)$$

noting that the modulus of the exponential term is unity, since every term in the curly brackets is real.

We can now evaluate the integral in (5.45).

$$\begin{aligned} \int_0^\chi |A_o(\xi)|^2 d\xi &= \frac{2}{N}\eta^2 \int_0^\chi \text{sech}^2 \left[\frac{\eta}{U} \xi \right] d\xi, \\ &= \frac{2U\eta}{N} \tanh \left[\frac{\eta}{U} \chi \right]. \end{aligned} \quad (5.48)$$

Finally, the amplitude A becomes

$$A(\chi, T) = \sqrt{\frac{2}{N}}\eta \exp[i \left(\frac{\sigma}{P} + r \right) \chi + i \frac{2U\eta}{P} \tanh \left(\frac{\eta}{U} \chi \right) - i \frac{P}{2U} T] \quad (5.49)$$

$$\times \text{sech} \left[\frac{\eta}{U} (\chi - UT) \right].$$

It is evident that, while the velocity of the envelope is amplitude independent, the velocity of the carrier wave does depend on the amplitude. The real part of (5.49) is plotted in Figure 5.1 for the times $T = 0, 8, 16$ and 24 . The dotted lines represent the envelope only. The parameter values used were $\sigma \simeq 0.8$, $N \simeq 0.4$ and $P \simeq -0.3$, which corresponds to $k = 1$ in Figure 4.4.

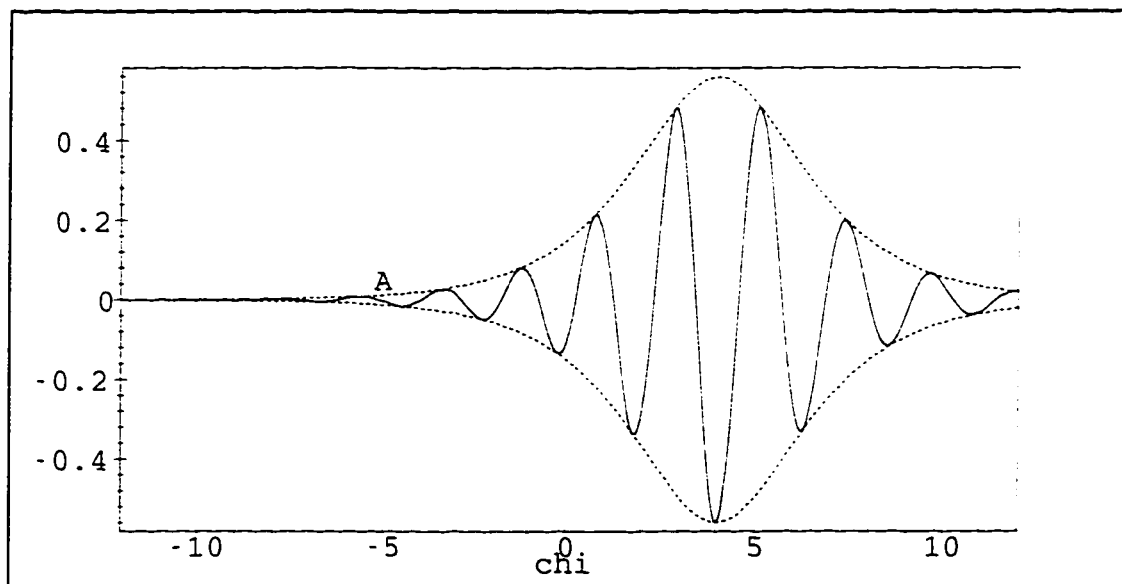
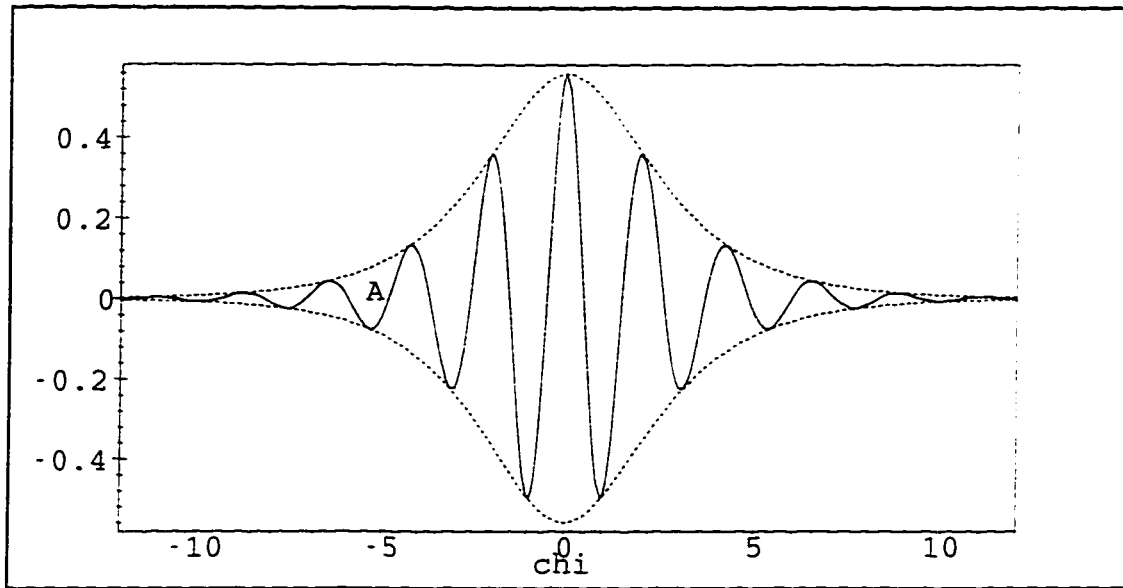


Figure 5.1: Soliton solution to Amplitude Equation in large space and slow time for $T=0$ and $T=8$. Continued on next page.

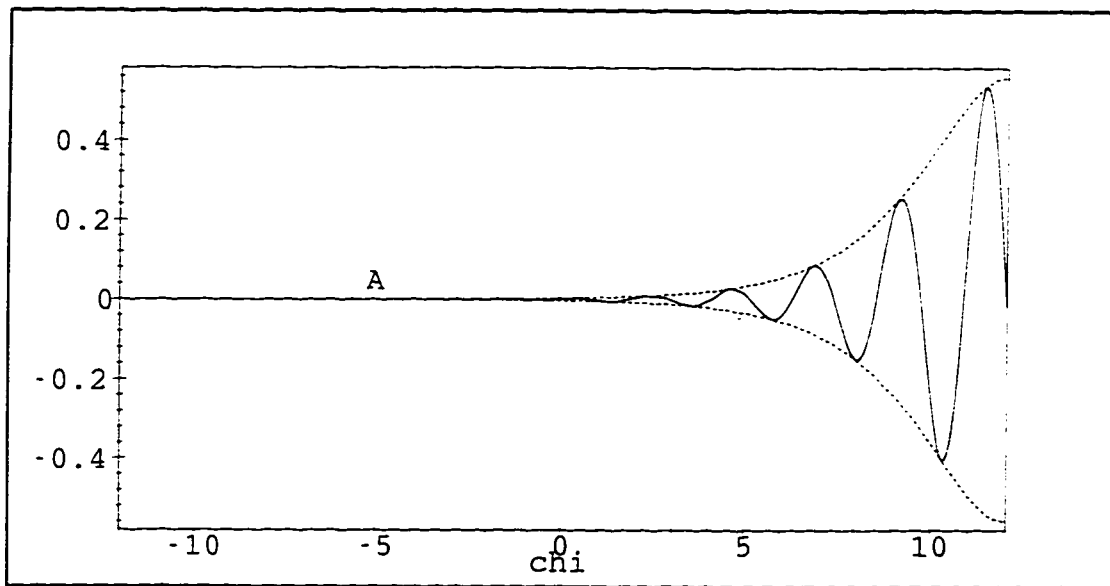
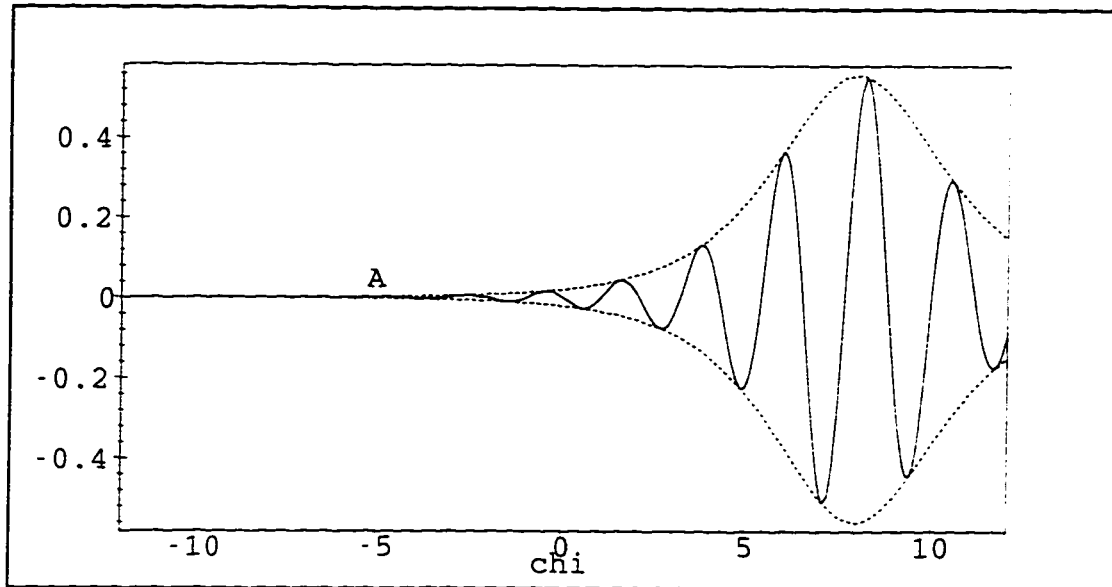


Figure 5.1, continued: Soliton solution to Amplitude Equation in large space and slow time for $T=16$ and $T=24$.

Chapter 6

Numerical Analysis

6.1 Introduction

There are numerous advantages to the computational approach when solving nonlinear PDEs in fluid dynamics. Most importantly, numerical simulations provide actual solutions to the fully nonlinear model. Of course, these solutions do contain a certain degree of error, but they are usually accurate enough for most purposes. Each computed solution also requires a set of specific parameters, and due to time constraints, the parameter space can only be sampled in a few places. However, such sampling often produces a meaningful picture of the influence of the parameters on the flow in general. A simulation may be initialized with data closely resembling real-world observations, which is difficult to do analytically. The behavior of the virtual flow can indicate whether the model captures enough of the relevant physical processes to describe, at least qualitatively, the real-world phenomenon under consideration. Numerically computed solutions can serve to verify the validity of an approximate theory based on the model, and often point the way toward further fruitful analytical investigation. Lastly, once a general analytical result is obtained, the exact physical structure of the evolving flow may

be visualized, for the parameter values assumed by the analytical work. Here we present numerical results for the original model equations, in a periodic channel of width L , for both realistic as well as highly idealized flow configurations.

6.2 The Algorithm

As a note to the reader, this section deals with the details of the numerical solver and may be skipped, with no loss in overall continuity. The algorithm is an explicit, finite-difference scheme which is leapfrog in time and central in space, while the Jacobian terms are approximated by the Arakawa (1966) scheme. The equations (2.92), (2.93) are first written in the form

$$h_t = -J \left(p + h \Delta h + \frac{1}{2} \nabla h \cdot \nabla h, h \right). \quad (6.1)$$

$$q_t = -J(p, q). \quad (6.2)$$

where $q = \Delta p + h - sy$.

Approximating the time derivatives by the central differences

$$h_t(t = t_k) \simeq \frac{h^{k+1} - h^{k-1}}{2\Delta t}, \quad q_t(t = t_k) \simeq \frac{q^{k+1} - q^{k-1}}{2\Delta t}. \quad (6.3)$$

we have

$$h^{k+1} = h^{k-1} - 2\Delta t J \left(p^k + h^k \Delta h^k + \frac{1}{2} \nabla h^k \cdot \nabla h^k, h^k \right), \quad (6.4)$$

$$q^{k+1} = q^{k-1} - 2\Delta t J(p^k, q^k), \quad (6.5)$$

where the superscripts $k-1$, k , and $k+1$ refer to evaluation at time t_{k-1} , t_k and t_{k+1} respectively. The time scheme can be thought of pictorially in the following way. For a time dependent quantity Q ,

$$Q^{k+1} = Q^{k-1} + \text{correction terms},$$

$$Q^{k+2} = Q^k + \text{correction terms},$$

$$Q^{k+3} = Q^{k+1} + \text{correction terms, and so on.}$$

We may view this as two processes working in tandem, exactly one iteration out of step. That is, the two processes follow a “leapfrog” pattern, where one calculates the quantities $Q^{2\lambda}$, and the other computes $Q^{2\lambda+1}$, for $\lambda \in \{0, 1, 2, \dots\}$. Such a procedure requires initial data at the first two time steps. However, it has the advantage that the error is only $O(\Delta t^2)$, rather than $O(\Delta t)$ as is the case with procedures based on one-sided derivatives. It is worth mentioning, that in approximating the lower layer equation (6.2) by (6.5), we are in fact tracking the evolution of the lower layer Potential Vorticity $q = \Delta p + h - sy$ (see Section 2.5).

We divide the spatial domain into an $m \times n$ grid where $x_{i+1} - x_i = \Delta x$ for $i \in \{0, m-1\}$ and $y_{j+1} - y_j = \Delta y$ for $j \in \{0, n-1\}$. Standard central difference formulas with an $O(\Delta x^2)$ error (or $O(\Delta y^2)$, whichever applies) are utilized for the spatial derivatives.

$$h_x(x = x_i) \simeq \frac{h_{i+1,j} - h_{i-1,j}}{2\Delta x}, \quad h_{xx}(x = x_i) \simeq \frac{h_{i+1,j} - 2h_{i,j} + h_{i-1,j}}{\Delta x^2}, \quad (6.6)$$

$$h_y(y = y_j) \simeq \frac{h_{i,j+1} - h_{i,j-1}}{2\Delta y}, \quad h_{yy}(y = y_j) \simeq \frac{h_{i,j+1} - 2h_{i,j} + h_{i,j-1}}{\Delta y^2}. \quad (6.7)$$

where $1 \leq i \leq m-1$, $1 \leq j \leq n-1$, with analogous formulas for p_x , p_{xx} , p_y and p_{yy} .

Special formulas are necessary at the boundaries of the (x, y) domain. The periodic boundary condition at x_0 and x_m is easily applied as follows. The expressions in (6.6) still hold, but whenever subscript $i = -1$ is called for, it is replaced by $i = m$, and similarly, $i = m+1$ is replaced by $i = 0$. Application of the Dirichlet boundary conditions on the channel walls is not so straightforward. If $j = n$, we do not have the luxury of looking at the $j+1$ node as it lies beyond

the boundary (similarly for $j - 1$ when $j = 0$). However we can utilize more points within the domain, to arrive at formulas which are still $O(\Delta y^2)$: For the boundary defined by $y = y_n$, we have

$$h_y(y = y_n) \simeq \frac{3h_{i,n} - 4h_{i,n-1} + h_{i,n-2}}{2\Delta y}, \quad (6.8)$$

$$h_{yy}(y = y_n) \simeq \frac{2h_{i,n} - 5h_{i,n-1} + 4h_{i,n-2} - h_{i,n-3}}{\Delta y^2}. \quad (6.9)$$

while for $y = y_o$,

$$h_y(y = y_o) \simeq \frac{-3h_{i,0} + 4h_{i,1} - h_{i,2}}{2\Delta y}. \quad (6.10)$$

$$h_{yy}(y = y_o) \simeq \frac{2h_{i,0} - 5h_{i,1} + 4h_{i,2} - h_{i,3}}{\Delta y^2}. \quad (6.11)$$

Setting $\Delta x = \Delta y$ for simplicity, the formula for the Jacobian of $A(x, y)$ and $B(x, y)$, evaluated at (x_i, y_j) is (Arakawa, 1966)

$$\begin{aligned} J(A, B) \simeq & -\frac{1}{12\Delta x^2} [(A_{i+1,j} - A_{i,j})(B_{i,j-1} + B_{i+1,j-1} - B_{i,j+1} - B_{i+1,j+1}) \\ & + (A_{i,j} - A_{i-1,j})(B_{i-1,j-1} + B_{i,j-1} - B_{i-1,j+1} - B_{i,j+1}) \\ & + (A_{i,j+1} - A_{i,j})(B_{i+1,j} + B_{i+1,j+1} - B_{i-1,j} - B_{i-1,j+1}) \\ & + (A_{i,j} - A_{i,j-1})(B_{i+1,j-1} + B_{i+1,j} - B_{i-1,j-1} - B_{i-1,j}) \\ & + (A_{i+1,j+1} - A_{i,j})(B_{i+1,j} - B_{i,j+1}) \\ & + (A_{i,j} - A_{i-1,j-1})(B_{i,j-1} - B_{i-1,j}) \\ & + (A_{i-1,j+1} - A_{i,j})(B_{i,j+1} - B_{i-1,j}) \\ & + (A_{i,j} - A_{i+1,j-1})(B_{i+1,j} - B_{i,j-1})]. \end{aligned} \quad (6.12)$$

Along-channel periodicity is enforced as explained above, and no special formulas are required at the channel walls since the Jacobian is only evaluated at $y_{i,1}$ through $y_{i,n-1}$. This scheme preserves energy and enstrophy, two quantities whose

accurate calculation is very desirable in fluid dynamics. Again, the associated error is only $O(\Delta x^2)$ and $O(\Delta y^2)$.

Finally, it is necessary to solve the Poisson problem.

$$\Delta p = q - h + sy, \quad (6.13)$$

to recover p from q . If this is the last calculation performed at each time iteration, then all quantities on the right hand side are already known. Thus, for each time step we want to solve

$$\Delta p^{k+1} = f(x, y). \quad (6.14)$$

where $f(x, y) = q^{k+1} - h^{k+1} + sy$, or in terms of central differences.

$$f(x_i, y_j) = \frac{p_{i+1,j} - 2p_{i,j} + p_{i-1,j}}{\Delta x^2} + \frac{p_{i,j+1} - 2p_{i,j} + p_{i,j-1}}{\Delta y^2}, \quad (6.15)$$

all evaluated at t_{k+1} . Now, if we stipulate that $\Delta x = \Delta y = c$ for some small constant c , then (6.15) reduces to

$$4p_{i,j} - p_{i+1,j} - p_{i-1,j} - p_{i,j+1} - p_{i,j-1} = -c^2 f(x_i, y_j), \quad (6.16)$$

for each $i \in \{0 \dots m\}$ and each $j \in \{1 \dots n - 1\}$, where periodicity is again enforced on the subscript i . If boundary data is prescribed at $j = 0$ and $j = n$, then there are $r = (m + 1)(n - 1)$ nodes in the domain for which p is unknown.

Numbering all these nodes sequentially from 1 to r we obtain a system of r equations in r unknowns. This can be written in the form $\mathbf{A}\mathbf{u} = \mathbf{b}$ where \mathbf{u} is composed of $p_{i,j}$, \mathbf{b} is composed of the right hand side of (6.15), and the entries of \mathbf{A} select the appropriate combinations of $p_{i,j}$ (Burden & Faires, 1993). Since \mathbf{A} is symmetric, positive-definite, we have a choice of several efficient routines.

Here we implement the Conjugate-Gradient scheme, which relies on the idea that solving $\mathbf{A}\mathbf{u} = \mathbf{b}$ is equivalent to minimizing the quadratic form

$$q(\mathbf{u}) = \langle \mathbf{u}, \mathbf{A}\mathbf{u} \rangle - 2 \langle \mathbf{u}, \mathbf{b} \rangle, \quad (6.17)$$

where the angle brackets represent the inner product of two vector quantities.

To see this, we consider q evaluated at $\mathbf{u} + t\mathbf{v}$, where \mathbf{u} and \mathbf{v} are vectors and t is some scalar. After a little algebra, it can be shown that

$$q(\mathbf{u} + t\mathbf{v}) = q(\mathbf{u}) + 2t \langle \mathbf{v}, \mathbf{A}\mathbf{u} - \mathbf{b} \rangle + t^2 \langle \mathbf{v}, \mathbf{A}\mathbf{v} \rangle. \quad (6.18)$$

Because \mathbf{A} is positive-definite, the coefficient of t^2 is positive and so q has a minimum in t , not a maximum. By taking the derivative of q and setting it equal to zero, we can determine the value of t where the minimum occurs. This value is given by

$$\hat{t} = \frac{\langle \mathbf{v}, \mathbf{A}\mathbf{u} - \mathbf{b} \rangle}{\langle \mathbf{v}, \mathbf{A}\mathbf{v} \rangle}. \quad (6.19)$$

When we substitute \hat{t} into (6.18) and simplify, we obtain

$$q(\mathbf{u} + \hat{t}\mathbf{v}) = q(\mathbf{u}) - \frac{\langle \mathbf{v}, \mathbf{b} - \mathbf{A}\mathbf{u} \rangle^2}{\langle \mathbf{v}, \mathbf{A}\mathbf{v} \rangle}. \quad (6.20)$$

Thus, $q(\mathbf{u} + \hat{t}\mathbf{v})$ is always closer to the minimum than $q(\mathbf{u})$ unless \mathbf{v} is orthogonal to the residual $\mathbf{b} - \mathbf{A}\mathbf{u}$, i.e. unless $\langle \mathbf{v}, \mathbf{b} - \mathbf{A}\mathbf{u} \rangle = 0$. More importantly, if $\mathbf{A}\mathbf{u} = \mathbf{b}$ then q cannot be reduced any further. This fact suggests an iterative process for finding the minimum q . Successive vectors $\mathbf{v}^{(r)}$ are chosen, each appropriate value $t^{(r)}$ is computed, and each approximation

$$\mathbf{u}^{(r+1)} = \mathbf{u}^{(r)} + t^{(r)}\mathbf{v}^{(r)}, \quad (6.21)$$

is closer to the solution of $\mathbf{A}\mathbf{u} = \mathbf{b}$. We note that the algorithm will be most efficient if the $\mathbf{v}^{(r)}$ are orthogonal to each other. A thorough discussion of the method is beyond the scope of this thesis, and we refer the reader to the book by Kincaid & Cheney (1991).

The above procedures have all been implemented in standard C, and the source code is given in Appendix C. The program was compiled and executed on Silicon Graphics workstations (Indigo, Indigo 2 and Power Challenge). Computation time required for one simulation ranged between several hours and two days, depending on the size of the domain, the resolution of the grid, and the number of time steps. The evolution of the flow was analyzed visually using *GASP* and *NCAR* libraries as well as the *Spyglass* software package.

6.3 Linear Theory Results

We can always align the model geometry so that the x axis is parallel with the mean flow. Following the same convention as in the rest of the thesis, x denotes the along-channel coordinate and y the cross-channel (or cross-shelf) coordinate. All experiments are performed in a channel which is periodic in x . For no normal flow on the channel walls we require that the x -derivatives of the streamfunctions h and p vanish on the boundaries. In practice, we fix the boundary data for all time. The upper layer thickness is initialized with an appropriate front profile, independent of x . To focus in on baroclinic effects, we initially set p equal to zero, which corresponds no mean flow in the lower layer. An appropriate perturbation is always imposed on p , and sometimes on h as well. The simulation then runs until numerical error begins to obscure important flow features (usually after several hundred thousand iterations).

We would first like to verify that the linear theory presented in Chapter 3 and

our numerical scheme are consistent with one another. These experiments will proceed as follows. The upper layer height is initialized with the gently sloping wedge front discussed in Section 3.3, plus a perturbation,

$$h(x, y, t = 0) = 1 + \alpha(y - \frac{L}{2}) + h'(x, y), \quad (6.22)$$

while the lower layer pressure is initialized with a perturbation only,

$$p(x, y, t = 0) = p'(x, y). \quad (6.23)$$

The perturbations are determined by the expressions in (3.30) and (3.29), and the parameters α and s are chosen so that linear theory holds (i.e. we are somewhere on the MSC). In this case we expect that the wavefields will not grow, but will simply propagate with the linear (real) phase speed given in (3.33). We therefore have the luxury of initializing the second time step (necessary in a leapfrog scheme) with the expected solutions at $t = \Delta t$.

Here we present two such experiments, at Points 1 and 2 (see Figure 3.1) on the MSC. For the Upper Branch, we chose Point 1, with $K^2 = 1.01$, $s = \alpha = 0.01$, so that $\frac{s}{\alpha} = 1$. This is almost exactly the point of marginal stability, (1,1). The perturbations imposed on h and p are

$$h' = p' = amp \sin(\frac{2\pi x}{x_{\max}}) \cos(\frac{\pi y}{L}). \quad (6.24)$$

where the amplitude amp is made sufficiently small that linear theory should be operative (see Figure 6.1). The perturbations are exactly the same for both streamfunctions, as is required on the Upper Branch. The complete profile of the upper layer is shown in Figure 6.2. Since Point 1 is exactly on the MSC, no growth (or decay) should be visible. The phase speed c_R has the value $-1.6 \times$

10^{-4} , from (3.33). Figure 6.3 is a time series of the upper layer perturbation. It demonstrates that the perturbation does not deform in any appreciable way, and its propagation speed is very small. A more precise calculation using the original data can show that any given point of constant phase propagates to the left, at a speed of -2.0×10^{-4} which closely matches the theoretical value.

A similar experiment was performed on the Lower Branch of the MSC, at Point 2. This time the initial parameters were $K^2 = 0.49$, $s = 0.012$, $\alpha = -0.01$, so that $\frac{s}{\alpha} = -1.23$. The phase speed c_R was calculated using (3.33) to be approximately 0.015. This time the wave speed is positive and the wave anomaly moves in the opposite direction to the first experiment. A time series of this process can be seen in Figure 6.4. Again, the wave perturbations in both layers move in unison, without much alteration. A peak which is followed throughout the simulation covers about 5 nondimensional length units in 400 nondimensional time units, for a phase speed of 0.016, remarkably close to the predicted value. To determine whether the flow was unstable in either experiment, the lower layer Kinetic Energy,

$$KE = \frac{1}{2} \int_{\min x}^{\max x} \int_0^L \nabla p \cdot \nabla p \, dy dx. \quad (6.25)$$

was tracked throughout both simulations. Some instability is inevitable in numerical simulations due to round-off errors, however in both cases the KE maintained its initial value to within 5% over a long time period, suggesting that very little growth had occurred.

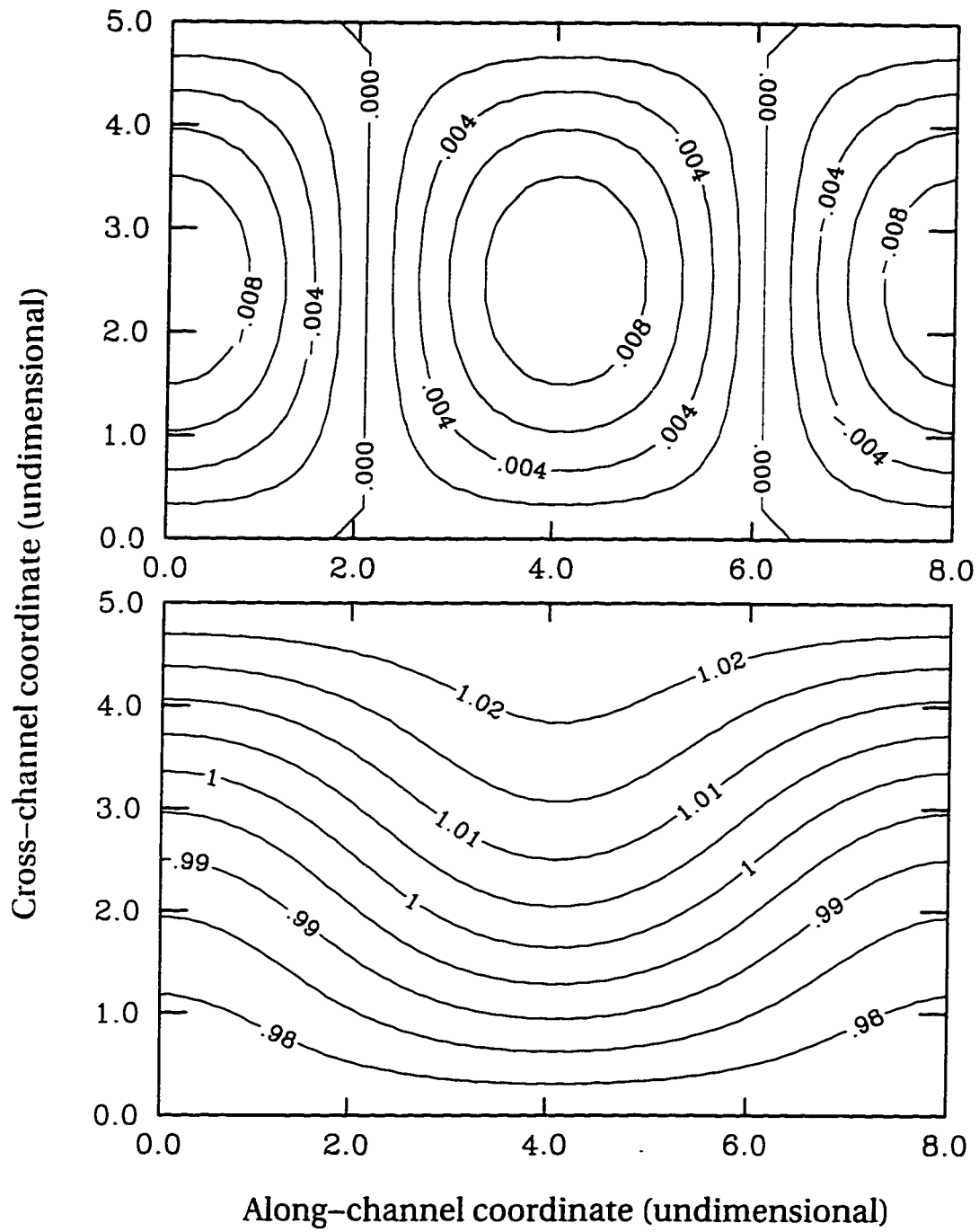


Figure 6.1: Typical perturbation imposed on upper layer thickness.
 Figure 6.2: Wedge front plus perturbation.

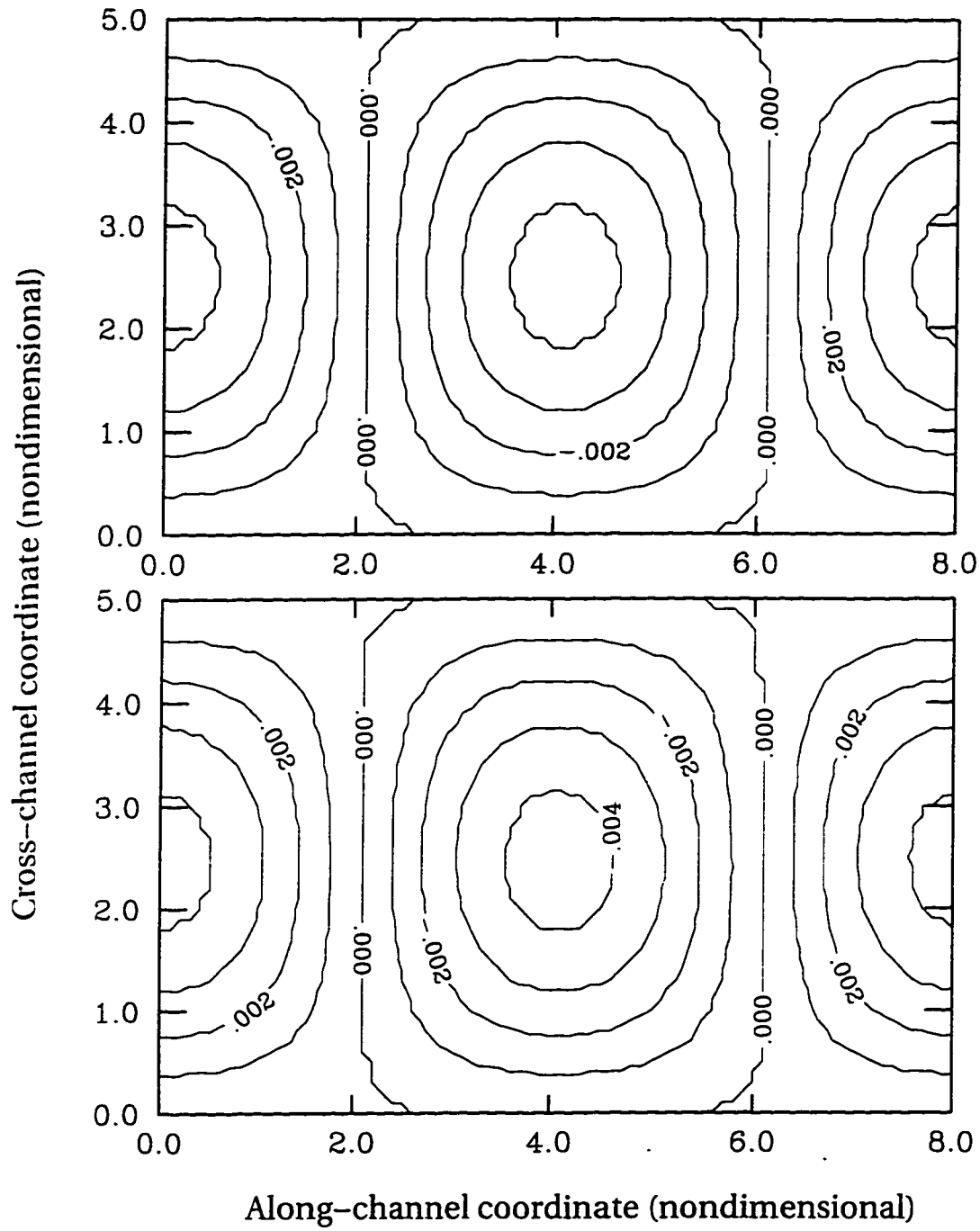


Figure 6.3: Time series of upper layer perturbation for wedge front at $t=1$ and $t=126$ (nondimensional time) on Upper Branch of MSC. Theoretical phase speed is -0.00016 . Continued on next page.

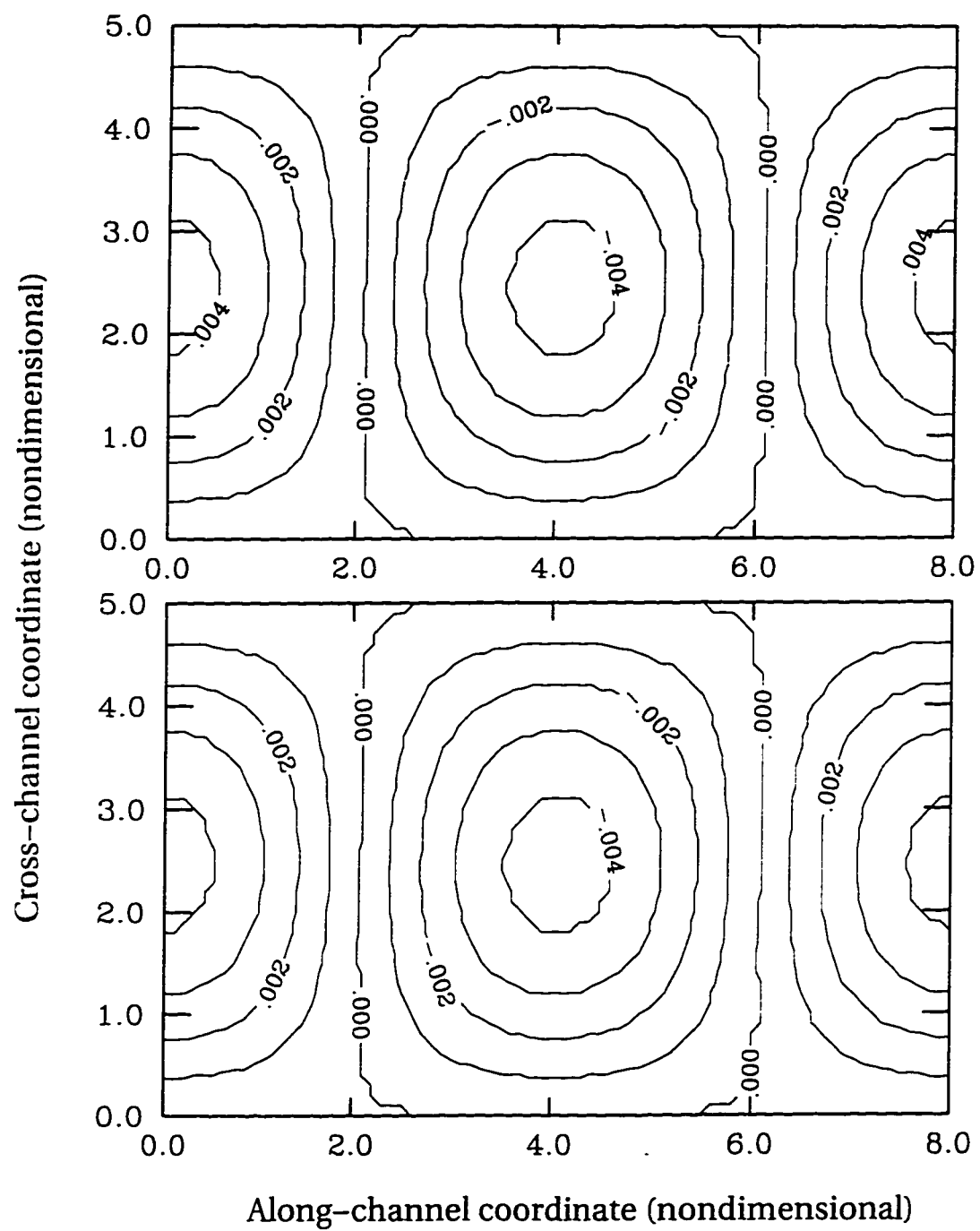


Figure 6.3 continued: Time series of upper layer perturbation for wedge front at $t=251$ and $t=376$ (nondimensional time).

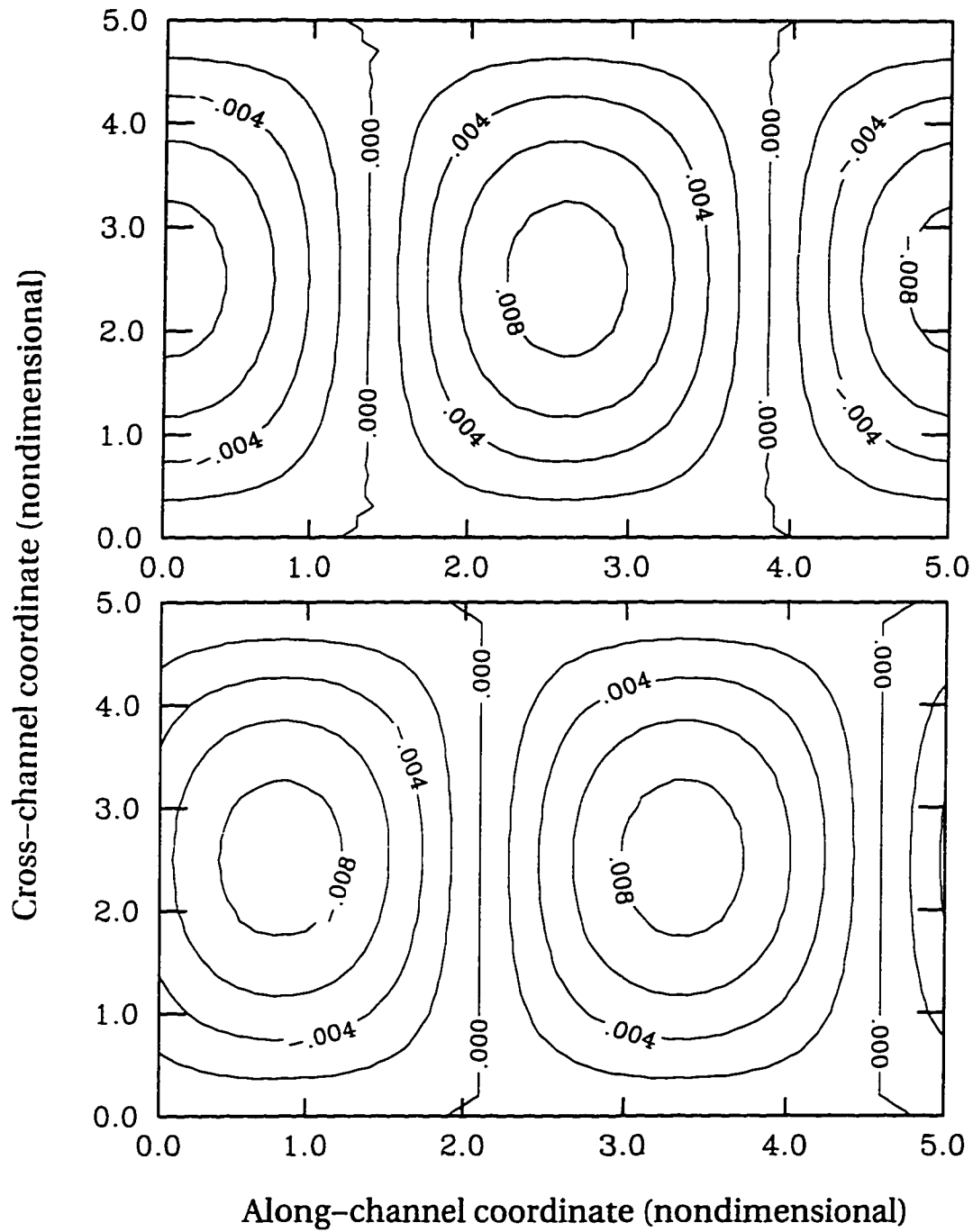


Figure 6.4: Time series of upper layer perturbation for wedge front at $t=1$ and $t=126$ (nondimensional time) on Lower Branch of MSC. Theoretical phase speed is 0.015. Continued on next page.

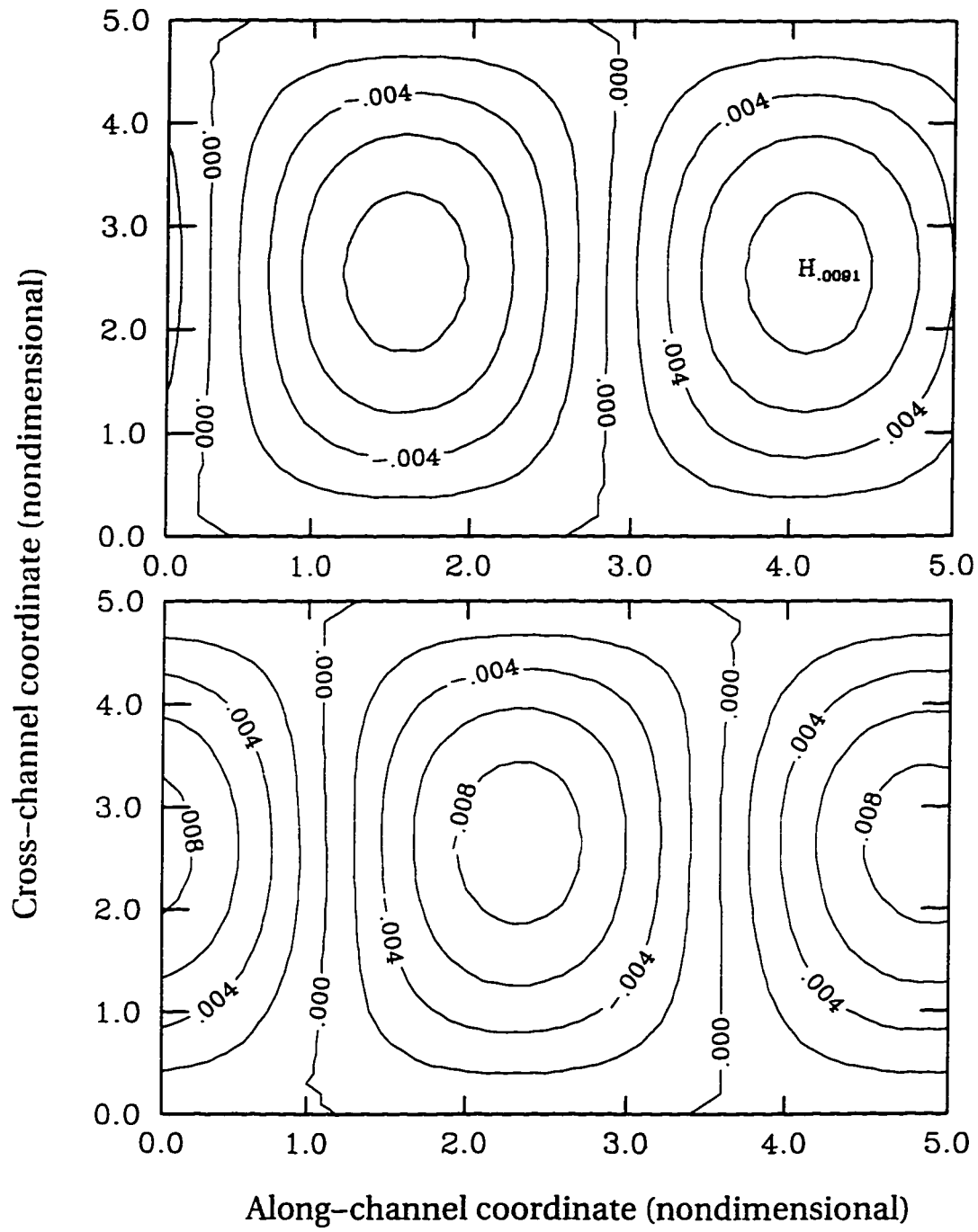


Figure 6.4 continued: Time series of upper layer perturbation for wedge front at $t=251$ and $t=376$ (nondimensional time).

6.4 Weakly Nonlinear Results

To investigate the behavior of a marginally unstable wedge front, we introduced the perturbed α and initialized the perturbation with the linear solution for the associated α_c . Moreover, the choice of the along-channel wavenumber k depended on the region under consideration (see Figures 4.2 through 4.6). A simulation was performed with $K^2 = 2.0$, $s = 0.078$, $\alpha_c = -0.01$ in a channel domain 10 units long by 5 units wide. The parameter δ was taken to be unity, which meant that $\alpha = -1.048 \times 10^{-2}$ by (4.14). To investigate the behavior of the perturbation in Region III (typical linear instability and nonlinear saturation) the value of k was taken as 1.26, which corresponded to two full waves in the x -direction.

The lower layer KE was tracked, which indicated the development of the flow. Figure 6.5 is a plot of the KE, normalized by its initial value, versus time. We see that there is an initial growth of the perturbation, followed by a saturation. This is consistent with the linear growth and nonlinear decay which our theory predicts. At time $t = 120$ however, the KE begins to increase rapidly and the flow becomes unphysical. The perturbation fields in both layers develop sharp peaks, often at the grid resolution, which may be a sign of numerical instability.

Many other precise wedge-front experiments were performed, at various points on both branches of the MSC. Unfortunately, the oscillatory signature of the perturbation, though predicted by weakly nonlinear theory, was never observed. Numerical error always prevented the onset of clearly periodic behavior. This is not to say that the numerical scheme is inappropriate, nor that the model is ill suited for computational integration. Indeed, many results were obtained for more complex initial configurations, which were not subject to such instability and agreed very well with real-world observations. Moreover, periodic weakly nonlinear interaction was observed for an isolated front, however this front did

not fall under the strict assumptions of our finite-amplitude theory. All these simulations will be discussed shortly.

Regarding the wedge-front (without an outcropping), we conclude that numerical verification is difficult, an assertion which may be worth investigating in itself. At this point in the research, it appears that the clamped Dirichlet boundary condition could be the origin for the difficulty. By fixing the upper layer thickness on both channel walls, we prevent the average slope of the isopycnal from changing. Individual anomalies are allowed to develop but the wedge shape is largely unchanged, which may be unphysical. On the other hand, if an outcropping exists, then the location of the front is determined by the dynamics of the model, and the front profile can deform accordingly. Such simulations are, in general, well behaved. It would be worthwhile to experiment with a fixed boundary condition on one wall, and a free boundary on the other wall, still requiring that the x -derivatives vanish there.

While investigating an isolated front with an outcropping, we found evidence for weakly-nonlinear interaction. The initial configuration was that of an upper layer jet (to be discussed further in the next section). A time series of the upper layer evolution can be seen in Figure 6.6. The front deforms horizontally into a gentle wave, then returns to its initial shape, then deforms again. This process repeated itself throughout the simulation. A plot of the lower layer KE versus time in Figure 6.7 demonstrates growth and decay at more or less equal intervals. Aside from the constant but small upward trend in the KE, we believe this periodic behavior indicative of weakly nonlinear processes. However, comparing this result with our analytical predictions is problematic, since the front is not linear in the cross-channel direction, and outcrops on the surface. Both are features which the theory does not take into account.

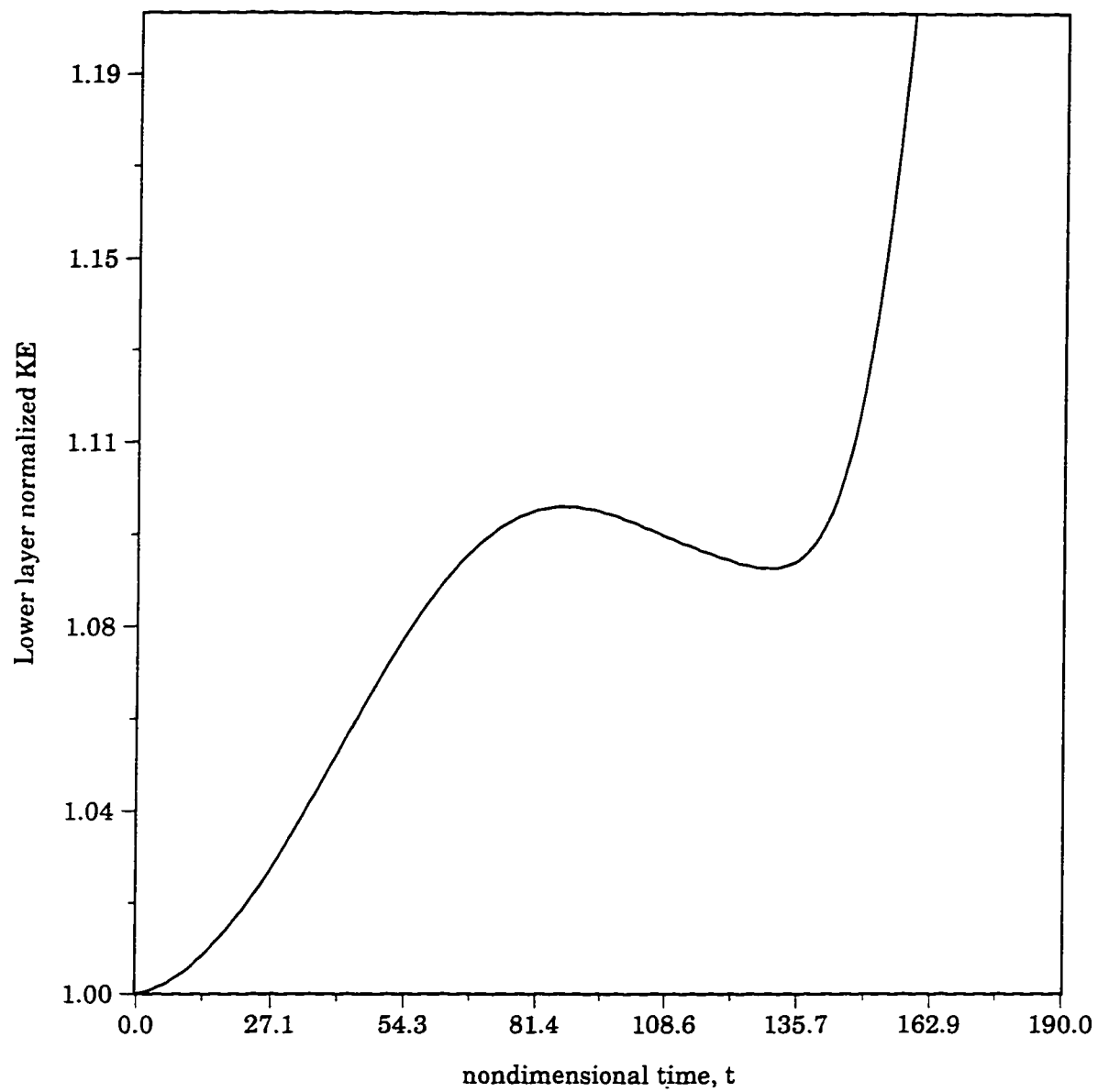


Figure 6.5: Normalized lower layer Kinetic Energy versus time for marginally-unstable wedge front simulation.

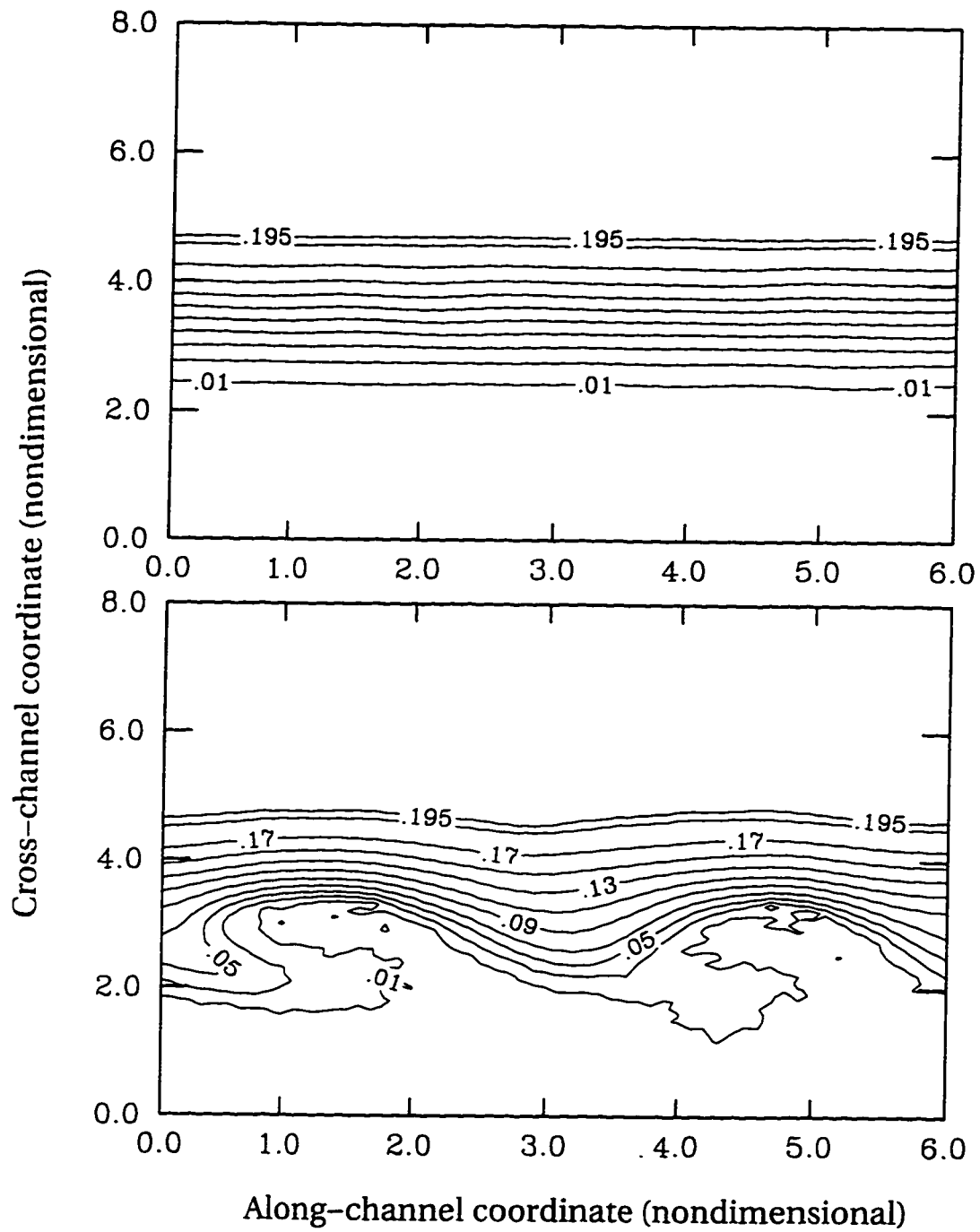


Figure 6.6: Time series of upper layer thickness for a weakly unstable isolated front at $t=1$ and $t=350$ (nondimensional time). Continued on next page.

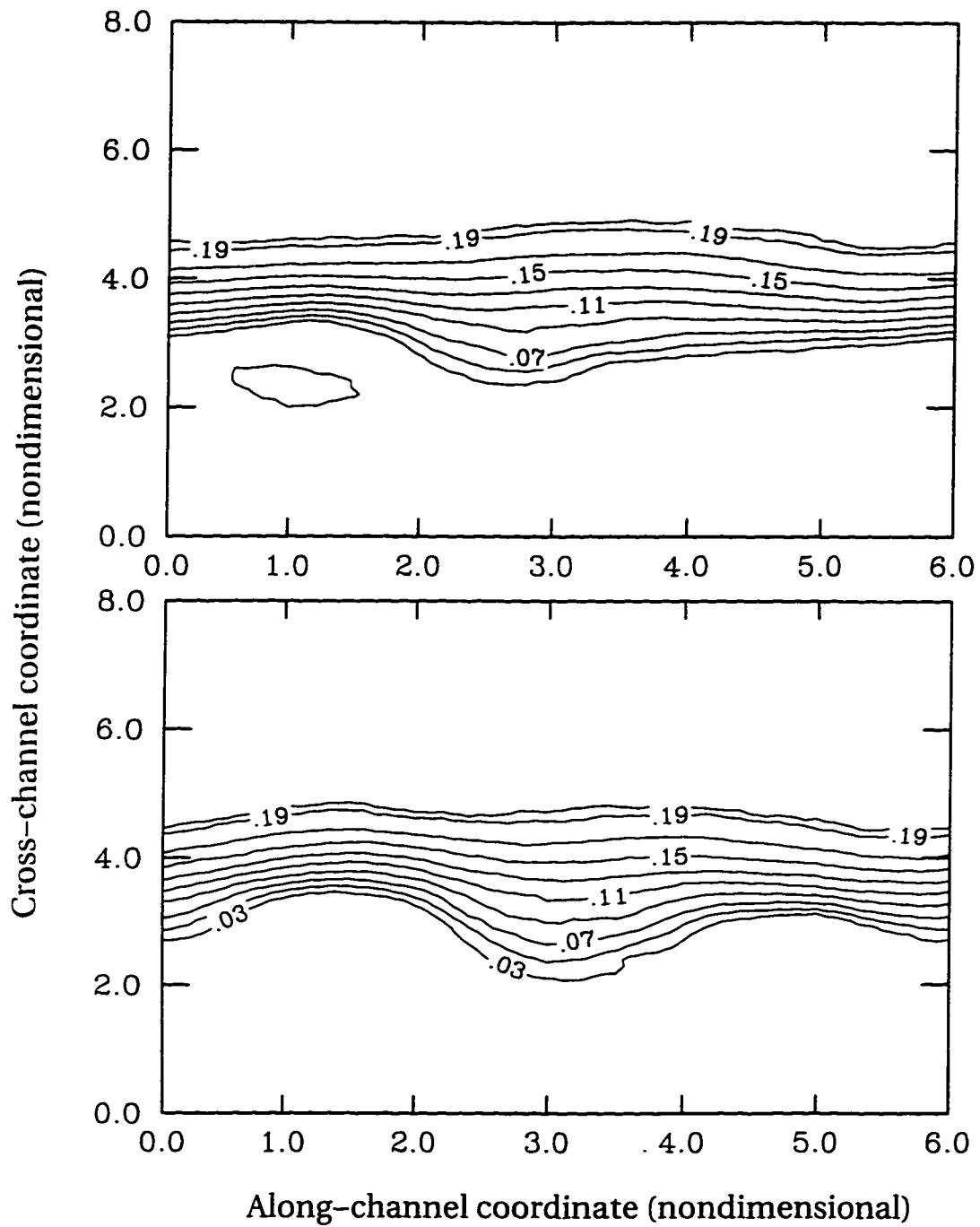


Figure 6.6, continued: Time series of upper layer thickness for a weakly unstable isolated front at $t=400$ and $t=490$ (nondimensional time).

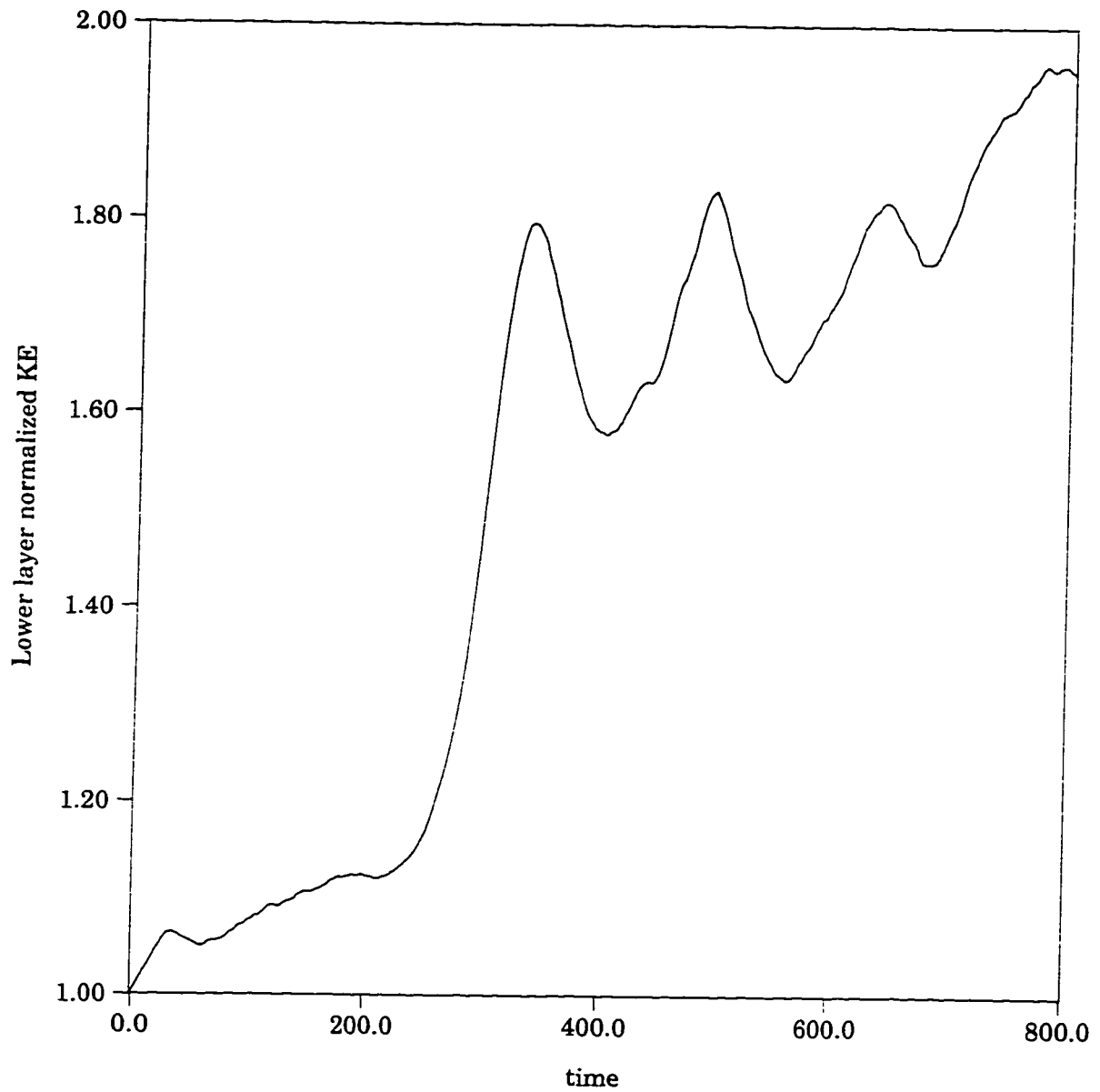


Figure 6.7: Normalized lower layer Kinetic Energy versus time for weakly-unstable isolated front simulation.

6.5 Jet Simulations

The isopycnal lines in cross-sections of surface currents such as the Gulf Stream or the Agulhas Current usually form a distinct, isolated front, which outcrops on the ocean surface (Gill, 1982). To leading order, the current is geostrophically determined (Robinson, 1983), so that along-channel velocities are greatest at the outcropping, where the y -derivatives of the isopycnals are at their maximum. In an attempt to mimic such conditions, a number of numerical simulations have been performed with a geometry shown in Figure 6.8. To excite the instability, the lower layer pressure was initialized with a random superposition of small waves. It was found that such a front readily deforms, after which warm-core eddies are shed, a process which seems to be heavily influenced by the bottom slope. Cold-core eddies were also observed.

In the following sections we will often give dimensional values for the space and time variables. Such quantities were calculated using the nondimensionalization scheme in Section 2.3 and typical scales for an oceanic shelf region (see Swaters, 1993). With $g' \simeq 0.01$, $\bar{h} \simeq 30$ m, $H \simeq 300$ m and $f_o \simeq 10^{-4}$, (2.29) defines $\delta \simeq 0.1$ and (2.30) predicts a lengthscale $L \simeq 10$ km. The internal Rossby radius associated with the upper layer is then approximately 6 km. The internal Rossby radius for the lower layer (or indeed, for the system as a whole) is $\delta^{-\frac{1}{4}}L$, or in this case roughly 17 km. Finally, the time scale as defined implicitly in (2.31) is 10^5 sec, or about 1.2 days.

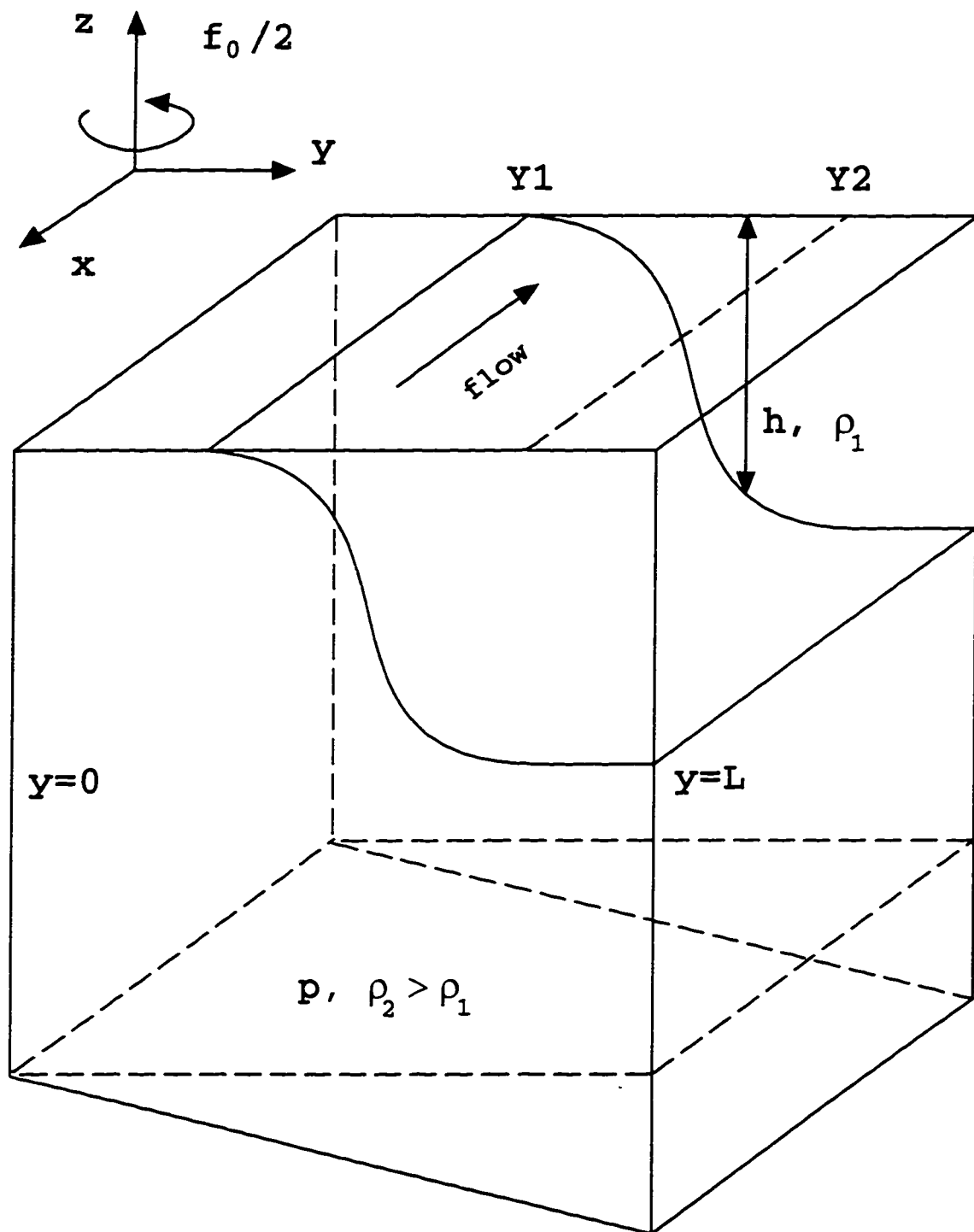


Figure 6.8: Isolated front profile (i.e. a jet)

6.5.1 Warm-Core Eddy Simulation

In a series of simulations, the initial upper layer thickness, h , was of the form

$$h = \begin{cases} 0 & \text{on } y \in (0, Y1] \\ \frac{1}{2}h_{\max}(\sin[\frac{\pi}{Y2-Y1}(y - y_{mid})]) + 1 & \text{on } y \in (Y1, Y2) \\ h_{\max} & \text{on } y \in [Y2, L] \end{cases} \quad (6.26)$$

where $y_{mid} = (Y1 + Y2)/2$ and the bottom was flat. Figures 6.9 and 6.10a show the evolution of h for $Y1 = 2$, $Y2 = 5$, and $h_{\max} = 0.1$ at $t = 0, 51, 102, 154$ and 207 . This corresponds to approximately 0, 59, 118, 178 and 240 days. The channel length and width were 6 and 8 units respectively, or in dimensional units, 60 and 80 km. In general, for a channel of this length, the front initially develops a wavenumber 2 instability. This wave then breaks and forms meanders. The meanders begin pinching off, i.e. warm-core eddies are shed by the current.

The resulting eddies are very reminiscent of vortices often observed near the afore-mentioned currents. In Figure 6.10a, one eddy has already split off and propagated away from the front while another eddy is just beginning to break away. Figure 6.10b shows that the lower layer pressure closely mimics the structure of the upper layer. An oblong high pressure cell whose center lies at $x \simeq 4.5$, $y \simeq 3.5$ is clearly discernible. These coordinates coincide with those of the isolated upper layer eddy. Since p is a streamfunction, a high pressure anomaly implies that an induced vortex exists in the lower layer.

The maximum current depth and velocity were varied in other simulations, as were the size of the domain and the size of the initial perturbation in the lower layer pressure. It was found that the dominant wavenumber of the deforming front (and therefore the number of vortices shed) is determined by the length of the channel. However this does not affect the intrinsic deformation wavelength.

Isolated Eddies are slightly elliptical in shape and most have a maximum diameter of 20-30 km (certainly larger than the Rossby radius of the upper layer).

Our studies show that the eddies may interact with each other, interact with the current, and eventually be reabsorbed by it. While outside the current, they propagate parallel to it but in the opposite direction. This behavior was noted in, for example, Chassignet *et al.* (1990) for a double gyre experiment using a multilayer, isopycnic numerical model. It is worth pointing out that, barring a serious asymmetry in the generation process, the eddies in our experiments have no tendency to propagate across the channel. This is in contrast with bottom-dwelling cold domes, which can acquire a cross-shelf velocity in the down-slope direction. An eddy's motion may, however, be perturbed through interactions with the lower layer.

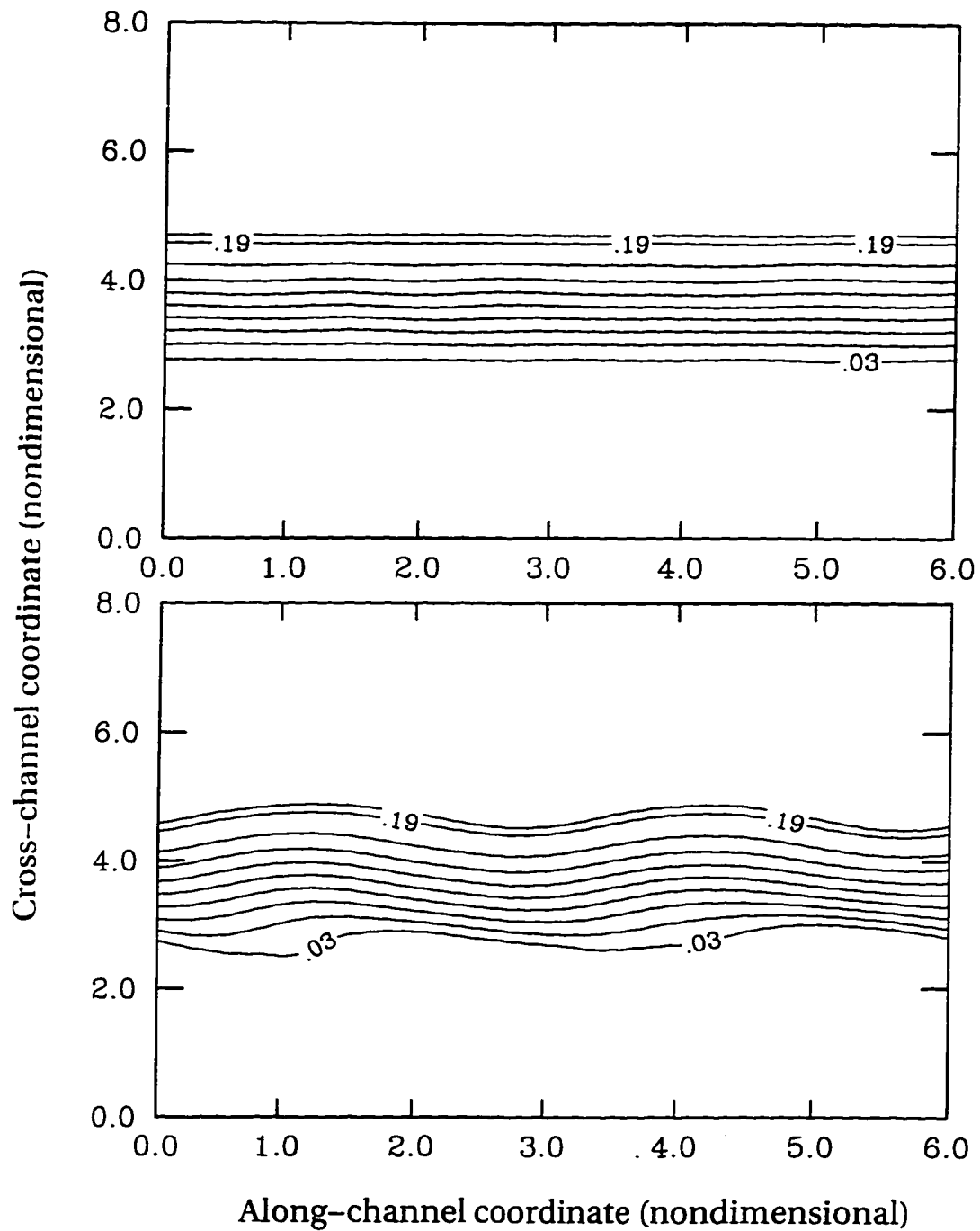


Figure 6.9: Time series of upper layer thickness for an isolated front at $t=0$ and $t=51$ (nondimensional time). Continued on next page.

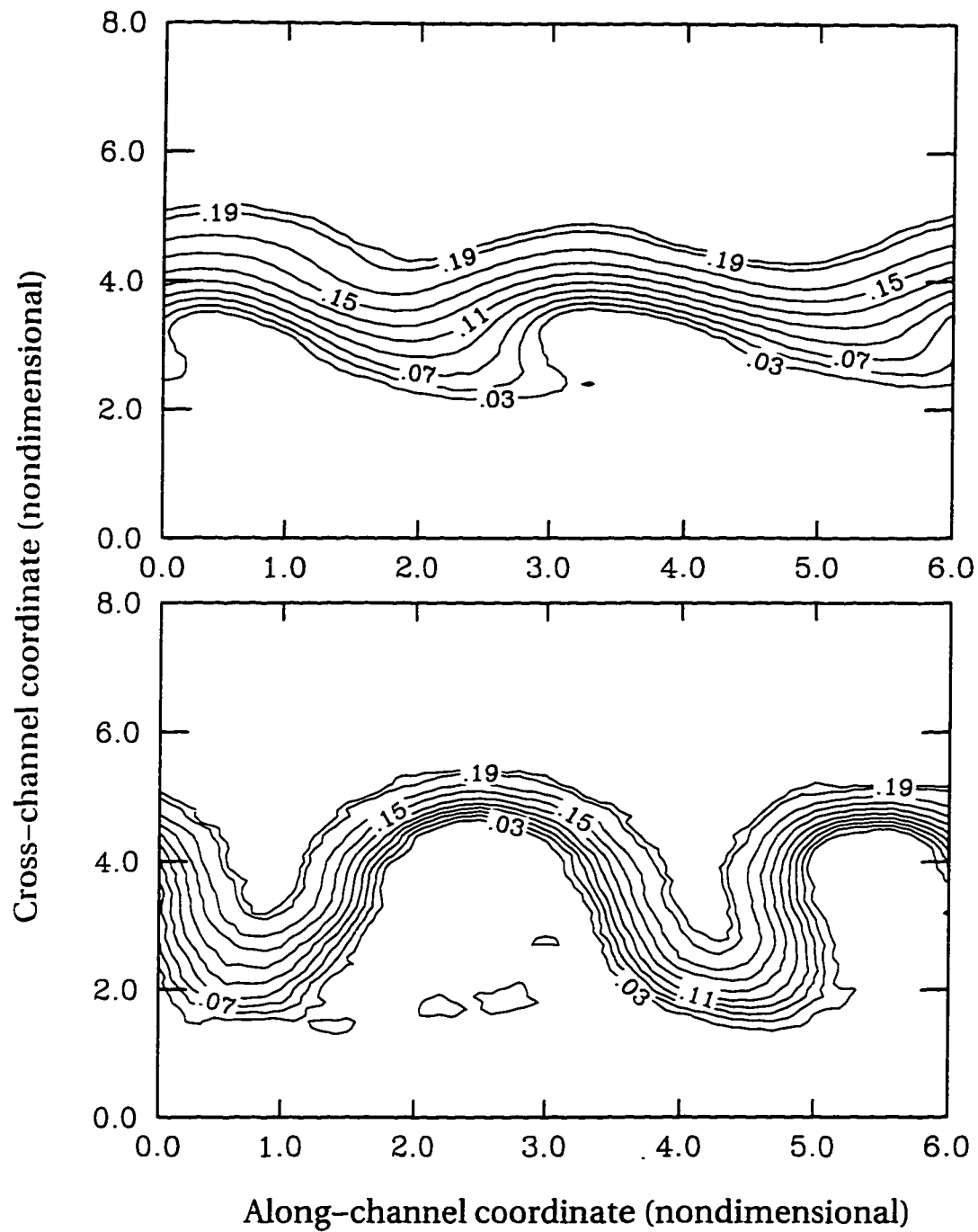


Figure 6.9, continued: Time series of upper layer thickness for an isolated front at $t=102$ and $t=154$ (nondimensional time). Continued on next page.

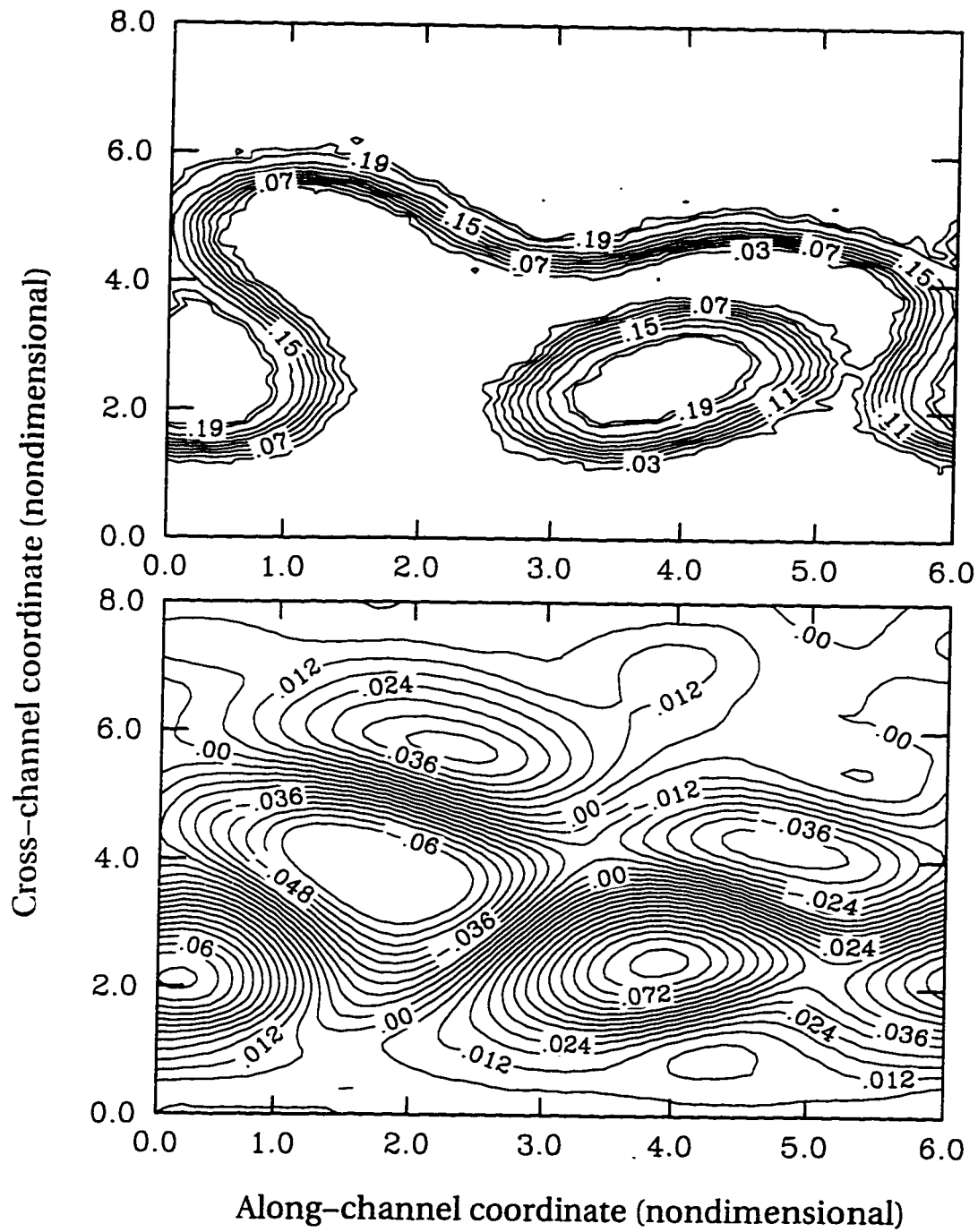


Figure 6.10 a: Upper layer thickness at $t = 206$.
 b: Lower layer geostrophic pressure at $t = 206$.

6.5.2 Cold-Core Eddy Simulation

The isolated front simulations described above sometimes produced cold-core eddies. This process seemed to be most affected by the bottom slope and the exact initial distribution of perturbations in the lower layer. The process usually begins with horizontal deformation of the front and meandering, as with the warm eddy simulations. However in some cases one of the waves is seen to break vigorously enough that it touches the crest of an adjacent wave. The two crests then merge, 'trapping' a pool of cold water within the jet. Thus, the cold-core eddy is just a (more or less) circular area away from the original front, where the upper layer thickness vanishes.

Here we present a simulation with the same initial conditions as above, but with a bottom slope of 0.039. In Figure 6.11 we see the time series of the upper layer thickness at $t = 0, 369, 416$ and 465 (i.e. $0, 427, 481$ and 538 days). The lower layer pressure does not show an induced eddy, however the model was never designed to capture such features. The vortex persisted largely unchanged for a long time. It propagated parallel to the current but, again, in the opposite direction.

Cold-core eddies are often seen in the vicinity of the Gulf Stream, especially where it leaves the coast. They cross the front and migrate into the warmer Sargasso Sea. Cold eddies in nature are usually circular for the majority of their existence (Robinson, 1983), a result which was also observed here. The cold eddies in this series of runs were generally smaller than warm eddies. This trend, while not usually observed in association with the Gulf Stream, was also noted in a numerical study by Bush *et al.* (1995).

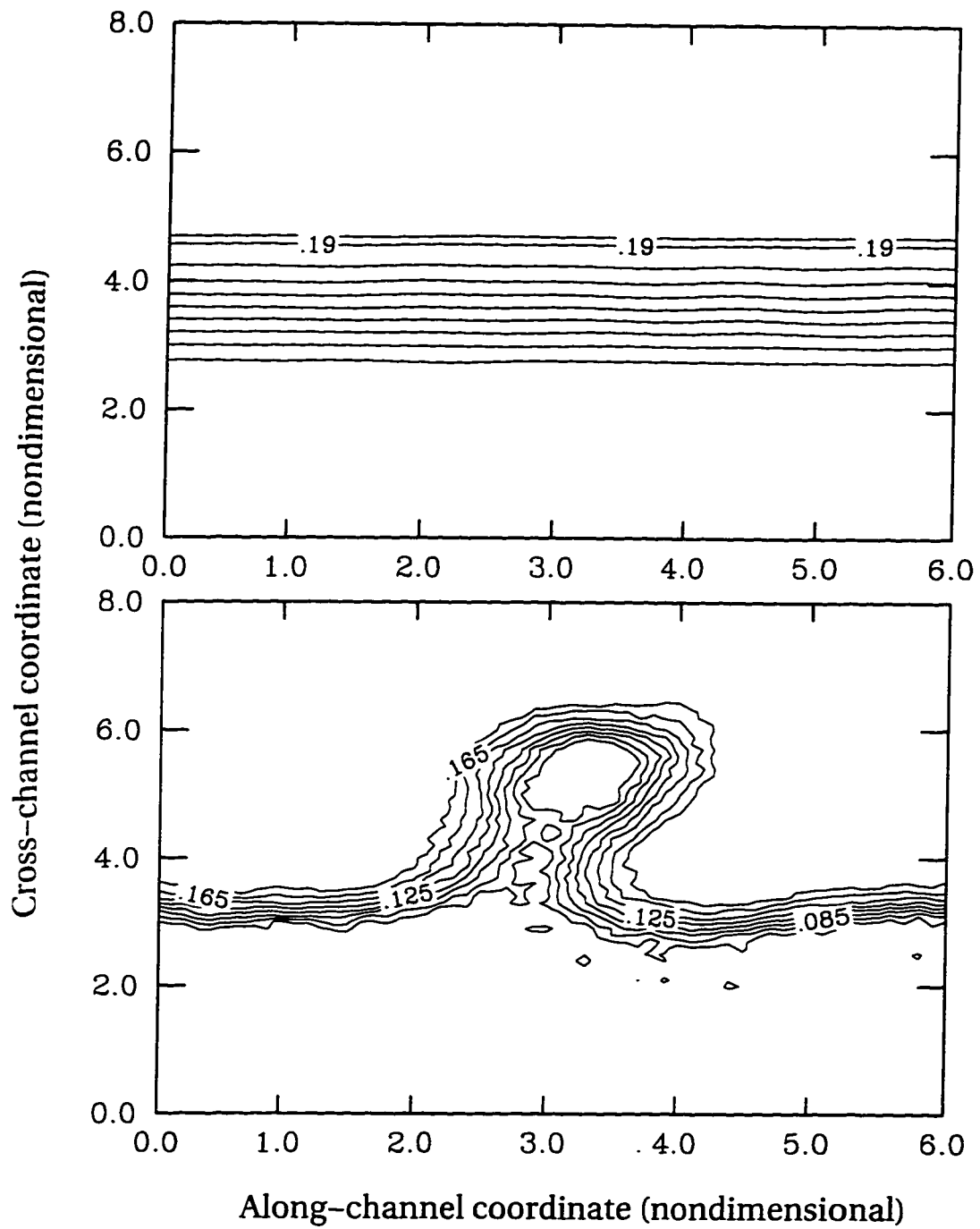


Figure 6.11: Time series of the upper layer thickness for an isolated front at $t=0$ and $t=370$ (nondimensional time). Continued on next page

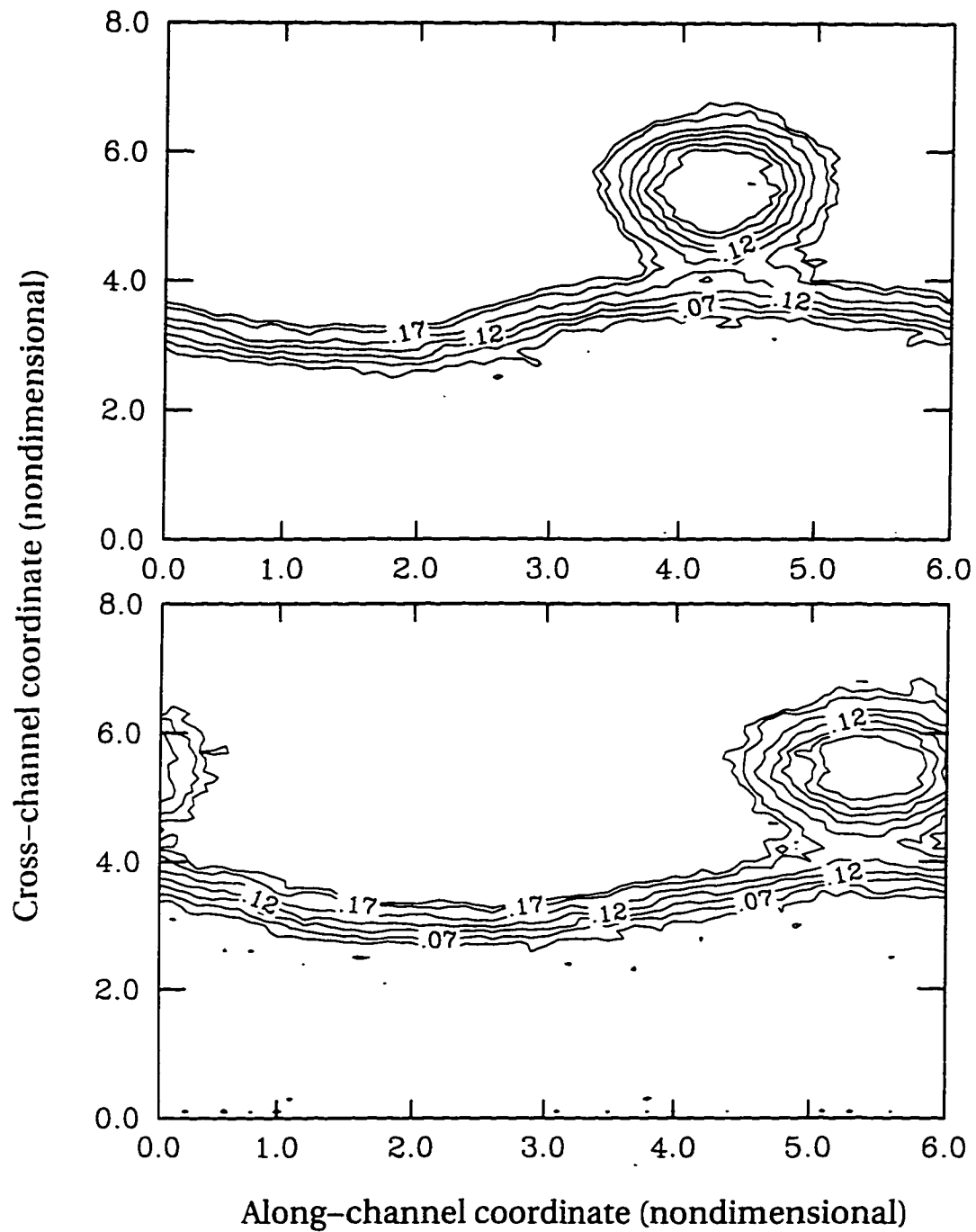


Figure 6.11, continued: Time series of the upper layer thickness for an isolated front at $t=418$ and $t=466$ (nondimensional time).

6.5.3 Effect of Bottom Slope

The present model incorporates a linearly-sloping bottom, which approximates the slanted topography of a continental shelf. The velocities of surface currents and fronts often become intensified near coastlines, where the ocean is typically very shallow (see Pond & Pickard (1983) for a discussion of westward intensification). This is when the ocean bottom plays an important role. In these simulations the bottom slope seemed to correlate directly with the time of the first warm eddy pinch-off. The results can be seen in Figure 6.12. We found that when s is between -0.195 and 0.039, the flow is most conducive to eddy formation. For $s > 0.039$ the instability is suppressed and the wave does not grow large enough to meander.

For $s < -0.195$, there is too much shear for coherent structures to form, or if they do form, they are very short-lived. The reason for this behavior is as follows. The bottom slope induces a topographic Rossby wave field in the lower layer. The Rossby waves naturally tend to propagate with the shallow water on their right. If the upper layer mean flow propagates in the same direction, then the lower layer is able to stabilize any developing large scale structures. If, on the other hand, waves in the slope water propagate in the opposite direction from the current, then instabilities are suppressed. This result is consistent with the observation that most warm and cold eddies are shed only after the Gulf Stream leaves the continental shelf. Bush *et al.* (1995) also proposed this possibility.

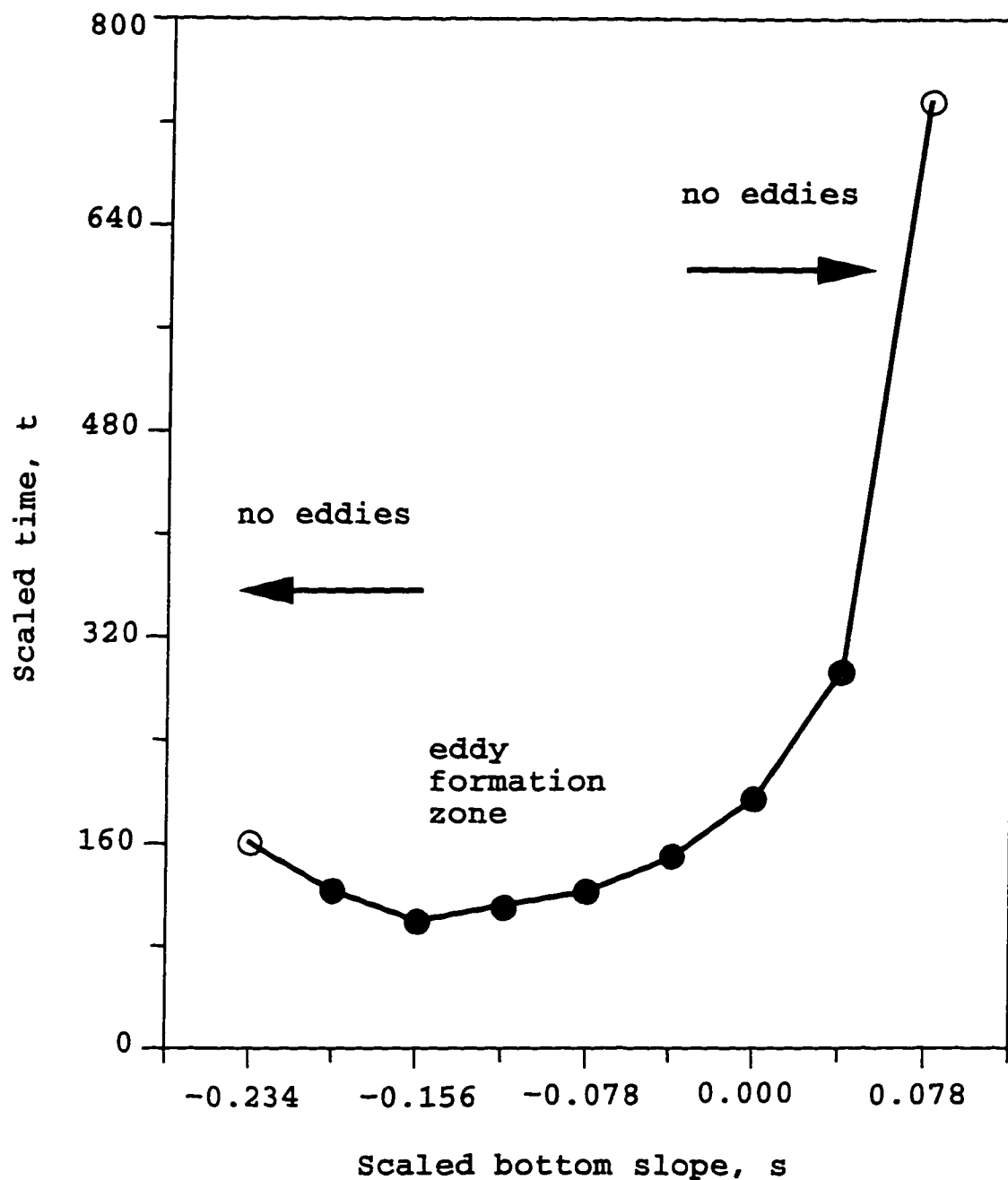


Figure 6.12: Time of first eddy pinch-off versus bottom slope, for isolated front simulation

6.6 Coupled Fronts

A current, such as the Gulf Stream, sometimes exhibits two outcroppings of one density surface (Gill, 1982). There are ample data involving these surface “coupled fronts” from laboratory experiments, most notably GKS, and Griffiths & Linden (1981). As an added motivation for this series of experiments, we can compare our results with those of primitive equation numerical models, for example Pavía (1992). A coupled front induces a shear flow (along-channel velocities in both directions). This is because the leading order x -velocity is proportional to the y -derivative of the isopycnal, as was explained in Chapter 2, the derivation of the model equations. The upper layer profiles we tested were a gaussian curve, a parabola, a cosine wave (from trough to trough) and several piecewise linear fronts. We required that the y -structure was approximately bell-shaped, but the exact function used did not have any crucial effect on frontal development. As for the coupled fronts in the previous section, a random perturbation was introduced into the lower layer pressure field to induce an instability in the flow.

Here we present results for a gaussian curve in the upper layer, where initially,

$$h = h_{\max} \exp[-a^2(y - y_{mid})^2]. \quad (6.27)$$

for all (x, y) in the domain. The general configuration is depicted in Figure 6.13. It should be stressed that, while the gaussian curve is strictly positive, its shape does approximate a coupled front fairly well. Profiles which actually outcrop on the surface were also tested, and did not exhibit markedly different behavior. These will be discussed later in the section.

A typical simulation can be summarized as follows. The current deforms asymmetrically and promptly breaks up into distinct eddies (in accordance with GKS) whose size is comparable to the width of the current, as reported by Griffiths &

Linden (1981). The eddies are elliptical, but with a very small eccentricity. They rotate clockwise, i.e. anti-cyclonically, where we mean that there is an overall rotation of the ellipse about its center. This is quite separate from the rotation of the fluid within the eddy, which is also anti-cyclonic due to the negative radial derivatives of h and leading order geostrophy.

Figure 6.14 shows four frames from a time series of such a break-up, where the parameters h_{\max} , a and y_{mid} had the values 0.5, 2.0 and 5.0 respectively. The domain was 12 units in the along-channel direction and 10 in the cross-channel direction (approximately 120 km by 100 km). The first frame is the initial configuration, and the other frames are at $t = 2, 4$ and 8 (i.e. 2, 5 and 9 days). Similar eddy development on a temporal scale of several days was observed by Pavía (1992) in numerical experiments using a Lagrangian, “particle-in-cell”, primitive equation algorithm.

Once formed, vortices in our simulations tend to be staggered about the line of horizontal shear and do not usually propagate in any direction. Their locations and translation can be influenced by a sloping bottom through strong anomalies in the lower layer pressure. However this effect is transitory, and yields no consistently preferred direction of motion. With a flat bottom, the arrangement of the eddies seems to be dictated by conservation of total momentum, which is zero for the initial current. We have observed that the emergent vortices are quite stable when isolated, but if any two come close to one another, they are likely to merge. The resulting oblong body is not so stable and can easily split into two separate eddies again. A merger can be seen in Figure 6.15a and a subsequent splitting in Figure 6.15b. These figures are a continuation of the time series in Figure 6.14.

The formation of nearly circular eddies for a coupled front was also noted by Pavía (1992) for the numerically-integrated $1\frac{1}{2}$ layer model introduced by Cushman-Roisin (1986). Since this is a barotropic model, and because the cou-

pled front does create a strong horizontal shear in the upper layer, it is likely that this particular instability is not primarily baroclinic. As in the jet simulations, the number of vortices produced is heavily influenced by the length of the channel domain. It should also be noted that the eddy development in a shear flow is very rapid, at least an order of magnitude faster than in the isolated front simulations, described above. This qualitative difference suggests another instability mechanism, in addition to the release of available potential energy. This is, again, a topic for future research.

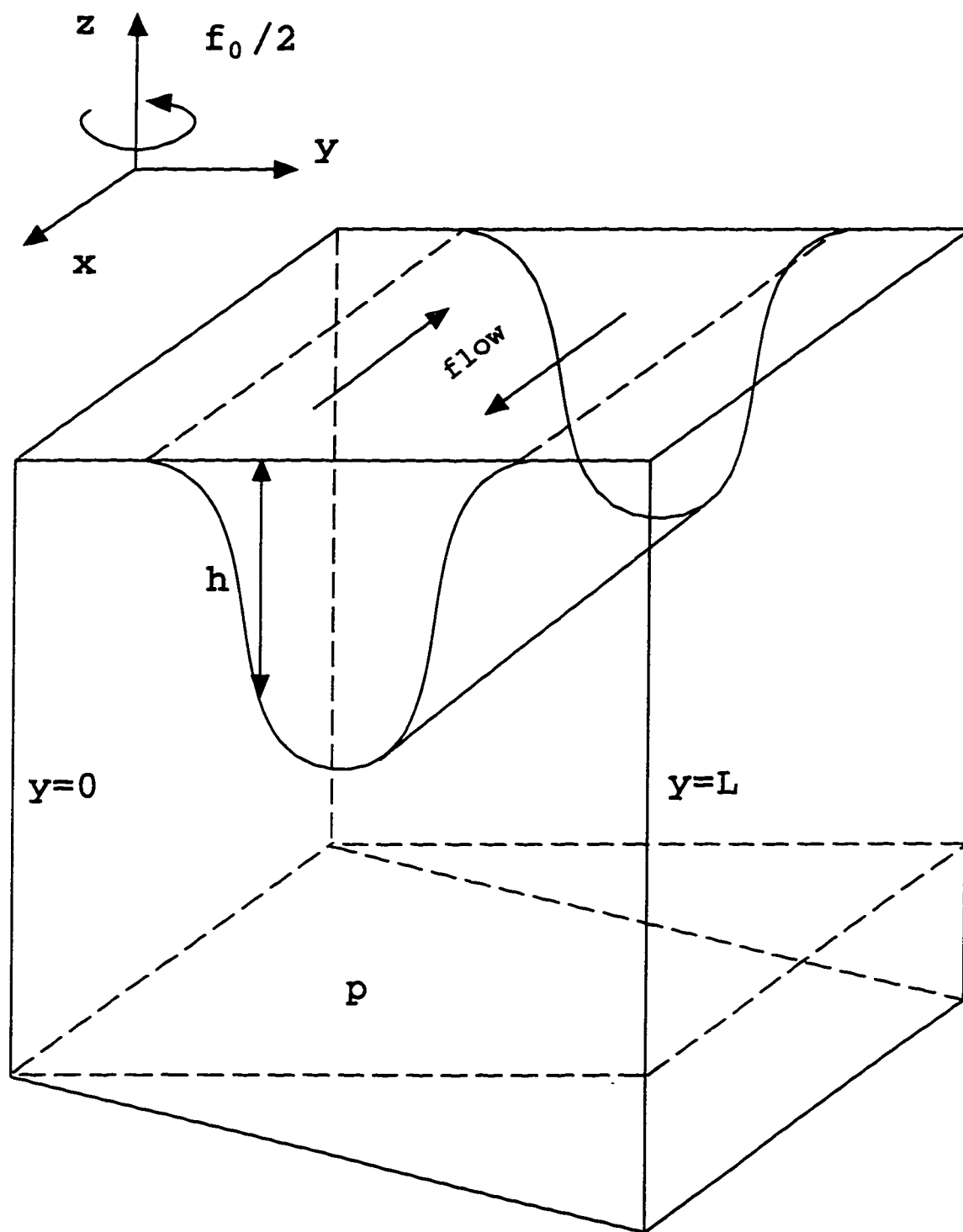


Figure 6.13: Coupled front profile
(i.e. a shear flow)

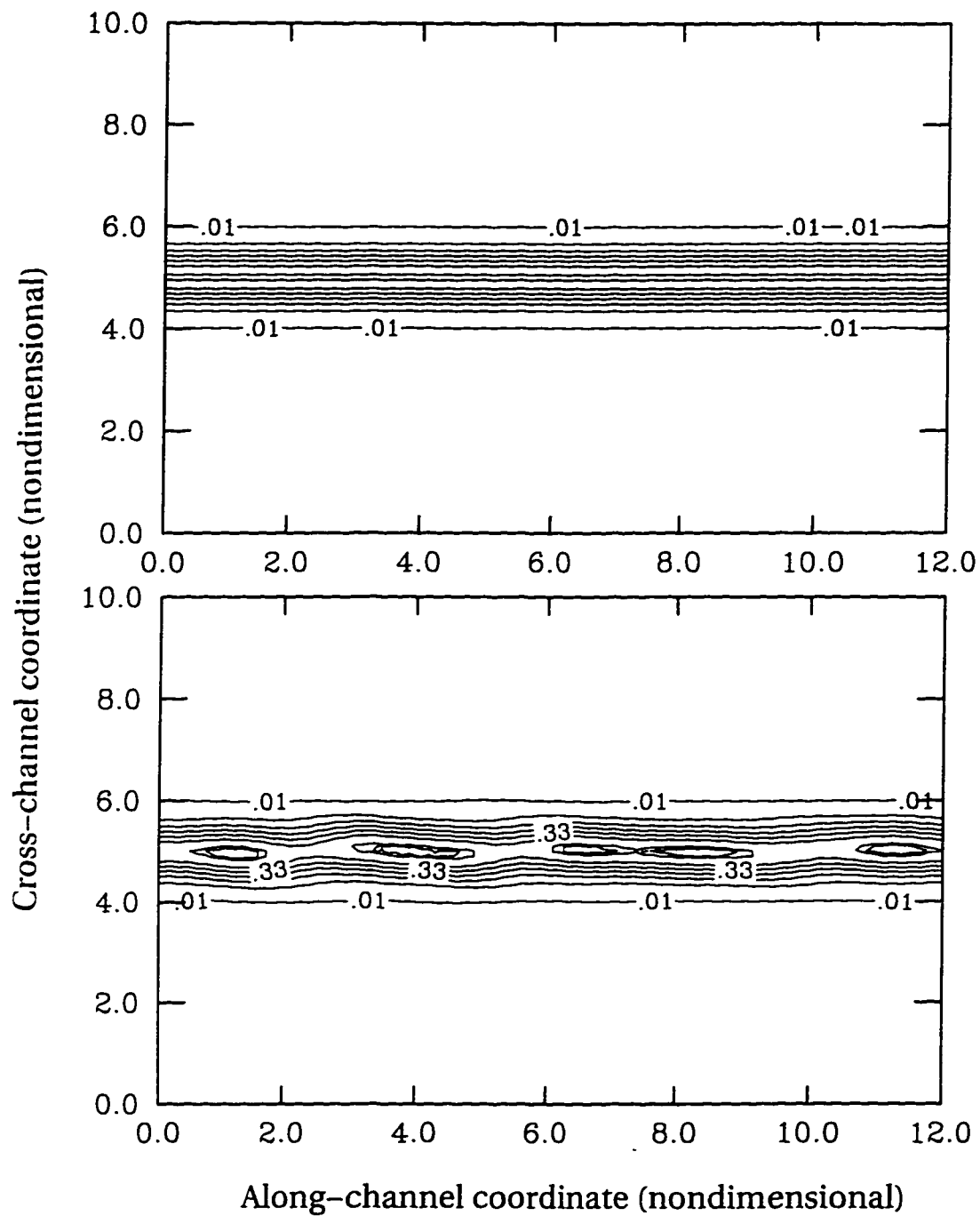


Figure 6.14: Time series of the upper layer thickness for a coupled front at $t=0$ and $t=2$ (nondimensional time). Continued on next page

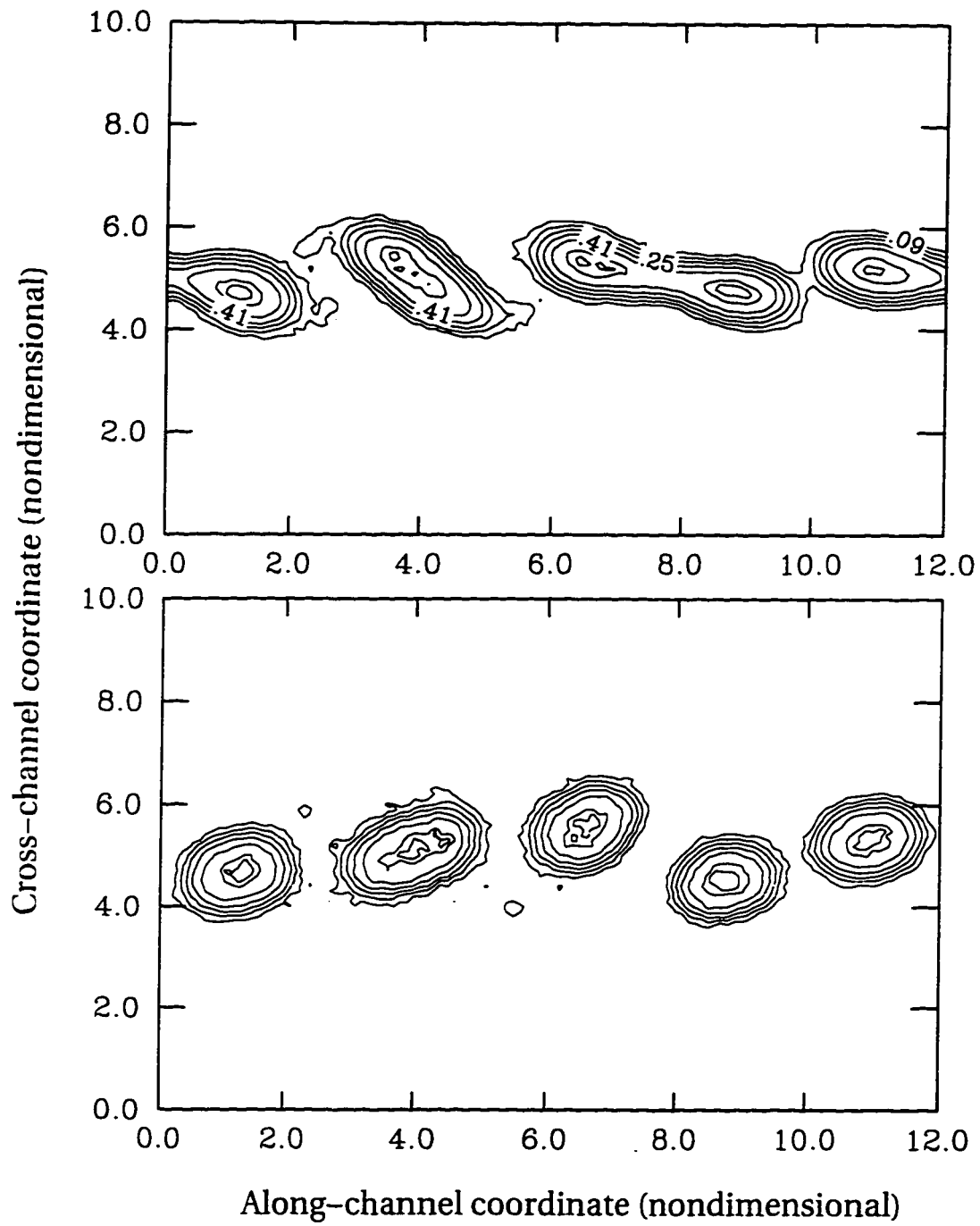


Figure 6.14, continued: Time series of the upper layer thickness for a coupled front at $t=4$ and $t=8$ (nondimensional time).

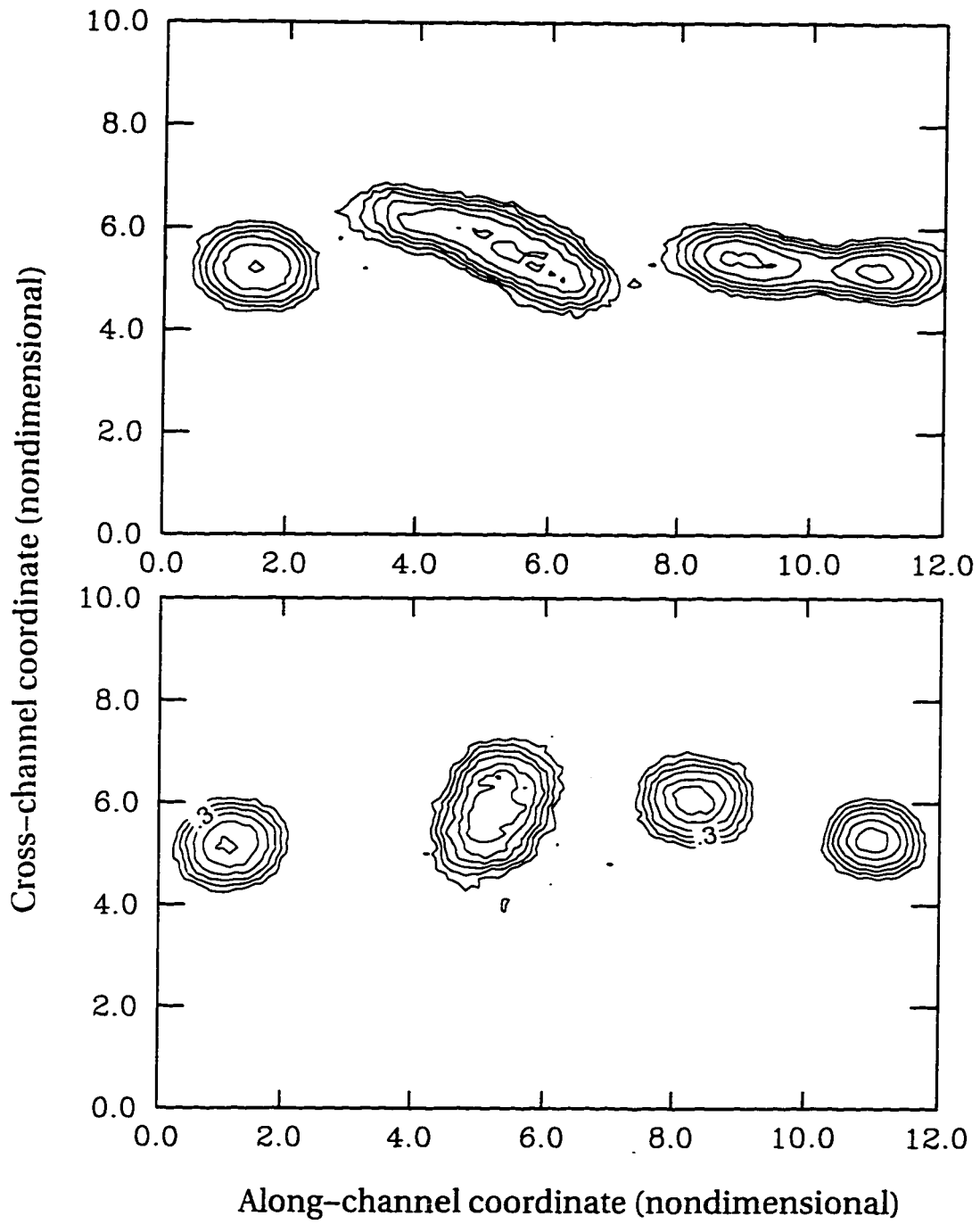


Figure 6.15: Upper layer thickness for a coupled front at $t=22$ and $t=40$ (nondimensional time).

6.7 A word about comparisons

Throughout this thesis we have referred to observational data from the world's oceans. In many ways this data compares favorably with results stemming from the present model. However, in cases where scales of motion differ to some degree, such comparisons can only be qualitative. Using the scalings discussed in Section 6.5, we find that warm core eddies in our jet simulations typically had a diameter of 30 km. This is considerably smaller than vortices produced in the Gulf Stream and other western boundary currents, which are often more than 100 km across (Robinson, 1983). In fact, the Gulf Stream exists mainly in the open ocean, not in the continental shelf region. Based on these considerations alone, a better analogy for our model may be the smaller "Algerian" and "California" currents, which exist close to the coast, and exhibit meandering and vortex-shedding on smaller spatial scales, (Paldor & Ghil, 1991).

As was mentioned previously, the time required for the first warm eddy pinch-off in our simulations is quite long, i.e. several months. However, there is nothing in the scaling for time (2.31) to suggest such a requirement. In fact, with the above mentioned depth ratio $\delta = 0.1$, we would expect the time scale to be quite reasonable and future numerical simulations may verify this claim with a better choice of parameters, such as perturbation size and maximum current depth. Finally, it is important to realize that the same physical processes are often at work on different scales. The present model and the analysis presented herein aim to elucidate the relative importance of these processes in general, rather than providing an accurate description of any particular oceanic feature.

Chapter 7

Conclusions

A two-layer model for buoyancy driven currents on a sloping shelf has been presented, based on Swaters (1993). The model investigates baroclinic destabilization, but unlike many previous models, does not rely on the quasigeostrophic approximation. The linear problem for a wedge-front profile yielded sufficient criteria for stability, and marginal stability curves involving the ratio of the interfacial slope to the bottom slope, and the along-channel wavenumber. We presented a weakly nonlinear theory for the said wedge profile. While this was a highly idealized configuration which did not actually allow for isopycnal outcroppings, the analysis retained the essential features of baroclinic instability through the release of available potential energy and saturation of growth through nonlinear interactions.

It was found that linear growth and nonlinear damping lead to oscillating solutions, namely Jacobi elliptic functions. It was also found that, under certain circumstances, a perturbation can experience explosive growth. The model is not, however, subject to ultraviolet catastrophe in the linear sense, as are some models with larger spatial scales. A more general equation, involving a large spatial variable as well as slow time, was also derived, and the existence of steadily

travelling soliton solutions was demonstrated. We believe this to be a significant result, in that it confirms the possibility of the emergence of stable, coherent, eddy-like structures.

Numerical experiments were performed in order to verify the theory, as well as to explore more realistic flow scenarios. Linear analysis results can be demonstrated computationally with little difficulty. Nonlinear saturation could be seen in some simulations, but a peculiar numerical instability prevented observations of oscillatory behavior. Simulations corresponding to realistic isolated and coupled fronts produced meandering, warm and cold core eddies in the upper layer, as well as lower layer induced eddies. Moreover, the rapidity of vortex shedding could be correlated with the bottom slope in a way consistent with observations of the Gulf Stream.

The research presented herein is a first step towards a full understanding of the Swaters (1993) model. The initial results have proven encouraging. Our finite amplitude theory predicts saturation of linear instabilities and the development of stable, large scale structures. Numerical experiments demonstrate behavior which mimics the most interesting aspects of buoyancy fronts, and is similar to behavior seen in much more robust, continuously stratified numerical models. This leads us to conjecture that the model embodies a good balance of appropriate scalings, simplifying assumptions and essential physical relationships. Future work should include establishing a clearer link between finite amplitude theory and numerical integration of the full equations. More realistic flow configurations should also be considered, perhaps a piecewise linear coupled front.

Bibliography

- [1] Arakawa, A., 1966: Computational Design for Long-Term Numerical Integration of the Equations of Fluid Motion: Two-Dimensional Incompressible Flow. Part 1. *J. Comp. Phys.* **1**, 119-143.
- [2] Burden, R. L. & Faires, J. D., 1993: *Numerical Analysis*, 5th edition, PWS Publishing. 768 pp.
- [3] Bush, A. B. G., McWilliams, J. C. & Peltier, W. R., 1995: The Formation of Oceanic Eddies in Symmetric and Asymmetric Jets. Part I: Early Time Evolution and Bulk Eddy Transports. *J. Phys. Oceanogr.* **25**, 1959-1979.
- [4] Bush, A. B. G., McWilliams, J. C. & Peltier, W. R., 1996: The Formation of Oceanic Eddies in Symmetric and Asymmetric Jets. Part II: Late Time Evolution and Coherent Vortex Formation. *J. Phys. Oceanogr.* **26**, 1825-1848.
- [5] Chassignet, E. P. & Cushman-Roisin, B., 1991: On the Influence of a Lower Layer on the Propagation of Nonlinear Oceanic Eddies. *J. Phys. Oceanogr.* **21**, 939-957.
- [6] Chassignet, E. P., Olson, D. B. & Boudra, D. B., 1990: Motion and Evolution of Oceanic Rings in a Numerical Model and in Observations. *J. Geophys. Res.* **95**, 22121-22140

- [7] Cushman-Roisin. B., 1986: Frontal Geostrophic Dynamics. *J. Phys. Oceanogr.* **16**, 132-143.
- [8] Cushman-Roisin, B., Sutyrin, G. G. & Tang, B., 1992: Two-layer geostrophic dynamics. Part I: Governing equations. *J. Phys. Oceanogr.* **22**, 117-127.
- [9] Cushman-Roisin. B., 1994: *Introduction to Geophysical Fluid Dynamics*, Prentice-Hall. 320 pp.
- [10] Cushman-Roisin, B. & Merchant-Both, S., 1995: Elliptical Warm-Core Rings in a Two Layer Ocean with Ambient Shear, *J. Fluid Mech.* **25**, 2011-2024.
- [11] Flierl. G. R.. 1984: Rossby Wave Radiation from a Strongly Nonlinear Warm Eddy. *J. Phys. Oceanogr.* **14**, 47-58.
- [12] Flierl. G. R.. Malanotte-Rizzoli. P. & Zabusky. N. J.. 1987: Nonlinear Waves and Coherent Vortex Structures in Barotropic β -plane Jets. *J. Phys. Oceanogr.* **17**, 1408-1438.
- [13] Ghil, M. & Paldor., N., 1994: A Model Equation for Nonlinear Wavelength Selection and Amplitude Evolution of Frontal Waves. *J. Nonlinear Sci.* **4**, 471-496.
- [14] Gill. A. E.. 1982: *Atmosphere-Ocean Dynamics*, Academic Press. 662 pp.
- [15] Griffiths, R. W. & Linden, P. F., 1981: The stability of buoyancy-driven coastal currents.
- [16] Griffiths, R. W. & Linden, P. F., 1982: Laboratory Experiments on Fronts.
- [17] Griffiths, R. W., Killworth, P. D. & Stern, M. E., 1982: Ageostrophic instability of ocean currents. *J. Fluid Mech.* **117**, 343-377.

- [18] Karsten, R. H. & Swaters, G. E., 1996: A note on the stability theory of buoyancy-driven ocean currents over a sloping bottom. *Z. angew. Math. Phys.* **47**, 28-38.
- [19] Kincaid, D. R. & Cheney, E. W., 1991: *Numerical Analysis: Mathematics of Scientific Computing*, Brooks/Cole Publishing, 690 pp.
- [20] Meacham, S., 1988: Non-Modal Baroclinic Instability, *Dyn. Atmos. Oceans* **12**, 19-45.
- [21] Mertz, G. & El-Sabh, M. I., 1989: An Autumn Instability Event in the Gaspé Current. *J. Phys. Oceanogr.* **19**, 148-156.
- [22] Mertz, G., Gratton, Y. & Gagné, J. A., 1990: Properties of Unstable Waves in the Lower St. Lawrence Estuary. *Atmosphere-Ocean* **28**, 230-240.
- [23] Milne-Thomson, L. M., 1950: *Jacobian Elliptic Function Tables*, Dover Publications, 123 pp.
- [24] Mooney, C. J. & Swaters, G. E., 1996: Finite-Amplitude Baroclinic Instability of a Mesoscale Gravity Current in a Channel. *Geophys. Astrophys. Fluid Dynamics*. **82**, 173-205.
- [25] Nagle, R. K. & Saff, E. B., 1993: *Fundamentals of Differential Equations and Boundary Value Problems*, Addison-Wesley Publishing, 777 pp.
- [26] Olson, D. B. & Evans, R. H., 1986: Rings of the Agulhas Current. *Deep-Sea Research* **33**, 27-42.
- [27] Paldor, N. & Ghil, M., 1991: Shortwave Instabilities of Coastal Currents. *Geophys. Astrophys. Fluid Dynamics*. **58**, 225-241.

- [28] Pavia, E. G., 1992: The Breakup of Frontal Filaments. *J. Phys. Oceanogr.* **22**, 399-403.
- [29] Pedlosky, J., 1970: Finite-Amplitude Baroclinic Waves. *J. Atmos. Sci.* **27**, 15-30.
- [30] Pedlosky, J., 1972: Finite-Amplitude Baroclinic Wave Packets. *J. Atmos. Sci.* **29**, 680-686.
- [31] Pedlosky, J., 1982: Finite-Amplitude Baroclinic Waves at Minimum Critical Shear. *J. Atmos. Sci.* **39**, 555-2127.
- [32] Pedlosky, J., 1983: The Growth and Decay of Finite-Amplitude Baroclinic Waves. *J. Atmos. Sci.* **40**, 1863-1876.
- [33] Pedlosky, J., 1984: The Equations for Geostrophic Motion in the Ocean. *J. Phys. Oceanogr.* **14**, 448-455.
- [34] Pedlosky, J., 1987: *Geophysical Fluid Dynamics*. 2nd edition. Springer. 710 pp.
- [35] Pond, S. & Pickard, G. L., 1983: *Introductory Dynamical Oceanography*, 2nd edition. Pergamon Press. 329 pp.
- [36] Robinson, A. R. (ed.), 1983: *Eddies in Marine Science*. Springer-Verlag. 609 pp.
- [37] Ross, S. L., 1974: *Differential Equations*. 2nd ed. John Wiley & Sons, 712 pp.
- [38] Swaters, G. E., 1991: On the baroclinic instability of cold-core coupled density fronts on a sloping continental shelf, *J. Fluid Mech.* **224**, 361-382.

- [39] Swaters, G. E. & Flierl, G. R., 1991: Dynamics of ventilated coherent cold eddies on a sloping bottom. *J. Fluid. Mech.* **223**, 565-587.
- [40] Swaters, G. E., 1993: On the baroclinic dynamics, Hamiltonian formulation, and general stability characteristics of density-driven surface currents and fronts over a sloping continental shelf, *Phil. Trans. R. Soc. Lond. A* **345**, 295-325.
- [41] Tan, B. & Liu, S., 1995: Collision Interactions of Solitons in a Baroclinic Atmosphere, *J. Atmos. Sci.* **52**, 1501-1512.
- [42] de Verdière, A. C., 1981: On Mean Flow Instabilities within the Planetary Geostrophic Equations. *J. Phys. Oceanogr.* **16**, 1981-1984.
- [43] Verzicco, R., Lalli, F. & Campana, E., 1997: Dynamics of baroclinic vortices in a rotating, stratified fluid: A numerical study. *Phys. Fluids*, **9**, 419-432.
- [44] Zauderer, E., 1989: *Partial Differential Equations of Applied Mathematics*. John Wiley & Sons, 891 pp.
- [45] Zwillinger, D., 1989: *Handbook of Differential Equations*, Academic Press, 787 pp.

Appendix A

Some Limits

A.1 Point a

At this point $N = 0$ and $\sigma < 0$, as in Figure 4.6. Equation (4.107) reduces to

$$R_T^2 = -\sigma(2R_o^2 - R^2). \quad (\text{A.1})$$

so that if we take the square root of both sides,

$$R_T = \sqrt{-\sigma} \sqrt{2R_o^2 - R^2}, \quad (\text{A.2})$$

i.e.

$$\frac{dR}{\sqrt{2R_o^2 - R^2}} = \sqrt{-\sigma} dT. \quad (\text{A.3})$$

Integrating from R_o to R and from 0 to T , results in the limiting case

$$R = \sqrt{2}R_o \sin(\sqrt{-\sigma}T + \frac{\pi}{4}). \quad (\text{A.4})$$

A.2 Point b

Here $\sigma = 0$ and $N > 0$, as in Figure 4.6. Equation (4.107) becomes

$$R_T^2 = -\frac{N}{2}(R^2 - R_o^2)^2 \leq 0. \quad (\text{A.5})$$

This is only possible if $R = R_o$ identically. We note that this solution does indeed satisfy the initial conditions

$$R(0) = R_o, \quad R_T(0) = \sigma R = 0, \quad (\text{A.6})$$

as we require. Thus the solution for all T is

$$R \equiv R_o. \quad (\text{A.7})$$

A.3 Region I

In this region $\sigma < 0$, $N < 0$. We first want to make sure that the snoidal solution in this region (i.e. **Case 2**) reduces to the solution (A.4) at Point a. Using the results of Subsection 4.3.1,

$$\begin{aligned} R &= \sqrt{\frac{2\sigma}{N}} P \\ &= \sqrt{\frac{2\sigma}{N}} \zeta \operatorname{sn}(\beta(\sqrt{-\sigma}T - \tau_o) | m^2), \end{aligned} \quad (\text{A.8})$$

where

$$\beta^2 = P_o^2 + \frac{1}{2} + \sqrt{\frac{1}{4} - P_o^2}, \quad \zeta^2 = P_o^2 + \frac{1}{2} - \sqrt{\frac{1}{4} - P_o^2}, \quad (\text{A.9})$$

$$\tau_o = -\frac{1}{\beta} \int_0^{Q_o} \frac{d\xi}{\sqrt{(1-\xi^2)(m^2-\xi^2)}}, \quad m^2 = \frac{\zeta^2}{\beta^2}, \quad (\text{A.10})$$

and

$$P_o = \sqrt{\frac{N}{2\sigma}} R_o. \quad (\text{A.11})$$

Taking the limit of the coefficient of $\text{sn}(\beta(\tau - \tau_o)|m^2)$ as $N \rightarrow 0^-$, we obtain.

$$\lim_{N \rightarrow 0^-} \sqrt{\frac{2\sigma}{N}} \zeta = \lim_{N \rightarrow 0^-} \sqrt{\frac{\sigma}{N} + R_o^2 - \sqrt{\frac{\sigma^2}{N^2} - \frac{2\sigma}{N} R_o^2}} = \sqrt{2} R_o. \quad (\text{A.12})$$

Taking the limit of the coefficient of T ,

$$\lim_{N \rightarrow 0^-} \beta \sqrt{-\sigma} = \lim_{N \rightarrow 0^-} \sqrt{\frac{N}{2\sigma} R_o^2 + \frac{1}{2} + \sqrt{\frac{1}{4} - \frac{N}{2\sigma} R_o^2}} \sqrt{-\sigma} = 1. \quad (\text{A.13})$$

Taking the limit of the parameter $m^2 = \frac{\zeta^2}{\beta^2}$,

$$\lim_{N \rightarrow 0^-} \frac{\zeta^2}{\beta^2} = \lim_{N \rightarrow 0^-} \frac{\frac{N}{2\sigma} R_o^2 + \frac{1}{2} - \sqrt{\frac{1}{4} - \frac{N}{2\sigma} R_o^2}}{\frac{N}{2\sigma} R_o^2 + \frac{1}{2} + \sqrt{\frac{1}{4} - \frac{N}{2\sigma} R_o^2}} = 0. \quad (\text{A.14})$$

Now we write τ_o as

$$\tau_o = -\frac{1}{\beta} \text{sn}^{-1}\left(\frac{\beta Q_o}{\zeta} \middle| \frac{\zeta^2}{\beta^2}\right). \quad (\text{A.15})$$

where $Q_o = \frac{1}{\beta} P_o$ and $\text{sn}^{-1}(\cdot)$ refers to the inverse Jacobi elliptic snoidal function.

Taking the limit of τ_o , after a little algebra, we obtain

$$\begin{aligned} \lim_{N \rightarrow 0^-} -\frac{1}{\beta} \text{sn}^{-1}\left(\frac{\beta Q_o}{\zeta} \middle| \frac{\zeta^2}{\beta^2}\right) &= -1 \cdot \text{sn}^{-1}\left(\lim_{N \rightarrow 0^-} \frac{\beta Q_o}{\zeta} \middle| \lim_{N \rightarrow 0^-} \frac{\zeta^2}{\beta^2}\right) \quad (\text{A.16}) \\ &= -\text{sn}^{-1}\left(\frac{1}{\sqrt{2}} \middle| 0\right) \\ &= -\arcsin\left(\frac{1}{\sqrt{2}}\right) \\ &= -\frac{\pi}{4}. \end{aligned}$$

Now, since $\text{sn}(u|0) = \sin(u)$ (Milne-Thomson, 1950), the limit of R is

$$\lim_{N \rightarrow 0^-} R = \sqrt{2} R_o \sin(\sqrt{-\sigma} T + \frac{\pi}{4}), \quad (\text{A.17})$$

which is the limiting case (A.4).

We now show that **Case 1** of Region I is a limit of **Case 2**. With R defined by (A.8) through (A.11), we take all the limits, as $P_o \rightarrow \frac{1}{2}$:

$$\lim_{P_o \rightarrow \frac{1}{2}} \zeta^2 = \frac{3}{4}, \quad (\text{A.18})$$

$$\lim_{P_o \rightarrow \frac{1}{2}} \beta^2 = \frac{3}{4}, \quad (\text{A.19})$$

$$\lim_{P_o \rightarrow \frac{1}{2}} m^2 = 1, \quad (\text{A.20})$$

$$\begin{aligned} \lim_{P_o \rightarrow \frac{1}{2}} \tau_o &= \lim_{P_o \rightarrow \frac{1}{2}} -\frac{1}{\beta} \int_0^{Q_o} \frac{d\xi}{\sqrt{(1-\xi^2)(m^2-\xi^2)}} \\ &= -\frac{2}{3} \int_0^{\frac{1}{\sqrt{3}}} \frac{d\xi}{1-\xi^2} \\ &= \frac{1}{\sqrt{3}} \ln \left| \frac{\sqrt{3}-1}{1+\sqrt{3}} \right|. \end{aligned} \quad (\text{A.21})$$

Now we take the limit of P ,

$$\begin{aligned} \lim_{P_o \rightarrow \frac{1}{2}} P &= \text{sn} \left(\frac{\sqrt{3}}{2} (\tau - \tau_o) | 1 \right) \\ &= \frac{\sqrt{3}}{2} \tanh \left(\frac{\sqrt{3}}{2} (\tau - \tau_o) \right) \\ &= \frac{1 - \sqrt{3} + (1 + \sqrt{3}) \exp[\sqrt{3}\tau]}{\sqrt{3} - 1 + (1 + \sqrt{3}) \exp[\sqrt{3}\tau]} \end{aligned} \quad (\text{A.22})$$

which agrees with the solution (4.115).

A.4 Region II

In this region $\sigma < 0$, $N > 0$. We wish to check that the cnoidal solution reduces to the solution (A.4) at Point a. Using the results of Subsection 4.3.2, **Case 2**,

$$R = \sqrt{\frac{-2\sigma}{N}}\beta \operatorname{cn} \left(\sqrt{\frac{\zeta^2}{\beta^2} + 1}\beta(\tau - \tau_o) \left| \left(1 + \frac{\zeta^2}{\beta^2}\right)^{-1} \right. \right),$$

where

$$\beta^2 = P_o^2 + \frac{1}{2} + \sqrt{\frac{1}{4} - P_o^2}, \quad (\text{A.23})$$

and

$$\zeta^2 = P_o^2 + \frac{1}{2} - \sqrt{\frac{1}{4} - P_o^2}. \quad (\text{A.24})$$

Taking the limit of the coefficient of the cnoidal function, as $N \rightarrow 0^+$,

$$\begin{aligned} \lim_{N \rightarrow 0^+} \sqrt{\frac{-2\sigma}{N}}\beta &= \lim_{N \rightarrow 0^+} \sqrt{R_o^2 + \frac{\sigma}{N} + \sqrt{\left(\frac{-\sigma}{N} + R_o^2\right)^2 - R_o^4}} \\ &= \lim_{N \rightarrow 0^+} \sqrt{R_o^2 + \frac{\sigma}{N} + \sqrt{\left(\frac{-\sigma}{N} + R_o^2\right)^2}} \\ &= \lim_{N \rightarrow 0^+} \sqrt{R_o^2 + \frac{\sigma}{N} - \frac{\sigma}{N} + R_o^2} \\ &= \sqrt{2}R_o. \end{aligned} \quad (\text{A.25})$$

Taking the limit of the coefficient of τ ,

$$\begin{aligned} \lim_{N \rightarrow 0^+} \sqrt{\frac{\zeta^2}{\beta^2} + 1}\beta &= \lim_{N \rightarrow 0^+} \sqrt{\zeta^2 + \beta^2} \\ &= \lim_{N \rightarrow 0^+} \sqrt{2\sqrt{\frac{N}{-2\sigma}R_o^2 + \frac{1}{4}}} \\ &= \lim_{N \rightarrow 0^+} \sqrt{2\sqrt{\frac{1}{4}}} \\ &= 1. \end{aligned} \quad (\text{A.26})$$

Taking the limit of $m^2 = \frac{\zeta^2}{\beta^2}$.

$$\begin{aligned} \lim_{N \rightarrow 0^+} \frac{\zeta^2}{\beta^2} &= \lim_{N \rightarrow 0^+} \frac{\frac{N}{2\sigma} R_o^2 + \frac{1}{2} + \sqrt{\frac{N}{-2\sigma} + \frac{1}{4}}}{-\frac{N}{2\sigma} R_o^2 - \frac{1}{2} + \sqrt{\frac{N}{-2\sigma} + \frac{1}{4}}} \\ &= \lim_{N \rightarrow 0^+} \frac{\frac{1}{2} + \frac{1}{2}}{-\frac{1}{2} + \frac{1}{2}}. \end{aligned} \quad (\text{A.27})$$

Clearly, m^2 tends to infinity, therefore,

$$\lim_{N \rightarrow 0^+} (1 + \frac{\zeta^2}{\beta^2})^{-1} = 0. \quad (\text{A.28})$$

We must also take the limit of τ_o :

$$\begin{aligned} \lim_{N \rightarrow 0^+} \tau_o &= \lim_{N \rightarrow 0^+} \frac{1}{\beta} (1 + \frac{\zeta^2}{\beta^2})^{-1/2} \int_{Q_o}^1 \frac{d\xi}{\sqrt{(\xi^2 + \zeta^2/\beta^2)(1 - \xi^2)}} \\ &= \lim_{N \rightarrow 0^+} (\zeta^2 + \beta^2)^{-1/2} \text{cn}^{-1}(\frac{1}{\beta} \sqrt{\frac{-N}{2\sigma}} R_o | (1 + \frac{\zeta^2}{\beta^2})^{-1}) \\ &= \lim_{N \rightarrow 0^+} 1 \cdot \text{cn}^{-1}(\frac{1}{\sqrt{2}} | 0) \\ &= \lim_{N \rightarrow 0^+} \arccos(\frac{1}{\sqrt{2}}) \\ &= \frac{\pi}{4}. \end{aligned} \quad (\text{A.29})$$

Therefore, the limit of R becomes

$$\begin{aligned} \lim_{N \rightarrow 0^+} R &= \sqrt{2} R_o \cos(\tau - \frac{\pi}{4}) \\ &= \sqrt{2} R_o \sin(\sqrt{-\sigma} T + \frac{\pi}{4}), \end{aligned} \quad (\text{A.30})$$

which exactly matches the solution at Point a, (A.4).

We now turn to Region II. **Case 3.** We show that it reduces to (A.7) at Point

b. Here the solution may be written as

$$R = \sqrt{\frac{-2\sigma}{N}} \beta \operatorname{dn} (\zeta(\tau - \tau_o)) | 1 - \frac{\zeta^2}{\beta^2}), \quad (\text{A.31})$$

where

$$\beta^2 = P_o^2 - \frac{1}{2} + \sqrt{P_o^2 + \frac{1}{4}} > 0, \quad (\text{A.32})$$

and

$$\zeta^2 = P_o^2 - \frac{1}{2} - \sqrt{P_o^2 + \frac{1}{4}} > 0. \quad (\text{A.33})$$

The limit of the coefficient of the dnoidal function is

$$\begin{aligned} \lim_{\sigma \rightarrow 0^-} \sqrt{\frac{-2\sigma}{N}} \beta &= \lim_{\sigma \rightarrow 0^-} \sqrt{R_o^2 + \frac{\sigma}{N} + \sqrt{-\frac{N}{2\sigma} R_o^2 + \frac{\sigma^2}{N^2}}} \\ &= \lim_{\sigma \rightarrow 0^-} \sqrt{R_o^2} \\ &= R_o. \end{aligned} \quad (\text{A.34})$$

Taking the limit of the parameter.

$$\begin{aligned} \lim_{\sigma \rightarrow 0^-} 1 - \frac{\zeta^2}{\beta^2} &= \lim_{\sigma \rightarrow 0^-} \frac{P_o^2 - \frac{1}{2} - \sqrt{P_o^2 + \frac{1}{4}}}{P_o^2 - \frac{1}{2} + \sqrt{P_o^2 + \frac{1}{4}}} \\ &= \lim_{\sigma \rightarrow 0^-} \frac{-2\sqrt{-\frac{N}{2\sigma} R_o^2 + \frac{1}{4}}}{\frac{N}{2\sigma} R_o^2 - \frac{1}{2} + \sqrt{-\frac{N}{2\sigma} R_o^2 + \frac{1}{4}}} \\ &= 0. \end{aligned} \quad (\text{A.35})$$

since the highest power of σ appears in the denominator. We see that the solution approaches

$$\begin{aligned} \lim_{\sigma \rightarrow 0^-} R &= \lim_{\sigma \rightarrow 0^-} R_o \operatorname{dn} (\zeta(\tau - \tau_o)) | 0 \\ &= R_o, \end{aligned} \quad (\text{A.36})$$

because $\text{dn } (u|0) = 1$ for any argument u (Milne-Thomson, 1950). This limit matches the solution (A.7), at Point b.

Presently we demonstrate that **Case 1** can be obtained as a limit of both **Case 2** and **Case 3**. The same procedure is followed as in Region I, above, and so we only give the highlights. We take the solution Q as defined in (4.154) and find the limit as $P_o \rightarrow \sqrt{2}$.

$$\begin{aligned}
\lim_{P_o \rightarrow \sqrt{2}} Q &= \lim_{P_o \rightarrow \sqrt{2}} \text{cn} \left(1 \times \sqrt{3}(\tau - \tau_o) \middle| \frac{1}{0+1} \right) \\
&= \lim_{P_o \rightarrow \sqrt{2}} \text{sech} \left(\sqrt{3}(\tau - \tau_o) \right) \\
&= \text{sech} \left(\sqrt{3}\tau - \ln\left(\frac{\sqrt{3}+1}{2}\right) \right) \\
&= \sqrt{2} \left(\left(\frac{\sqrt{3}-1}{2} \right) \exp[\sqrt{3}\tau] + \left(\frac{\sqrt{3}+1}{2} \right) \exp[-\sqrt{3}\tau] \right)^{-1}
\end{aligned} \tag{A.37}$$

which agrees with (4.146). Now taking Q as defined by (4.163).

$$\begin{aligned}
\lim_{P_o \rightarrow \sqrt{2}} Q &= \lim_{P_o \rightarrow \sqrt{2}} \text{dn} \left(\sqrt{3}(\tau - \tau_o) \middle| 1 \right) \\
&= \lim_{P_o \rightarrow \sqrt{2}} \text{sech} \left(\sqrt{3}(\tau - \tau_o) \right) \\
&= \text{sech} \left(\sqrt{3}\tau - \ln\left(\frac{\sqrt{3}+1}{2}\right) \right) \\
&= \sqrt{2} \left(\left(\frac{\sqrt{3}-1}{2} \right) \exp[\sqrt{3}\tau] + \left(\frac{\sqrt{3}+1}{2} \right) \exp[-\sqrt{3}\tau] \right)^{-1}
\end{aligned} \tag{A.38}$$

and this again matches (4.146).

A.5 Region III

The solution is

$$R = \sqrt{\frac{2\sigma}{N}} P_{\max} \operatorname{dn} \left(P_{\max} \sqrt{\frac{\sigma}{2}} T - \tau'_o \middle| 1 - \frac{P_{\min}^2}{P_{\max}^2} \right), \quad (\text{A.39})$$

with

$$P_{\min}^2 = \left(\frac{N}{2\sigma} R_o^2 + \frac{1}{2} \right) - \frac{1}{2} \sqrt{\frac{2N}{\sigma} R_o^2 + 1}, \quad (\text{A.40})$$

$$P_{\max}^2 = \left(\frac{N}{2\sigma} R_o^2 + \frac{1}{2} \right) + \frac{1}{2} \sqrt{\frac{2N}{\sigma} R_o^2 + 1}. \quad (\text{A.41})$$

and

$$\tau'_o = \int_{Q_o}^1 \frac{dQ}{\sqrt{(1-Q^2)(Q^2 - (P_{\min}/P_{\max})^2)}}. \quad (\text{A.42})$$

Taking the limit of the coefficient of the dnoidal function,

$$\begin{aligned} \lim_{\sigma \rightarrow 0^+} \sqrt{\frac{2\sigma}{N}} P_{\max} &= \lim_{\sigma \rightarrow 0^+} \sqrt{R_o^2 + \frac{\sigma}{N} + \sqrt{\frac{2\sigma}{N} R_o^2 + \frac{\sigma^2}{N^2}}} \\ &= \lim_{\sigma \rightarrow 0^+} \sqrt{R_o^2} \\ &= R_o. \end{aligned} \quad (\text{A.43})$$

Taking the limit of the parameter,

$$\begin{aligned} \lim_{\sigma \rightarrow 0^+} 1 - \frac{P_{\min}^2}{P_{\max}^2} &= \lim_{\sigma \rightarrow 0^+} 1 - \frac{\left(\frac{N}{2\sigma} R_o^2 + \frac{1}{2} \right) - \frac{1}{2} \sqrt{\frac{2N}{\sigma} R_o^2 + 1}}{\left(\frac{N}{2\sigma} R_o^2 + \frac{1}{2} \right) + \frac{1}{2} \sqrt{\frac{2N}{\sigma} R_o^2 + 1}} \\ &= \lim_{\sigma \rightarrow 0^+} \frac{2\sqrt{\frac{2N}{\sigma} R_o^2 + 1}}{\frac{N}{\sigma} R_o^2 - 1 + \sqrt{\frac{2N}{\sigma} R_o^2 + 1}} \\ &= 0, \end{aligned} \quad (\text{A.44})$$

since the denominator increases faster than the numerator. Now.

$$\begin{aligned}\lim_{\sigma \rightarrow 0^-} R &= \lim_{\sigma \rightarrow 0^-} R_o \, \mathbf{dn} \left(P_{\max} \sqrt{\frac{\sigma}{2}} T - \tau_o' | 0 \right) \\ &= R_o.\end{aligned}\tag{A.45}$$

Again, this matches the solution (A.7) at Point b.

Appendix B

Expressions for σ

B.1 Upper Branch, $l^2 - 2 > 0$

$$\begin{aligned}
\sigma = & \frac{1}{96} k^2 \left(-2 L^3 l^6 \%1 - 48 k^2 l^6 K^4 \%2 \sqrt{l^2 - 2} - 48 l^8 K^4 \%2 \sqrt{l^2 - 2} \right. \\
& + 3 l^2 K^4 \%1 L + 48 k^2 (-1)^n l^6 K^4 \sqrt{l^2 - 2} + 48 l^6 K^4 \%2 \sqrt{l^2 - 2} \\
& + 48 (-1)^n \sqrt{l^2 - 2} l^8 K^4 - 24 \%1 L l^8 K^4 + 24 \%1 L k^2 l^6 K^4 \\
& + L^3 K^4 \%1 l^4 + 1536 \delta^2 K^8 L \%1 l^4 + 48 (-1)^{(1+n)} l^6 \sqrt{l^2 - 2} K^4 \\
& + 96 K^{16} \delta^2 L \%1 l^4 - L^3 K^2 \%1 l^4 - k^2 L^3 K^4 \%1 l^2 \\
& - 3072 \delta^2 K^{10} L \%1 l^4 + 96 (-1)^{(1+n)} k^2 l^6 \sqrt{l^2 - 2} K^2 \\
& + 2 k^2 L^3 K^4 \%1 l^4 + 96 (-1)^{(1+n)} l^8 \sqrt{l^2 - 2} K^2 \\
& + 2304 K^{12} \delta^2 L \%1 l^4 + 2 L^3 l^6 K^4 \%1 + k^2 L^3 K^2 \%1 l^2 \\
& + 48 (-1)^{(1+n)} l^6 \sqrt{l^2 - 2} - 768 K^{14} \delta^2 L \%1 l^4 - 2 k^2 L^3 \%1 l^4 \\
& + 15 k^2 K^4 L \%1 + 24 \%1 L l^8 - 48 \%1 L k^2 l^6 K^2 \\
& - 12 k^2 K^4 L \%1 l^4 - 36 l^6 K^4 L \%1 - 12 k^2 K^4 L \%1 l^2 \\
& \left. + 72 \%1 L l^6 K^2 - 48 \%1 L l^8 K^2 + 24 \%1 L k^2 l^6 - 36 \%1 L l^6 \right)
\end{aligned}$$

$$\begin{aligned}
& -12k^2 L l^4 \%1 + 48k^2 (-1)^n l^6 \sqrt{l^2 - 2} - 96l^6 \%2 K^2 \sqrt{l^2 - 2} \\
& + 96 \%2 l^8 K^2 \sqrt{l^2 - 2} + 24k^2 L l^4 K^2 \%1 + 96 (-1)^n l^6 K^2 \sqrt{l^2 - 2} \\
& + 96k^2 l^6 K^2 \%2 \sqrt{l^2 - 2} - 48k^2 l^6 \%2 \sqrt{l^2 - 2} - 48 \%2 l^8 \sqrt{l^2 - 2} \\
& + 48l^6 \%2 \sqrt{l^2 - 2} + 48 (-1)^n \sqrt{l^2 - 2} l^8 - 15k^2 L K^2 \%1 \\
& - 3 L l^2 K^2 \%1 + 12k^2 L l^2 \%1) / (K^{10} L \%1 l^4 \\
& (16 - 32 K^2 + 24 K^4 - 8 K^6 + K^8)) \\
& \%1 := \sin(\sqrt{l^2 - 2} L) \\
& \%2 := \cos(\sqrt{l^2 - 2} L)
\end{aligned}$$

B.2 Upper Branch, $l^2 - 2 < 0$

$$\begin{aligned}
\sigma = & \frac{1}{96} k^2 \left(-48 \%1 L l^8 K^2 + 24 \%1 L k^2 l^6 - 48 \%1 L k^2 l^6 K^2 \right. \\
& + 96 \%1 l^6 \sqrt{2 - l^2} K^2 - 96 k^2 l^6 \%1 \sqrt{2 - l^2} K^2 \\
& + 48 k^2 l^6 \%1 \sqrt{2 - l^2} - 96 l^8 \%1 \sqrt{2 - l^2} K^2 \\
& + 192 (-1)^{(1+n)} \%2 l^6 \sqrt{2 - l^2} K^2 + 96 (-1)^{(1+n)} l^8 \%2 \sqrt{2 - l^2} \\
& - 24 L k^2 l^6 + 96 (-1)^{(1+n)} k^2 l^6 \%2 \sqrt{2 - l^2} \\
& + 96 (-1)^{(1+n)} l^8 \%2 K^4 \sqrt{2 - l^2} + 1536 \delta^2 K^8 l^4 L \%1 - 2 l^6 L^3 \%1 \\
& + 48 l^8 \sqrt{2 - l^2} K^4 - 48 l^6 \sqrt{2 - l^2} K^4 + 2 l^6 L^3 + 15 L k^2 K^4 \%1 \\
& - 12 L k^2 l^4 K^4 \%1 + 96 \%2 l^6 \sqrt{2 - l^2} (-1)^n K^4 - 12 k^2 l^2 L K^4 \%1 \\
& - 3072 \delta^2 K^{10} l^4 L \%1 + 96 \delta^2 K^{16} l^4 L \%1 + 3 l^2 K^4 L \%1 \\
& - 768 \delta^2 K^{14} l^4 L \%1 + 2 k^2 L^3 l^4 K^4 \%1 + 2 l^6 L^3 K^4 \%1 \\
& + 24 \%1 L l^8 K^4 + 24 \%1 L k^2 l^6 K^4 - 48 \%1 l^6 \sqrt{2 - l^2} K^4 \\
& + 48 k^2 l^6 \%1 \sqrt{2 - l^2} K^4 + 48 l^8 \%1 \sqrt{2 - l^2} K^4 + 48 k^2 l^6 \sqrt{2 - l^2} K^4 \\
& \left. + l^4 K^4 L^3 \%1 - l^4 K^2 L^3 \%1 + 2304 \delta^2 K^{12} l^4 L \%1 - 2 k^2 L^3 l^4 \%1 \right)
\end{aligned}$$

$$\begin{aligned}
& -36 l^6 K^4 L \%1 + k^2 L^3 l^2 K^2 \%1 - k^2 L^3 l^2 K^4 \%1 - 24 L k^2 l^6 K^4 \\
& + 12 k^2 l^2 L K^4 - 15 L k^2 K^4 + 12 L k^2 l^4 K^4 - 2 k^2 L^3 l^4 K^4 \\
& + 768 \delta^2 K^{14} l^4 L - 96 \delta^2 K^{16} l^4 L + k^2 L^3 l^2 K^4 - k^2 L^3 l^2 K^2 \\
& - 1536 \delta^2 K^8 l^4 L + 3072 \delta^2 K^{10} l^4 L - 2304 \delta^2 K^{12} l^4 L - 24 L l^8 \\
& + 96 (-1)^{(1+n)} k^2 l^6 \%2 K^4 \sqrt{2-l^2} + 48 L l^8 K^2 - 12 L k^2 l^2 \\
& + 12 k^2 l^4 L + 36 l^6 L - 3 l^2 K^4 L - 48 \%1 l^6 \sqrt{2-l^2} + 24 \%1 L l^8 \\
& - 2 l^6 L^3 K^4 + l^4 K^2 L^3 + 48 L k^2 l^6 K^2 - l^4 K^4 L^3 + 36 l^6 K^4 L \\
& + 2 k^2 L^3 l^4 + 15 k^2 L K^2 - 24 L k^2 l^4 K^2 - 48 l^6 \sqrt{2-l^2} \\
& + 48 l^8 \sqrt{2-l^2} - 24 L l^8 K^4 + 48 l^8 \%1 \sqrt{2-l^2} + 48 k^2 l^6 \sqrt{2-l^2} \\
& - 72 l^6 L K^2 + 3 L l^2 K^2 + 192 k^2 l^6 \%2 (-1)^n \sqrt{2-l^2} K^2 \\
& + 192 l^8 \%2 (-1)^n K^2 \sqrt{2-l^2} - 12 L k^2 l^4 \%1 + 72 l^6 L \%1 K^2 \\
& - 3 l^2 K^2 L \%1 - 15 k^2 L K^2 \%1 - 96 l^8 \sqrt{2-l^2} K^2 - 36 l^6 L \%1 \\
& + 24 L k^2 l^4 K^2 \%1 + 12 k^2 l^2 L \%1 - 96 k^2 l^6 \sqrt{2-l^2} K^2 \\
& + 96 \%2 l^6 \sqrt{2-l^2} (-1)^n + 96 l^6 \sqrt{2-l^2} K^2) / (l^4 L (-1 + \%1) \\
& (-2 + K^2)^4 K^{10}) \\
& \%1 := e^{(-2\sqrt{2-l^2} L)} \\
& \%2 := e^{(-\sqrt{2-l^2} L)}
\end{aligned}$$

B.3 Lower Branch

$$\begin{aligned}
\sigma = & \frac{1}{96} k^2 \left(-48 (-1)^n l^8 K^4 \sqrt{l^2+2} - 48 (-1)^n k^2 l^6 K^4 \sqrt{l^2+2} \right. \\
& - 48 (-1)^n l^6 K^4 \sqrt{l^2+2} - 15 k^2 K^4 L \%1 - 12 k^2 K^4 L \%1 l^2 \\
& + 36 l^6 K^4 L \%1 + 12 k^2 K^4 L \%1 l^4 - 2 L^3 l^6 \%1 - L^3 K^4 \%1 l^4 \\
& \left. + k^2 L^3 K^4 \%1 l^2 + 2304 K^{12} \delta^2 L \%1 l^4 - L^3 K^2 \%1 l^4 \right)
\end{aligned}$$

$$\begin{aligned}
& + 96 K^{16} \delta^2 L \%1 l^4 + 2 k^2 L^3 K^4 \%1 l^4 - 3 K^4 \%1 l^2 L \\
& + 48 l^8 \%2 \sqrt{l^2 + 2} K^4 + 24 \%1 L k^2 l^6 K^4 + 48 l^6 K^4 \%2 \sqrt{l^2 + 2} \\
& + 24 \%1 L l^8 K^4 + 48 k^2 l^6 K^4 \%2 \sqrt{l^2 + 2} + 1536 \delta^2 K^8 L \%1 l^4 \\
& - 2 k^2 L^3 \%1 l^4 + 2 L^3 l^6 K^4 \%1 + 3072 \delta^2 K^{10} L \%1 l^4 \\
& + k^2 L^3 K^2 \%1 l^2 + 768 K^{14} \delta^2 L \%1 l^4 + 24 \%1 L l^8 \\
& + 24 \%1 L k^2 l^6 + 36 \%1 L l^6 + 12 k^2 \%1 l^4 L - 15 k^2 L K^2 \%1 \\
& - 48 (-1)^n \sqrt{l^2 + 2} l^8 + 48 \%1 L k^2 l^6 K^2 + 48 l^8 \%2 \sqrt{l^2 + 2} \\
& + 48 l^6 \%2 \sqrt{l^2 + 2} - 48 (-1)^n l^6 \sqrt{l^2 + 2} - 96 k^2 (-1)^n l^6 \sqrt{l^2 + 2} K^2 \\
& + 96 k^2 l^6 K^2 \%2 \sqrt{l^2 + 2} + 48 \%1 L l^8 K^2 + 24 k^2 L K^2 \%1 l^4 \\
& + 72 l^6 L K^2 \%1 - 3 L K^2 \%1 l^2 + 12 k^2 \%1 l^2 L \\
& + 96 l^8 \%2 \sqrt{l^2 + 2} K^2 - 48 k^2 (-1)^n l^6 \sqrt{l^2 + 2} \\
& - 96 (-1)^n l^6 \sqrt{l^2 + 2} K^2 + 96 l^6 K^2 \%2 \sqrt{l^2 + 2} \\
& - 96 (-1)^n l^8 K^2 \sqrt{l^2 + 2} + 48 k^2 l^6 \%2 \sqrt{l^2 + 2} \Big) / (K^{10} L \%1 l^4 \\
& (16 + 32 K^2 + 24 K^4 + 8 K^6 + K^8)) \\
& \%1 := \sin(\sqrt{l^2 + 2} L) \\
& \%2 := \cos(\sqrt{l^2 + 2} L)
\end{aligned}$$

Appendix C

Numerical Solver

```
/* ***** */
/* Program DDC12.C */
/* Density Driven Current */
/* Programmer: Matt Reszka */
/* Department of Mathematics */
/* University of Alberta */
/* 16 06 97 */
/* Finite Difference Scheme for the coupled PDE pair contained in
/* ON THE BAROCLINIC DYNAMICS, HAMILTONIAN FORMULATION
/* AND GENERAL STABILITY CHARACTERISTICS OF DENSITY-
/* DRIVEN SURFACE CURRENTS AND FRONTS OVER A SLOPING
/* CONTINENTAL SHELF by Gordon E. Swaters, Professor of Mathematics
/* Phil. Trans. R. Soc. Lond. A 345, 295-325
/* ***** */

/* ***** */
/* Programming notes: */
/* Compiled on a Silicon Graphics Indigo workstation, using the syntax
/* cc -O3 -o ddc12 ddc12.c -lm
/* Leapfrog finite difference in time. Central finite difference in space.
/* Jacobian terms approximated using Arakawa (1966) Scheme.
/* Variables h and q integrated forward in time, p recovered from q using a
/* Conjugate-Gradient Poisson-problem solver. Smoothly periodic channel in x.
/* Clamped Dirichlet boundary conditions on y. Data dumped to 3
/* files: one for h, one for p (both in binary format), and one control
/* file (text format) containing derived quantities such as the KE.
/* ***** */
```



```

/* "Si apud bibliothecam, hortulum habes, nihil geerit." */

/* include necessary header files */
#include <stdio.h>
#include <stdlib.h>
#include <math.h>
#include <time.h>
#include <sys/time.h>

/* define constants */
#define PI 3.1415926535897932
#define MINX (0.0)
#define MAXX (6.0)
#define MINY (0.0)
#define MAXY (8.0)
#define s 0.0
#define a 2.0
#define hmax 0.1
#define XINC 80
#define YINC 160
#define TINC 1000000
#define TSKIP 2000
#define XSKIP 1
#define YSKIP 1
#define dx ((MAXX - MINX) / XINC)
#define dy dx
#define dx2 (dx * dx)
#define dy2 (dy * dy)
#define dt 0.0004
#define N (XINC * (YINC - 1))
#define TNODES (TINC / TSKIP + 1)
#define YNODES (YINC / YSKIP + 1)
#define XNODES (XINC / XSKIP)

#define H_FILE "jet1b-h.dat"
#define P_FILE "jet1b-p.dat"
#define HAM_FILE "jet1b-ham.dat"
#define digits 10000
#define HFRIC 0.0
#define FRIC 0.0
#define ROBFIL 0.005
#define TITLE "DDC 1.2"

/* double precision PI */
/* minimum x value for xy region */
/* maximum x value for xy region */
/* minimum y value for xy region */
/* maximum y value for xy region */
/* bottom slope (assumed positive) */
/* parameter within h0 */
/* half of h0_max */
/* x increments for xy region */
/* y increments for xy region */
/* t increments for time */
/* save data every TSKIP t-increments */
/* save data every XSKIP x-increments */
/* save data every YSKIP y-increments */
/* delta x for xy region */
/* delta y for xy region */
/* delta x squared */
/* delta y squared */
/* delta t for time */
/* size of system for poisson solver */
/* number of time-slices saved */
/* number of nodes saved in y dir. */
/* number of nodes saved in x dir. */

/* file name for h data */
/* file name for p data */
/* file name for Hamiltonian data */
/* factor used in saving real numbers */
/* horizontal friction coefficient */
/* upper layer friction coefficient */
/* value of Robert filter */
/* program title */

```

```

/* declare variables */
double x, y, t;
double H;
double KElo, KEup;
double M, M2;
double Ens;
double PertKE;
double initH;
double initKElo;
double initKEup;
double initM, initM2;
double initEns;
double initPertKE;
int i, j, k, ip, im, jp, jm;
int ipp, imm, jpp, jmm;
time_t thetime;

/* x, y and time */
/* Hamiltonian (invariant) */
/* KE of upper and lower layers */
/* Mass, Mass^2 (invariant) */
/* Enstrophy */
/* Perturbation KE (upper layer) */
/* initial Hamiltonian */
/* initial KE of lower layer */
/* initial KE of upper layer */
/* initial Mass and Mass^2 */
/* initial Enstrophy */
/* initial upper Perturbation KE */
/* counter variables */
/* counter variables */
/* current time from system clock */

double h0 [XINC+1][YINC+1];
double h1 [XINC+1][YINC+1];
double h [XINC+1][YINC+1];
double p0 [XINC+1][YINC+1];
double p1 [XINC+1][YINC+1];
double p [XINC+1][YINC+1];
double q0 [XINC+1][YINC+1];
double q1 [XINC+1][YINC+1];
double q [XINC+1][YINC+1];
double vfrc [XINC+1][YINC+1];
double A1 [XINC+1][YINC+1];
short int output [XINC+1];
short int tag1, tag2;

/* solution matrix for h at t - 2dt */
/* solution matrix for h at t - dt */
/* solution matrix for h at t */
/* solution matrix for p at t - 2dt */
/* solution matrix for p at t - dt */
/* solution matrix for p at t */
/* intermediate solution at t - 2dt */
/* intermediate solution at t - dt */
/* intermediate solution at t */
/* used in friction for q */
/* term 1 of equation 1 */
/* binary output array */
/* needed for FORTRAN-readable data */

double b [N+1];
double soln [N+1];

/* RHS vector in Poisson solver */
/* solution to Poisson equation */

FILE *H_stream;
FILE *P_stream;
FILE *Ham_stream;

/* output file (h data) */
/* output file (p data) */
/* output file (Hamiltonian) */

void ret (int car) /* force carriage return */
{
    int mm;
    for (mm = 1; mm <= car; mm++)
        printf ("\n");
}

```

```

}

double fmax (double num1, double num2) /* return the max of two f. p. numbers */
{
    if (num1 >= num2) return (num1);
    else return (num2);
}

double Sqr (double num) /* square a floating point number */
{
    return (num * num);
}

double f (double x, double y) /* IC and BC for h */
{
    /* return (hmax * exp (- Sqr (a * (y - MAXY / 2.0)))); */
    /* return (hmax + a * (y - MAXY / 2.0)); */
    if (y < 4.0) return (0.0);
    if (y > 7.0) return (2.0 * hmax);
    else return (hmax * sin ((y - 5.5) * PI / 3.0) + hmax);
}

double g (double x, double y) /* IC and BC for p */
{
    return (0.0);
}

/* finite difference approximations for derivatives */

double Dx (double ar[][YINC+1], int m, int n)
{
    if ((n == 0) || (n == YINC)) return (0.0);
    if (m == 0) return ((ar[1][n] - ar[XINC-1][n]) / (2.0 * dx));
    if (m == XINC - 1) return ((ar[0][n] - ar[XINC-2][n]) / (2.0 * dx));
    else return ((ar[m+1][n] - ar[m-1][n]) / (2.0 * dx));
}

double Dxx (double ar[][YINC+1], int m, int n)
{
    if ((n == 0) || (n == YINC)) return (0.0);
    if (m == 0) return ((ar[1][n] - 2.0 * ar[0][n] + ar[XINC-1][n])
        / dx2);
    if (m == XINC - 1) return ((ar[0][n] - 2.0 * ar[XINC-1][n]

```

```

        + ar [XINC-2][n]) / dx2);
    else return ((ar [m+1][n] - 2.0 * ar [m][n] + ar [m-1][n]) / dx2);
}

double Dy (double ar[][YINC+1], int m, int n)
{
    if (n == 0) return ((4.0 * ar [m][1] - 3.0 * ar [m][0] - ar [m][2])
        / (2.0 * dy));
    if (n == YINC) return ((ar [m][YINC-2] - 4.0 * ar [m][YINC-1]
        + 3.0 * ar [m][YINC]) / (2.0 * dy));
    else return ((ar [m][n+1] - ar [m][n-1]) / (2.0 * dy));
}

double Dyy (double ar[][YINC+1], int m, int n)
{
    if (n == 0) return ((2.0 * ar [m][0] - 5.0 * ar [m][1]
        + 4.0 * ar [m][2] - ar [m][3]) / dy2);
    if (n == YINC) return ((2.0 * ar [m][YINC] - 5.0 * ar [m][YINC-1]
        + 4.0 * ar [m][YINC-2] - ar [m][YINC-3]) / dy2);
    else return ((ar [m][n+1] - 2.0 * ar [m][n] + ar [m][n-1]) / dy2);
}

double Top (double y) /* bottom topography */
{
    return (s * y);
}

void Solver (void) /* Poisson equation solver */
{
    int i, j;                /* counter variables */
    double sum;              /* temporary sum */
    double norm;             /* norm squared */
    double d, w;             /* weights */

    double c [N+1];          /* temporary vector */
    double r [N+1];          /* temporary vector */
    double z [N+1];          /* temporary vector */

    /* set up b, using BC, q and h */

    for (i = 0; i <= XINC - 1; i++)
    {
        b [i+1] = - dx2 * (q [i][YINC-1] - h [i][YINC-1])

```

```

        + Top (MAXY - dy)) + g (MINX + i * dx, MAXY);
    b [XINC*(YINC-2)+1+i] = - dx2 * (q [i][1] - h [i][1]
        + Top (MINY + dy)) + g (MINX + i * dx, MINY);
}

for (j = 2; j <= YINC - 2; j++)
{
    y = MINY + j * dy;
    for (i = 0; i <= XINC - 1; i++)
    {
        b [(YINC-j-1)*XINC+i+1] = - dx2 * (q [i][j] + Top (y)
            - h [i][j]);
    }
}

/* conjugate gradient algorithm for Ax = b (note: x is 'soln') */

norm = 0;

for (i = 1; i <= N; i++)
{
    r [i] = b [i] - 4.0 * soln [i];
}

for (i = 1; i <= N - XINC; i++)
{
    r [i] = r [i] + soln [XINC+i];
    r [XINC+i] = r [XINC+i] + soln [i];
}

for (j = 0; j <= YINC - 2; j++)
{
    for (i = 1; i <= XINC - 1; i++)
    {
        r [j*XINC+i] = r [j*XINC+i] + soln [j*XINC+i+1];
        r [j*XINC+i+1] = r [j*XINC+i+1] + soln [j*XINC+i];
    }
}

for (j = 1; j <= YINC - 1; j++)
{
    r [(j-1)*XINC+1] = r [(j-1)*XINC+1] + soln [j*XINC];
    r [j*XINC] = r [j*XINC] + soln [(j-1)*XINC+1];
}

```

```

}

for (i = 1; i <= N; i++)
{
    c [i] = r [i];
    norm = norm + Sqr (r [i]);
}

while (norm >= 0.00000001)
{
    sum = 0;

    for (i = 1; i <= N; i++)
    {
        z [i] = 4.0 * c [i];
    }

    for (i = 1; i <= N - XINC; i++)
    {
        z [i] = z [i] - c [XINC+i];
        z [XINC+i] = z [XINC+i] - c [i];
    }

    for (j = 0; j <= YINC - 2; j++)
    {
        for (i = 1; i <= XINC - 1; i++)
        {
            z [j*XINC+i] = z [j*XINC+i] - c [j*XINC+i+1];
            z [j*XINC+i+1] = z [j*XINC+i+1] - c [j*XINC+i];
        }
    }

    for (j = 1; j <= YINC - 1; j++)
    {
        z [(j-1)*XINC+1] = z [(j-1)*XINC+1] - c [j*XINC];
        z [j*XINC] = z [j*XINC] - c [(j-1)*XINC+1];
    }

    for (i = 1; i <= N; i++)
    {
        sum = sum + c [i] * z [i];
    }
}

```

```

        w = norm / sum;
        d = 0;

        for (i = 1; i <= N; i++)
        {
            soln [i] = soln [i] + w * c [i];
            r [i] = r [i] - w * z [i];
            d = d + r [i] * r [i];
        }

        for (i = 1; i <= N; i++)
        {
            c [i] = r [i] + d / norm * c [i];
        }
        norm = d;
    }

    /* update p */

    for (j = 1; j <= YINC - 1; j++)
    {
        for (i = 0; i <= XINC - 1; i++)
        {
            p [i][j] = soln [(YINC-j-1)*XINC+i+1];
        }
    }
}

void Setup (void) /* initial housekeeping */
{
    double amp, tr, num, wn0, wn1;
    double max_h0y;
    int i1, j1, n0, n1;

    double arc1 [XINC+1][YINC+1];
    double arc2 [XINC+1][YINC+1];

    tag1 = 0;
    tag2 = 2 * XNODES;

    /* save header info */

    fprintf (Ham_stream, "%14.10f\n", 0.0);

```

```

fprintf (Ham_stream, "%14.10f\n", TINC * dt);
fprintf (Ham_stream, "%14.10f\n", MINY);
fprintf (Ham_stream, "%14.10f\n", MAXY);
fprintf (Ham_stream, "%14.10f\n", MINX);
fprintf (Ham_stream, "%14.10f\n", MAXX);
fprintf (Ham_stream, "%14.10f\n", dt);
fprintf (Ham_stream, "%14.10f\n", dy);
fprintf (Ham_stream, "%14.10f\n", dx);
fprintf (Ham_stream, "%d\n", TNODES);
fprintf (Ham_stream, "%d\n", YNODES);
fprintf (Ham_stream, "%d\n", XNODES);

/* set initial h, p and q */

n0 = 2;
wn0 = n0 * PI / MAXX;
n1 = 5;
wn1 = n1 * PI / MAXX;
amp = 0.02;
max_h0y = 0.0;

printf ("n0 = %d n1 = %d wn0 = %5.2f wn1 = %5.2f\n", n0, n1, wn0, wn1);

for (i = 0; i <= XINC - 1; i++)
{
    x = MINX + i * dx;
    for (j = 0; j <= YINC; j++)
    {
        y = MINY + j * dy;
        h0 [i][j] = f (x, y);
        p0 [i][j] = g (x, y);
    }
}

/* time (&thetime);
   srand48 (thetime);
*/
for (i = n0; i <= n1; i++)
{
    for (j = n0; j <= n1; j++)
    {
        tr = 2.0 * PI * drand48 ();
        num = drand48 ();
        arcl [i][j] = num * cos (tr);
    }
}

```



```

        arc2 [i][j] = num * sin (tr);
    }
}

for (j = 0; j <= YINC - 1; j++)
{
    y = MINY + j * dy;
    for (i = 0; i <= XINC - 1; i++)
    {
        x = MINX + i * dx;
        for (il = n0; il <= n1; il++)
        {
            for (jl = n0; jl <= n1; jl++)
            {
                amp = 1.0 / sqrt (Sqr (il * 2.0 * PI / MAXX)
                    + Sqr (jl * PI / (MAXY - MINY)));
                p0 [i][j] = p0 [i][j] + amp
                * (arc1 [il][jl] * cos (2.0 * PI * x * il / MAXX)
                - arc2 [il][jl] * sin (2.0 * PI * x * il / MAXX))
                * sin (jl * PI * (y - MINY) / (MAXY - MINY))
                * (cos ((2.0 * jl + 1.0) * PI * (y - MAXY / 2.0) / MAXY) + 1.0) * 0.5;
            }
        }
        if (Dy (h0, i, j) > max_h0y) max_h0y = Dy (h0, i, j);
    }
}

printf ("max h0y = %8.5f\n", max_h0y);

initKElo = 0;
initKEup = 0;
for (i = 0; i <= XINC - 1; i++)
{
    for (j = 0; j <= YINC - 1; j++)
    {
        initKElo = initKElo + Sqr (Dx (p0, i, j))
            + Sqr (Dy (p0, i, j));
        initKEup = initKEup + h0 [i][j]
            * (Sqr (Dx (h0, i, j))
            + Sqr (Dy (h0, i, j)));
    }
}
initKElo = dx * dy * initKElo;

```

```

initKEup = dx * dy * initKEup;

amp = sqrt (initKEup / initKElo * 0.5);

for (i = 0; i <= XINC - 1; i++)
{
    for (j = 0; j <= YINC; j++)
    {
        p0 [i][j] = amp * p0 [i][j];
        p1 [i][j] = p0 [i][j];
        h1 [i][j] = h0 [i][j];
        h [i][j] = h1 [i][j];
        p [i][j] = p1 [i][j];
    }
}

for (j = 0; j <= YINC; j++)
{
    y = MINY + j * dy;
    for (i = 0; i <= XINC - 1; i++)
    {
        q0 [i][j] = h0 [i][j] + Dxx (p0, i, j) + Dyy (p0, i, j)
                    - Top (y);
        q1 [i][j] = h1 [i][j] + Dxx (p1, i, j) + Dyy (p1, i, j)
                    - Top (y);
        vfrc [i][j] = 0.0;
    }
}

for (j = 1; j <= YINC - 1; j++)
{
    for (i = 0; i <= XINC - 1; i++)
    {
        soln [(YINC-j-1)*XINC+i+1] = p1 [i][j];
    }
}

initKElo = 0;
initKEup = 0;
initM = 0;
initM2 = 0;
initEns = 0;
initPertKE = 0;

```

```

for (i = 0; i <= XINC - 1; i++)
{
    x = MINX + i * dx;
    for (j = 0; j <= YINC - 1; j++)
    {
        y = MINY + j * dy;
        initKElo = initKElo + Sqr (Dx (p0, i, j))
            + Sqr (Dy (p0, i, j));
        initKEup = initKEup + h0 [i][j]
            * (Sqr (Dx (h0, i, j))
            + Sqr (Dy (h0, i, j)));
        initM = initM + h0 [i][j];
        initM2 = initM2 + Sqr (h0 [i][j]);
        initEns = initEns + Sqr (q0 [i][j] - h0 [i][j] + Top (y));
        initPertKE = initPertKE + (h0 [i][j] - f (x, y))
            * (Sqr (Dx (h0, i, j))
            + Sqr (Dy (h0, i, j) - a));
    }
}
initKElo = dx * dy * initKElo;
initKEup = dx * dy * initKEup;
initH = 0.5 * (initKElo - initKEup);
initM = dx * dy * initM;
initM2 = dx * dy * initM2;
initEns = dx * dy * initEns;
initPertKE = dx * dy * initPertKE;
printf ("ef = %8.5f\n", initKElo / initKEup);

/* save initial h0, p0 */

for (j = 0; j <= YNODES - 1; j++)
{
    y = MINY + j * dy;
    fwrite (&tag1, 2, 1, H_stream);
    fwrite (&tag2, 2, 1, H_stream);
    for (i = 0; i <= XNODES - 1; i++)
    {
        output [i] = digits * h0 [i*XSKIP][j*YSKIP];
    }
    fwrite (output, 2, XNODES, H_stream);
    fwrite (&tag1, 2, 1, H_stream);
    fwrite (&tag2, 2, 1, H_stream);
}

```

```

/* save initial p0 */

for (j = 0; j <= YNODES - 1; j++)
{
    fwrite (&tag1, 2, 1, P_stream);
    fwrite (&tag2, 2, 1, P_stream);
    for (i = 0; i <= XNODES - 1; i++)
    {
        output [i] = digits * p0 [i*XSKIP][j*YSKIP];
    }
    fwrite (output, 2, XNODES, P_stream);
    fwrite (&tag1, 2, 1, P_stream);
    fwrite (&tag2, 2, 1, P_stream);
}

/* save initial H, KElo, KEup, M, M2 and Ens */

fprintf (Ham_stream, "%16.10f", 0.0);
fprintf (Ham_stream, "%16.10f", initH);
fprintf (Ham_stream, "%16.10f", initKElo);
fprintf (Ham_stream, "%16.10f", initKEup);
fprintf (Ham_stream, "%16.10f", initM);
fprintf (Ham_stream, "%16.10f", initM2);
fprintf (Ham_stream, "%16.10f", initEns);
fprintf (Ham_stream, "%16.10f", initPertKE);
fprintf (Ham_stream, "\n");

/* if any term is 0, set it to 1 (for future normalization) */

if (initH == 0) initH = 1.0;
if (initKElo == 0) initKElo = 1.0;
if (initKEup == 0) initKEup = 1.0;
if (initM == 0) initM = 1.0;
if (initM2 == 0) initM2 = 1.0;
if (initEns == 0) initEns = 1.0;

/* save initial normalized H, KElo and KEup */

fprintf (Ham_stream, "%16.10f", 0.0);
fprintf (Ham_stream, "%16.10f", initH / initH);
fprintf (Ham_stream, "%16.10f", initKElo / initKElo);
fprintf (Ham_stream, "%16.10f", initKEup / initKEup);
fprintf (Ham_stream, "%16.10f", initM / initM);

```

```

fprintf (Ham_stream, "%16.10f", initM2 / initM2);
fprintf (Ham_stream, "%16.10f", initEns / initEns);
fprintf (Ham_stream, "%16.10f", initPertKE);
fprintf (Ham_stream, "\n");

/* save initial h1, p1, and Hamiltonian data */

if (TSKIP == 1)
{
    for (j = 0; j <= YNODES - 1; j++)
    {
        fwrite (&tag1, 2, 1, H_stream);
        fwrite (&tag2, 2, 1, H_stream);
        for (i = 0; i <= XNODES - 1; i++)
        {
            output [i] = digits * h1 [i*XSKIP][j*YSKIP];
        }
        fwrite (output, 2, XNODES, H_stream);
        fwrite (&tag1, 2, 1, H_stream);
        fwrite (&tag2, 2, 1, H_stream);
    }

    for (j = 0; j <= YNODES - 1; j++)
    {
        fwrite (&tag1, 2, 1, P_stream);
        fwrite (&tag2, 2, 1, P_stream);
        for (i = 0; i <= XNODES - 1; i++)
        {
            output [i] = digits * p1 [i*XSKIP][j*YSKIP];
        }
        fwrite (output, 2, XNODES, P_stream);
        fwrite (&tag1, 2, 1, P_stream);
        fwrite (&tag2, 2, 1, P_stream);
    }

    fprintf (Ham_stream, "%16.10f", dt);
    fprintf (Ham_stream, "%16.10f", initH / initH);
    fprintf (Ham_stream, "%16.10f", initKElo / initKElo);
    fprintf (Ham_stream, "%16.10f", initKEup / initKEup);
    fprintf (Ham_stream, "%16.10f", initM / initM);
    fprintf (Ham_stream, "%16.10f", initM2 / initM2);
    fprintf (Ham_stream, "%16.10f", initEns / initEns);
    fprintf (Ham_stream, "%16.10f", initPertKE);

```

```

        fprintf (Ham_stream, "\n");
    }
    fflush (NULL);
}

void SaveData (void) /* save data to disk files */
{
    /* save h */

    for (j = 0; j <= YNODES - 1; j++)
    {
        fwrite (&tag1, 2, 1, H_stream);
        fwrite (&tag2, 2, 1, H_stream);
        for (i = 0; i <= XNODES - 1; i++)
        {
            output [i] = digits * h1 [i*XSKIP][j*YSKIP];
        }
        fwrite (output, 2, XNODES, H_stream);
        fwrite (&tag1, 2, 1, H_stream);
        fwrite (&tag2, 2, 1, H_stream);
    }

    /* save p */

    for (j = 0; j <= YNODES - 1; j++)
    {
        fwrite (&tag1, 2, 1, P_stream);
        fwrite (&tag2, 2, 1, P_stream);
        for (i = 0; i <= XNODES - 1; i++)
        {
            output [i] = digits * p1 [i*XSKIP][j*YSKIP];
        }
        fwrite (output, 2, XNODES, P_stream);
        fwrite (&tag1, 2, 1, P_stream);
        fwrite (&tag2, 2, 1, P_stream);
    }

    /* determine Hamiltonian */
    /* (invariant if h and p are zero on the boundaries) */

    KElo = 0;
    KEup = 0;
    M = 0;

```

```

M2 = 0;
Ens = 0;
PertKE = 0;
for (i = 0; i <= XINC - 1; i++)
{
    x = MINX + i * dx;
    for (j = 0; j <= YINC - 1; j++)
    {
        y = MINY + j * dy;
        KElo = KElo + Sqr (Dx (p1, i, j))
            + Sqr (Dy (p1, i, j));
        KEup = KEup + h1 [i][j]
            * (Sqr (Dx (h1, i, j))
            + Sqr (Dy (h1, i, j)));
        M = M + h1 [i][j];
        M2 = M2 + Sqr (h1 [i][j]);
        Ens = Ens + Sqr (q1 [i][j] - h1 [i][j] + Top (y));
        PertKE = PertKE + (h1 [i][j] - f (x, y))
            * (Sqr (Dx (h1, i, j))
            + Sqr (Dy (h1, i, j) - a));
    }
}

KElo = dx * dy * KElo;
KEup = dx * dy * KEup;
H = 0.5 * (KElo - KEup);
M = dx * dy * M;
M2 = dx * dy * M2;
Ens = dx * dy * Ens;
PertKE = dx * dy * PertKE;

/* save Hamiltonian and its 2 terms */

fprintf (Ham_stream, "%16.10f", t);
fprintf (Ham_stream, "%16.10f", H / initH);
fprintf (Ham_stream, "%16.10f", KElo / initKElo);
fprintf (Ham_stream, "%16.10f", KEup / initKEup);
fprintf (Ham_stream, "%16.10f", M / initM);
fprintf (Ham_stream, "%16.10f", M2 / initM2);
fprintf (Ham_stream, "%16.10f", Ens / initEns);
fprintf (Ham_stream, "%16.10f", PertKE);
fprintf (Ham_stream, "\n");

```

```

    printf ("%14.10f\n", H / initH);

    fflush (NULL);
}

void main (void)
{
    printf ("%s", TITLE);
    ret (1);

    /* open data files */
    if ((H_stream = fopen (H_FILE, "wb")) == NULL)
    {
        printf ("Cannot open output file.\n");
        exit (1); /* exit program */
    }
    if ((P_stream = fopen (P_FILE, "wb")) == NULL)
    {
        printf ("Cannot open output file.\n");
        exit (1); /* exit program */
    }
    if ((Ham_stream = fopen (HAM_FILE, "w")) == NULL)
    {
        printf ("Cannot open output file.\n");
        exit (1); /* exit program */
    }

    /* initial setup of all variables and conditions */

    Setup ();

    /* finite difference approximation loop */

    for (k = 2; k <= TINC; k++)
    {
        t = k * dt;
        if (abs (H / initH) > 1000) exit (0);

        for (j = 0; j <= YINC; j++)
        {
            for (i = 0; i <= XINC - 1; i++)
            {
                A1 [i][j] = p1 [i][j]

```



```

        + h1 [i][j] * (Dxx (h1, i, j)
        + Dyy (h1, i, j))
        + 0.5 * (Sqr (Dx (h1, i, j))
        + Sqr (Dy (h1, i, j)));
    }
}

for (i = 0; i <= XINC - 1; i++)
{
    ip = i + 1;
    im = i - 1;
    if (ip == XINC) ip = 0;
    if (im == - 1) im = XINC - 1;

    for (j = 1; j <= YINC - 1; j++)
    {
        jp = j + 1;
        jm = j - 1;

        h [i][j] = h0 [i][j]
        + 2.0 * dt / (12.0 * dx2)
        * ((h1 [i][jm] + h1 [ip][jm] - h1 [i][jp] - h1 [ip][jp])
        * (A1 [ip][j] - A1 [i][j])
        + (h1 [im][jm] + h1 [i][jm] - h1 [im][jp] - h1 [i][jp])
        * (A1 [i][j] - A1 [im][j])
        + (h1 [ip][j] + h1 [ip][jp] - h1 [im][j] - h1 [im][jp])
        * (A1 [i][jp] - A1 [i][j])
        + (h1 [ip][jm] + h1 [ip][j] - h1 [im][jm] - h1 [im][j])
        * (A1 [i][j] - A1 [i][jm])
        + (h1 [ip][j] - h1 [i][jp]) * (A1 [ip][jp] - A1 [i][j])
        + (h1 [i][jm] - h1 [im][j]) * (A1 [i][j] - A1 [im][jm])
        + (h1 [i][jp] - h1 [im][j]) * (A1 [im][jp] - A1 [i][j])
        + (h1 [ip][j] - h1 [i][jm]) * (A1 [i][j] - A1 [ip][jm]))

        + (2.0 * dt * HFRIC / dx2) * (h0 [im][j] + h0 [ip][j]
        + h0 [i][jm] + h0 [i][jp] - 4.0 * h0 [i][j]);

        if (h [i][j] < 0.0) h [i][j] = 0.0;

        q [i][j] = q0 [i][j]
        + 2.0 * dt / (12.0 * dx2)
        * ((q1 [i][jm] + q1 [ip][jm] - q1 [i][jp] - q1 [ip][jp])
        * (p1 [ip][j] - p1 [i][j])

```

```

+ (q1 [im][jm] + q1 [i][jm] - q1 [im][jp] - q1 [i][jp])
* (p1 [i][j] - p1 [im][j])
+ (q1 [ip][j] + q1 [ip][jp] - q1 [im][j] - q1 [im][jp])
* (p1 [i][jp] - p1 [i][j])
+ (q1 [ip][jm] + q1 [ip][j] - q1 [im][jm] - q1 [im][j])
* (p1 [i][j] - p1 [i][jm])
+ (q1 [ip][j] - q1 [i][jp]) * (p1 [ip][jp] - p1 [i][j])
+ (q1 [i][jm] - q1 [im][j]) * (p1 [i][j] - p1 [im][jm])
+ (q1 [i][jp] - q1 [im][j]) * (p1 [im][jp] - p1 [i][j])
+ (q1 [ip][j] - q1 [i][jm]) * (p1 [i][j] - p1 [ip][jm])

+ (2.0 * dt * FRIC / dx2) * (vfrc [im][j] + vfrc [ip][j]
+ vfrc [i][jm] + vfrc [i][jp] - 4.0 * vfrc [i][j]);

    } /* j loop */
} /* i loop */

/* solve Poisson equation to obtain p from q */

Solver ();

/* extrapolate values of q on boundaries */

{
    for (i = 0; i <= XINC - 1; i++)
    {
        q [i][0] = h [i][0] + Dyy (p, i, 0)
            - Top (MINY);
        q [i][YINC] = h [i][YINC] + Dyy (p, i, YINC)
            - Top (MAXY);
    }
}

/* update h, p and q */

for (i = 0; i <= XINC - 1; i++)
{
    for (j = 1; j <= YINC - 1; j++)
    {
        y = MINY + j * dy;

        q1 [i][j] = q1 [i][j] + 0.5 * ROBFIL
            * (q0 [i][j] - 2.0 * q1 [i][j])

```

```

        + q [i][j]);

        h1 [i][j] = h1 [i][j] + 0.5 * ROBFIL
            * (h0 [i][j] - 2.0 * h1 [i][j]
            + h [i][j]);

        h0 [i][j] = h1 [i][j];
        h1 [i][j] = h [i][j];
        p0 [i][j] = p1 [i][j];
        p1 [i][j] = p [i][j];
        q0 [i][j] = q1 [i][j];
        q1 [i][j] = q [i][j];

        vfrc [i][j] = q0 [i][j] - h0 [i][j] + Top (y);
    }
    q0 [i][0] = q1 [i][0];
    q1 [i][0] = q [i][0];
    q0 [i][YINC] = q1 [i][YINC];
    q1 [i][YINC] = q [i][YINC];

    vfrc [i][0] = q0 [i][0] - h0 [i][0] + Top (MINY);
    vfrc [i][YINC] = q0 [i][YINC] - h0 [i][YINC] + Top (MAXY);
}

/* save data at certain intervals of t, x, and y */

if (k % TSKIP == 0)
{
    SaveData ();
}

} /* k loop */

/* close data files */
fclose (H_stream);
fclose (P_stream);
fclose (Ham_stream);
}

```